# Alma Mater Studiorum – Università di Bologna
## in cotutela con Université de Lyon


## DOTTORATO DI RICERCA IN

# Chimica

Ciclo   29

**Settore Concorsuale di afferenza:**       **03/C2**

**Settore Scientifico disciplinare:**       **CHIM/04**


TITOLO TESI

## Presentata da: Yu Zhang

## Catalytic upgrading of oxygenated building blocks in lignocellulose-based biorefineries


| Coordinatore Dottorato | Relatore |
|---|---|
| **Prof. Aldo Roda** | **Prof.ssa.Stefania Albonetti** |
| | Relatore |
| | **Dr. Chloé Thieuleux** |


**Esame finale anno 2017**

N°d'ordre   NNT : xxx

<div align="center">

**THESE de DOCTORAT DE L'UNIVERSITE DE LYON**

Délivrée par

**L'Université Claude Bernard Lyon 1**

**Ecole Doctorale de Lyon**

N° ED206

**Spécialité de doctorat** : **Chimie**

**Discipline** : **Chimie Industrielle Durable**

Soutenue publiquement le 19 Janvier 2017

Par

**M. Yu ZHANG**

</div>

# Catalytic upgrading of oxygenated building blocks in lignocellulose-based biorefineries

<div align="center">

**Directeur de thèses: Mme. Stefania Albonetti**

**Co-Directeur de thèses : Mme. Chloè Thieuleux and Mme. Elsje Alessandra Quadrelli**

</div>

**Jury:**

| | |
|---|---|
| Dr. Chloé THIEULEUX | Membre in jury |
| Prof. Stefania ALBONETTI | Membre in jury |
| Prof. Pascal FONGARLAND | Membre in jury |
| Dr.Francesco Di RENZO | Rapporteur |
| Prof.Fabrizio CAVANI | Membre in jury |
| Dr.Carlo LUCARELLI | Rapporteur |

# UNIVERSITE CLAUDE BERNARD - LYON 1

| | |
|---|---|
| Président de l'Université | M. le Professeur Frédéric FLEURY |
| Président du Conseil Académique | M. le Professeur Hamda BEN HADID |
| Vice-président du Conseil d'Administration | M. le Professeur Didier REVEL |
| Vice-président du Conseil Formation et Vie Universitaire | M. le Professeur Philippe CHEVALIER |
| Vice-président de la Commission Recherche | M. Fabrice VALLÉE |
| Directeur Général des Services | M. Alain HELLEU |

## COMPOSANTES SANTE

| | |
|---|---|
| Faculté de Médecine Lyon Est – Claude Bernard | Directeur : M. le Professeur J. ETIENNE |
| Faculté de Médecine et de Maïeutique Lyon Sud – Charles Mérieux | Directeur : Mme la Professeure C. BURILLON |
| Faculté d'Odontologie | Directeur : M. le Professeur D. BOURGEOIS |
| Institut des Sciences Pharmaceutiques et Biologiques | Directeur : Mme la Professeure C. VINCIGUERRA |
| Institut des Sciences et Techniques de la Réadaptation | Directeur : M. X. PERROT |
| Département de formation et Centre de Recherche en Biologie Humaine | Directeur : Mme la Professeure A-M. SCHOTT |

## COMPOSANTES ET DEPARTEMENTS DE SCIENCES ET TECHNOLOGIE

| | |
|---|---|
| Faculté des Sciences et Technologies | Directeur : M. F. DE MARCHI |
| Département Biologie | Directeur : M. le Professeur F. THEVENARD |
| Département Chimie Biochimie | Directeur : Mme C. FELIX |
| Département GEP | Directeur : M. Hassan HAMMOURI |
| Département Informatique | Directeur : M. le Professeur S. AKKOUCHE |
| Département Mathématiques | Directeur : M. le Professeur G. TOMANOV |
| Département Mécanique | Directeur : M. le Professeur H. BEN HADID |
| Département Physique | Directeur : M. le Professeur J-C PLENET |
| UFR Sciences et Techniques des Activités Physiques et Sportives | Directeur : M. Y.VANPOULLE |
| Observatoire des Sciences de l'Univers de Lyon | Directeur : M. B. GUIDERDONI |
| Polytech Lyon | Directeur : M. le Professeur E.PERRIN |
| Ecole Supérieure de Chimie Physique Electronique | Directeur : M. G. PIGNAULT |
| Institut Universitaire de Technologie de Lyon 1 | Directeur : M. le Professeur C. VITON |
| Ecole Supérieure du Professorat et de l'Education | Directeur : M. le Professeur A. MOUGNIOTTE |
| Institut de Science Financière et d'Assurances | Directeur : M. N. LEBOISNE |

*Excellence is an art won by training and habitation. We do not act rightly because we have virtue or excellence, but rather we have those because we have acted rightly. We are what we repeatedly do. Excellence, then, is not an act but a habit."*

*Aristotle (384 BC - 322 BC)*

# Abstract

This PhD project is focused on the gas phase hydrogenation of furfural over iron and magnesium oxides. Numerous catalysts with different iron and magnesium molar ratios, were prepared by co-precipitation or impregnation methods and were tested for the reduction of furfural (FU) using methanol as hydrogen donor. Furfuryl alcohol (FAL) and 2-methyl furfural (MFU) were the main products obtained, demonstrating that Mg/Fe/O systems can promote sequential hydrogenation-hydrogenolysis reaction. Impregnated catalysts demonstrated to be more active and selective towards MFU than co-precipitated ones. Reported data demonstrated that product distribution was strongly influenced by the iron content and from the resulting acid and redox properties of the material. As a matter of fact, the introduction of iron on the surface of the basic oxide led to the addition of Lewis acidity and redox capacity in the system, significantly enhancing FU conversion and MFU production. The activation of different species on the catalyst surface has been studied by in situ DRIFTS and FTIR. The results reveal that the MgO basicity favors methanol activation and FeOx redox capacity might be the responsible of furfuryl alcohol hydrogenolysis.

# Résumé

Cette thèse porte sur l'hydrogénation en phase gazeuse du furfural sur des oxydes de fer et de magnésium. De nombreux catalyseurs avec différents ratio molaires en fer et magnésium ont été préparés par des méthodes de co-précipitation ou d'imprégnation. Ils ont été ensuite testés lors de la réduction du furfural (FU) en utilisant du méthanol comme donneur d'hydrogène. L'alcool furfurylique (FAL) et le 2-methyl furfural (MFU) étaient les principaux produits obtenus démontrant alors que les systèmes Mg/Fe/O peuvent favoriser la réaction séquentielle d'hydrogénation-hydrogénolyse. Les catalyseurs imprégnés se sont révélés plus actif et sélectif vis-à-vis des MFU que ceux préparés par co-précipitation. Les données rapportées ont montré que la distribution du produit était fortement influencée par la teneur en fer et par l'acide résultant, ainsi que les propriétés d'oxydoréduction du matériau. En effet, l'introduction de fer à la surface d'oxyde basique a conduit à l'addition d'acidité de Lewis et de potentiel d'oxydoréduction dans le système, améliorant significativement la conversion de FU et la production de MFU. L'activation des différentes espèces à la surface du catalyseur a été étudié in situ par DRIFTS et FTIR. Les résultats révèlent que la basicité du MgO favorise l'activation du méthanol et que le potentiel d'oxydoréduction du FeOx pourrait être responsable de l'hydrogénolyse de l'alcool furfurylique.

# Preface

This thesis is intended to provide a fundamental investigation on the hydrogen transfer reduction of furfural. Thus, in chapter I, a comprehensive introduction of furan compounds utilization was presented. Further, we present a review of the different transformation strategies for the upgrading of furfurals towards fuels and chemicals and related hydrogen transfer reduction process in biomass conversion. In Chapter II, we carried out experiments for handling of furfural reduction into methyl furan, including co-precipitated and impregnated catalytic system. Properties of active sites were investigated and characterized by ex situ techniques such as acid base analysis, $H_2$ TPR, Raman spectra. Chapter III is focuses on mechanistic investigations. Detailed analysis by in situ DRIFT and FT-IR were performed. The manuscript ends up with a general conclusion where some perspectives are put forward.

The work reported in this thesis was carried out between C2P2 Lab Lyon and University of Bologna, within SINCHEM project support.

# Contents

# Chapter I Overview on Biomass Utilization

Facing energy shortage, biomass is considered as a renewable energy source because its inherent energy comes from the sun and it can regrow in a relatively short time. Recently, there has been a strong political and technical focus on using biomass to produce transportation fuels and organic chemicals. Replacement of petroleum-derived supplements with chemicals from biomass will play a key role in sustaining the growth of the chemical industry.

Biomass is an abundant and sustainable resource. Three general components of biomass can be distinguished: starches, triglycerides, and lignocellulose.[1] Starches are biopolymers of glucose in which glucose molecular was lined by α-glycosidic bonds, and may be fully hydrolysis into monomers. The monomers have been extensively used as feedstock for the production of first generation bio-alcohol such as bio-ethanol, deriving from starch components of food crops such as wheat shell, corn, and sugar cane, is probably the most well established bio-fuel production process.[2] Triglycerides can be obtained from both plant and animals sources (such as vegetable oils and animal grace), and are used as feedstock for the production of biodiesel via the transesterification of lipids with an alcohol, such as methanol, to form a mixture of mono-alkyl esters of long-chain fatty acids (such as Fatty Acid Methyl Ester). In the latter process, since glycerol is formed as side product but it can be recycled for other industrial uses. Among these trans-esterification process bases is used as catalyst conventionally, such as NaOH or KOH.[3] One concept should be emphasized here. Using starches and triglycerides as feedstock to produce fuel and chemicals is generally regarded as unsustainable because it seize the limited food resources for chemicals rather than feeding humans. Additionally, using edible starches and triglycerides as feedstock are consistently more costly compared to using fossil-based feedstock. Consequently, more effort in the utilization of starches and triglycerides has shift to exploit sources of waste, such as un-edible oils and waste cooking oil, as potential feedstock. Lignocellulosic biomass is the inedible parts and most abundant biomass resources. The components diagram was shown in **Figure 1.1**, it was reported by Wyman Charles *et al*.[4] lignocellulosic biomass is composed of 40-50% cellulose (glucose polymer linked through β-glycosidic bonds), 25-35% hemicelluloses (amorphous polymer of pentose sugars) and 15-20% lignin (amorphous phenolic polymer). Since it is abundant and inexpensive, lignocellulosic biomass is difficult to directly use. Several pretreatment steps were required before

transformation into monomeric sugars. The pretreatment processes employ a combination of physical such as high energy milling and chemical processes such as acidic hydrolysis, and it was thought to be the most costly steps in lignocellulosic biomass utilization due to its low selectivity and high energy input.
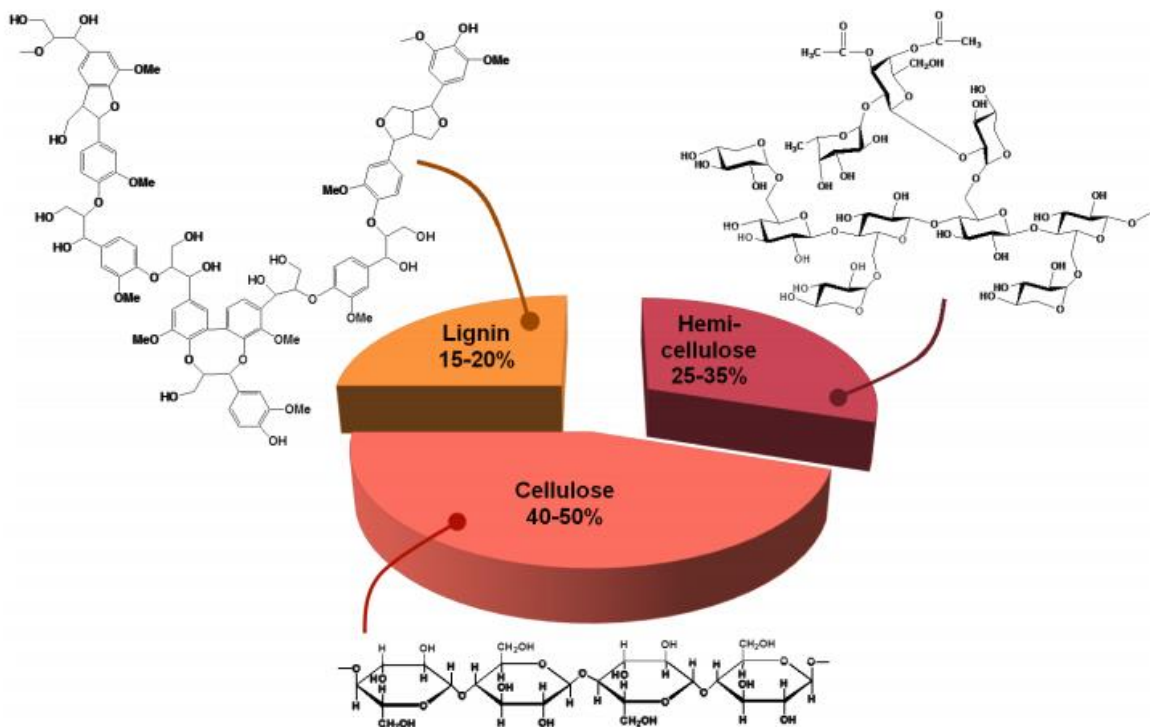


**Figure 1.1** General composition of lignocellulosic biomass and representative structures of constituent components represented from Ref.[4]

After pretreatment, different transformation routes were integrated to satisfy various production desires. Among these transformations, the main principle is using it rather than directly flaring it. Thus in order to facile the transformation, there are two approaches was established: thermochemical processes and platform sequential transfer processes, and both of them were shown in **Figure 1.2**
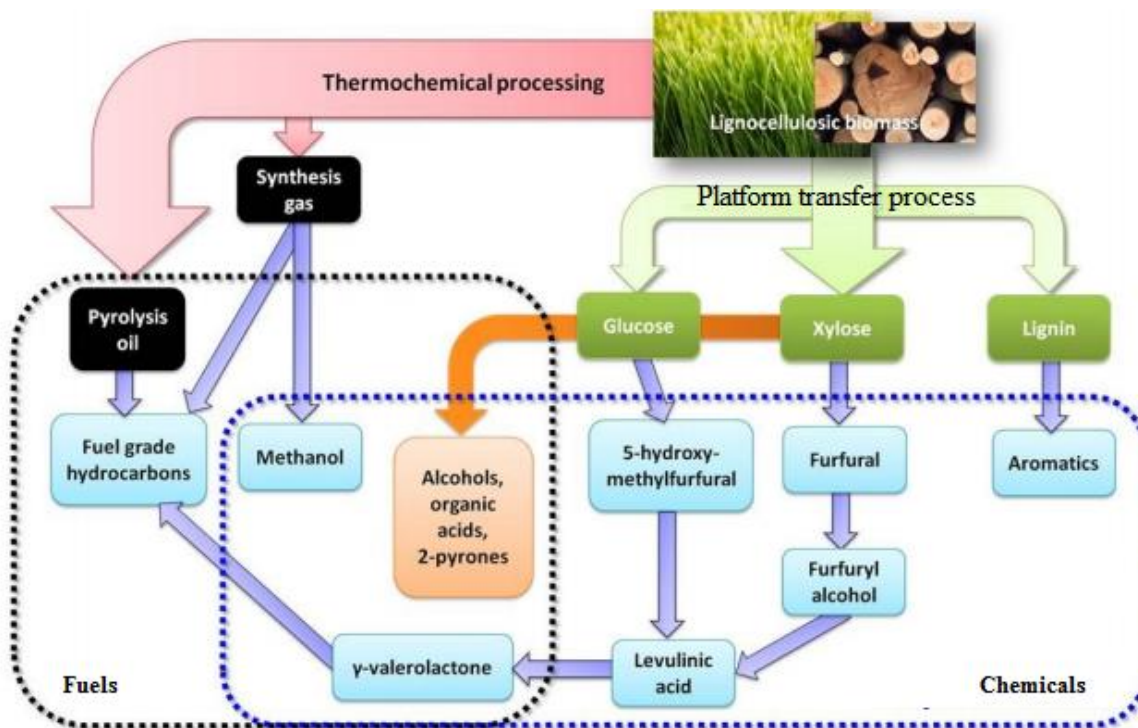
**Figure 1.2** Processes of the conversion of biomass through thermochemical and platform sequential transfer process strategies to fuel and platform chemicals

The well-developed strategies for the production of bio-derived jet fuel are lignocellulose gasification integrated with Fisher–Tropsch Synthesis. The process is easy coupling with established industrial chemical process. Among the procedures, four stages were involved. At beginning with pretreatment, during this stage, biomass was dried and grinded. After that, a powder will be obtained. The second stage was gasification, after heating in a high temperature; it was transformed into synthesis gas flow. After purification, the Fischer-Tropsch process will convert synthesis gas into liquid hydrocarbon.

During sequence transformation several platform compounds were discovered. These called building block chemicals can be produced from sugars via biological or chemical transformation processes. The top sugar-based building blocks are furfural (FUR), hydroxymethylfurfural (HMF), Furfural 2,5-furan dicarboxylic acid (FDCA), levulinic acid (LA), glycerol, sorbitol, and xylitol/arabinitol. So among these platform compounds we focused on the furfural upgrading because its transfer process was easily couple with established industrial process and scale up into pilot synthesis and real application.

## 1.1 Catalytic conversion of furfurals into fuel and chemicals

Biomass is mainly from wood resources, as a penitential fuel, it has a high oxygen content which lowers significantly the heating values. Thus, hydrogenation is an alternative to produce fuel compounds from biomass molecules. Several efficient approaches have been developed for highly selective transformation of furfural (FUR) into fuel and fine chemicals including: dehydration, oxidation, hydrogenation and carbon-carbon coupling.
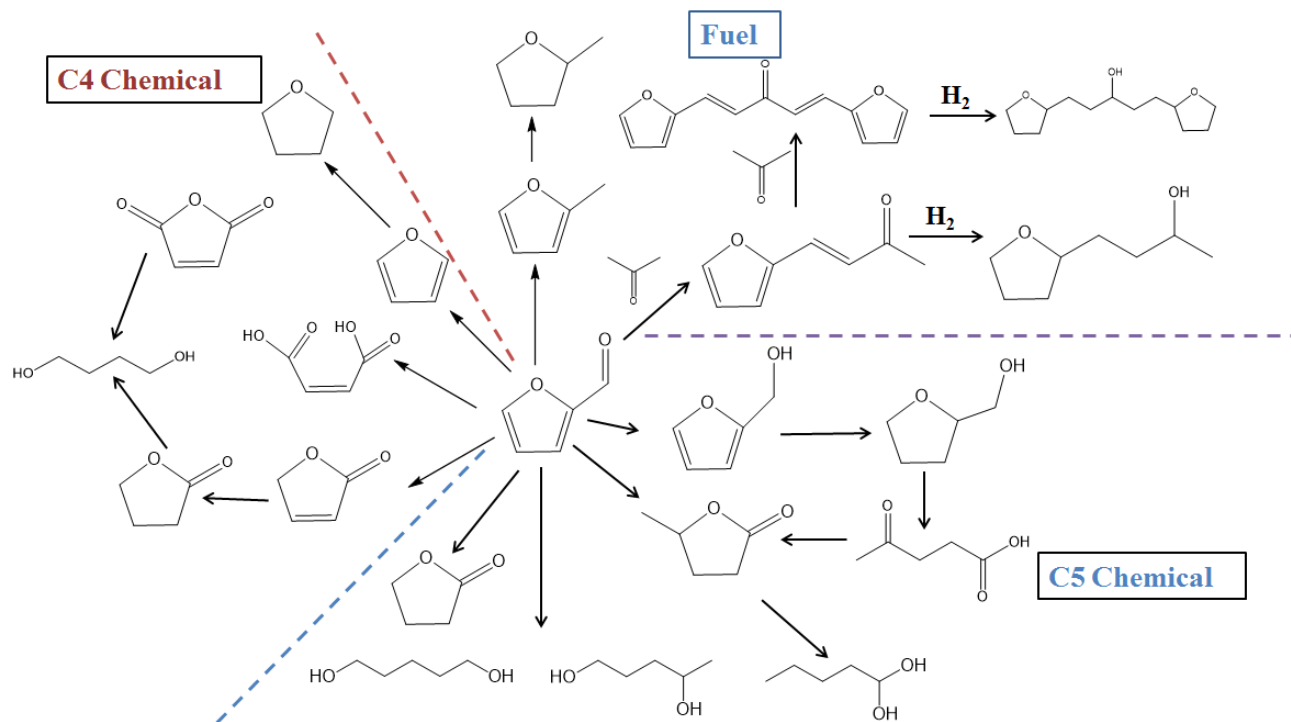


**Figure 1.3** Summary of furfural conversion into value chemicals and fuel

The most common processes to remove oxygen from biomass derived compounds are dehydration and hydrogenation where hydrodeoxygenation is the main route to reduce oxygen contents. The section on hydrogenation reactions is the longest section as it encompasses a wide number of products, most of them already commercialized. These include products and biofuels derived from furfuryl alcohol, tetrahydrofurfuryl alcohol, methylfuran, tetrahydromethylfuran, and cyclopentanone. The extensive compilation of furfural based compounds transformation routes were summarized in **Figure 1.3**.

### 1.1.1  Furfuryl Alcohol, Methyl Furan and their Derivatives.

16

Furfuryl alcohol (2-furanmethanol, FAL) is the most important chemical derived from FUR, having a broad spectrum of applications in the chemical industry. FAL production utilizes 65% of the overall FUR produced. FAL is primarily used for the production of resins for use as high-quality cores and molds for metal casting in the foundry industry, as a reactive solvent for phenolic resins in the refractory industry, as a viscosity reducer for epoxy resins, in the manufacture of polyurethane foams and polyesters, and as a chemical building block for the synthesis of tetrahydrofurfuryl alcohol (THFA) and pharmaceuticals (such as antiulcer ranitidine), and in the manufacture of fragrances. Other relevant chemicals that can be obtained from FAL include ethyl furfuryl ether, levulinic acid (LA), γ-valerolactone (GVL); the latter two products can also be synthesized directly from FUR.

From the view of industrial manufacture, FAL is produced through chemical catalytic hydrogenation of FUR processes, which can be accomplished in gas or liquid phase. FUR hydrogenation could also lead to the formation of some other chemicals besides FAL, such as 2-methylfuran (MFU) through hydrogenolysis of side chains the C–OH bond, tetrahydrofurfuryl alcohol (THFA, via deep hydrogenation of the furan ring of FAL), and 2-methyl tetrahydrofuran (MTHF, from the hydrogenation of MFU).[5] Other minor products include furan and tetrahydrofuran, different pentanediols, 2-pentanone and 2-pentanol, cyclopentanone and cyclopentanol could also be formed in particular condition, but they are not the main goals for FUR upgrading, due to less atomic economic.

### 1.1.2. Gas-Phase Hydrogenation of Furfural.

The industrial gas-phase process is essentially conducted by feeding FUR into an evaporator system comprising a packed column, a circulating pump, and a heater to maintain the FUR temperature at 120°C.[6, 7] Gas hydrogen was introduced from the bottom of the reaction column in a countercurrent of liquid FUR that flows downwards. The reaction products are condensed, and FAL is separated by distillation and residual FUR is recycled.

The gas-phase process was first reported in 1929 by using Cu on asbestos as the catalyst,[8] after that the use of copper chromite was reported in 1937 by Du Pont de Nemours.[9] Later, Quaker Oats Company achieved 99% furfuryl alcohol yields at 130–170°C by using Cu supported on $Na_2O \cdot xSiO_2$.[10] Similarly, many other Cu based catalystic systems and metals

such as Pt, Pd, Co, Fe, Ni, and Zn have been attempted for this process, mainly to overcome the environmental concerns when chromium components were used in copper chromite catalysts. The experimental conditions and catalytic results of relevant catalytic systems are summarized in **Table 1.1**. Many systems contain copper species which was believed as the active phase and most employing support was silica. The simply comparison is not reasonable, because the experiments are carried out under various conditions. The $H_2$/FUR molar ratio reported in literature was range from 2 to 900 and the reaction temperatures range between 130 and 200 °C and time-on-stream values was range from 0.25 to 80 h. However, according to **Table 1.1**, it can be informed that the best catalytic performance to synthesis FAL is obtained via using the CuCa/SiO$_2$ catalyst.[11] More interesting, it remained stable after running 80 h reaction and provided a FAL yield of 99% with a low $H_2$/FUR molar ratio of 5 at the low reaction temperature (130°C). However, in the absence of Ca and at higher reaction temperature (170°C), it still achieved of 97% FAL yield after 5 h of reaction with a similar liquid hourly space velocity (LHSV) of 0.5 h$^{-1}$.[12] Therefore, the challenge in the gas-phase hydrogenation of FUR to FAL lies in the inhibition of the pathways that generate 2-methylfuran and furan when high conversions of FUR are obtained because FAL is an active intermediate, which is difficult to highly selective synthesis of FAL in high reaction temperature. As regard to investigate the influence of catalyst towards FAL selectivity, the strong metal support interaction metal oxides was proposed to be a key fact, it was demonstrated by Somorjai and co-workers, in which TiO$_2$-supported Pt was used as catalyst.[13] it indicated that an active furfuryl-oxygen intermediate species were formed by a charge-transfer interaction between an oxygen vacancy of TiO$_2$ and furfural and the species is rapidly hydrogenated. The role of the Pt/TiO$_2$ interface is simply to facilitate hydrogen spill to form this furfuryl-oxygen intermediate, this reaction pathway is an order of magnitude faster than when Pt is not supported on TiO$_2$.

The occurrence of catalyst deactivation complicates the application of Cu-based catalysts in gas phase processes. This deactivation is more severe at higher FUR partial pressures, making a thorough kinetic study of FUR hydrogenation difficult.[14] A possible explanations of the observed catalyst deactivation, the formation of coke, catalyst poisoning by adsorption of FUR or other reaction products, a change in the oxidation state of the copper species, and sintering of the copper particles during the catalytic process have been proposed.

Recently, the deactivation of copper chromite catalyst was studies by J.A.Dumesic *et al*. in which it pointed that the main cause for deactivation of copper chromite catalysts was the strong adsorption of species derived from FUR and FAL.[15] Moreover, when Cu sites were covered by Cr species which could form by the decomposition of copper chromite, it will significantly decrease the FAL selectivity. Nevertheless, it has very recently been demonstrated that the stability of copper chromite can be improved by deposition of a thin alumina layer *via* atomic layer deposition, which inhibited coke formation, Cu agglomeration, and blocking of the copper particles by chromite species.[16]

**Table 1.1** summary of Gas-Phase Hydrogenation of Furfural to FAL over Catalysts

| Catalyst | Reaction condition | | | Results | | |
|---|---|---|---|---|---|---|
| | Space Velocity $(h^{-1})$ | Temp. (°C) | Time (h) | FUR.Con.(%) | FAL Yield (%) | Ref. |
| Cu/SiO$_2$ | 0.5 (LHSV) | 170 | 4 | 98 | 97 | [12] |
| Cu/SiO$_2$ | 0.5 (WHSV) | 140 | 10 | 98 | 73 | [17] |
| Cu/SiO$_2$ | 2.3 (LHSV) | 290 | 0.25 | 77 | 63 | [18] |
| Cu/MgO | 4.8 (WHSV) | 180 | 5 | 98 | 96 | [19] |
| Cu/SBA-15 | 1.5 (WHSV) | 170 | 1 | 92 | 85 | [20] |
| Cu/ZnO | 0.5 (WHSV) | 220 | 10 | 95 | 31 | [17] |
| Cu/Carbon | NA[a] | 225 | 1 | 1.6μmol.g$^{-1}$s$^{-1}$ [b] | 68% select. [c] | [21] |
| Ni/SiO$_2$ | 10 (WHSV) | 220 | NA[a] | 84 | 31 | [22] |
| Pt/SiO$_2$ | 1300 (GHSV) | 200 | 0.5 | 0.2μmol.g$^{-1}$s$^{-1}$ [b] | 13% select. [c] | [23] |
| CuCr/TiO$_2$ | 1.2 (WHSV) | 140 | 0.5 | 90 | 79 | [24] |
| CuCo/SiO$_2$ | 3.1 (WHSV) | 200 | 12 | 65 | 64 | [25] |
| CuCa/SiO$_2$ | 0.33 (LHSV) | 130 | 80 | 100 | 99 | [11] |
| Cu$_2$Cr$_2$O$_5$ | 52 (WHSV) | 200 | 4 | 22μmol.g$^{-1}$s$^{-1}$ [b] | 98% select. [c] | [15] |
| CuNiMgAl oxide | 4000 (GHSV) | 220 | 36 | 80 | 64 | [26] |

(a) NA: not available, (b) Reaction rate was presented in the reference instead of conversion number, (c) Selectivity to FAL were given instead of yield, LHSV= Liquid hourly space velocity, WHSV=Weight hourly space velocity GHSV=Gas hourly space velocity

### 1.1.3. Liquid-Phase Hydrogenation of Furfural.

The first liquid-phase hydrogenation of FUR was invented by Quaker Oats Company in 1933 where Ni/MgO catalyst was employed as catalyst,[27] the process required accurate control to avoid the deep hydrogenation to form tetrahydrofurfuryl alcohol. Meanwhile, reduced copper chromite has been widely used as catalyst and it achieved more than 90% yield of FAL. When higher pressure and higher temperature was attempted, the FAL selectivity was improved to 98% at 140 °C using 10 MPa $H_2$ by adding alkaline earth oxides such as CaO and BaO in copper chromite.[28] when copper chromite was supported on CaO, the FAL yield could reach close to 98% at low $H_2$ pressures.[29]

In order to facilitate industrial operations, the liquid-phase hydrogenation of FUR was performed by primary mixing copper chromite with FUR to form an initial slurry, after that, the slurry was continuously fed into a tubular bubble reactor along with $H_2$.[30] In the outlet, the slurry was de-pressurized, and excess $H_2$ is recycled into the reactor, the liquid phase was rectified to obtain pure FAL. Since high yield of FAL was obtained from the process, but the main drawback of chromium-based catalysts is the risk of environmental pollution, most of chromium compounds are toxic, and for this reason, extensive effort has been devoted to develop more environmentally friendly catalysts. **Table 1.2** summarizes the liquid phase catalytic systems used for this reaction. From the results, it can be said that liquid-phase hydrogenation of FUR to produce FAL always leads to better catalytic results than these obtained in the gas phase process, many catalysts can produce around 100% FAL yields, although high $H_2$ pressures are required. Most studies are using $H_2$ pressures is 1-2 MPa and reaction temperatures is between 60 and 180 °C. Since the operation condition was different, in general, high FAL yields could been obtained under very different experimental conditions and with multicomponent catalysts in which Ni and Cu are mainly presented as the active sites. Almost full transformation into FAL has been reported by using pure FUR or FUR diluted in water, ethanol or isopropanol. The deactivation of Cu-based catalysts is believed to the agglomeration and copper species leaching. In order to limit the copper deactivation, atomic layer deposition has recently been developed by

J.A.Dumesic *et al.* the synthesis strategy was demonstrated to be a desirable approach to stabilize copper-based catalysts for liquid-phase catalytic reactions.[31] Similarly, layer deposition of an alumina overcoat was conducted, in which the Cu particles was in encapsulation by an amorphous alumina overcoat. After that process high temperature calcination produced multiple pore structure in coating alumina layer, thus more active copper species could be exposed but still maintaining the stabilizing interaction with low coordination copper sites on the surface that prevent leaching and agglomeration. In contrast, Pt/C catalysts have been reported to not undergo deactivation after being used for three cycles.[32] Also in this work, the author carried out kinetic analysis. The experimental data was fully fitted with the Langmuir–Hinshelwood dual-site mechanism in which it contained two different active sites for the molecular adsorption of $H_2$ and FUR/FAL species. It concluded that the reaction between adsorbed FUR and adsorbed hydrogen is the rate-controlling step.

**Table1.2** Summary of different catalytic system for liquid-phase hydrogenation of furfural

| Catalyst | Reaction condition | | | Results | | |
|---|---|---|---|---|---|---|
| | Solvent | Temp. (°C) | Time (h) | FUR.Con.(%) | FAL Yield (%) | Ref. |
| Ni-alloy | No | 100 | 6 | 100 | 100 | [33] |
| Cu/Al$_2$O$_3$ | Water | 90 | 2 | 81 | 81 | [34] |
| Co/SBA-15 | Ethanol | 150 | 1.5 | 92 | 88 | [35] |
| Ru/Zr-MOF | Water | 20 | 4 | 95 | 95 | [36] |
| Pt-Sn/SiO$_2$ | Isopropanol | 100 | 4 | 100 | 96 | [37] |
| Rh-Sn/SiO$_2$ | Isopropanol | 100 | 4 | 14 | 13 | [38] |
| In-ReOx/SiO2 | Water | 50 | NA[a] | 100 | 97 | [39] |
| Pd-Cu/MgO | Water | 100 | 1.3 | 100 | 99 | [40] |
| Cu-Co/SBA-15 | Isopropanol | 170 | 4 | 99 | 80 | [41] |
| NiFeB/SiO2 | Isopropanol | 100 | 4 | 100 | 100 | [42] |

| | | | | | | |
|---|---|---|---|---|---|---|
| CuAlFe oxide/Ca(OH)$_2$ | None | 160 | 0.3 | 99 | 98 | [43] |
| CuCr mixed oxide | n-Octane | 200 | 4 | 95 | 78 | [44] |
| CuFe mixed oxide | n-Octane | 200 | 4 | 87 | 84 | [45] |
| CuMgAl mixed oxide | Isopropanol | 110 | 1 | 63 | 63 | [46] |
| CuZnCrZr mixed oxide | Isopropanol | 170 | 3.5 | 100 | 96 | [47] |
| CuNiMgAl mixed oxdie | Ethanol | 200 | 2 | 93 | 83 | [48] |

a) NA = not available

An alternative approach for liquid phase hydrogenation of FUR is one-step hydrogenation–esterification of FUR to form furfuryl esters was reported by A.Corma *et.al*. The produce furfuryl esters can be used as fuel agents for partly blending with petrol diesel due to its high energy density.[49] The hydrogenation–esterification of furfural based compounds to furfuryl esters was proposed to be an alternative route to upgrading furan based compounds. Similarly Zheng *et al*. investigated the hydrogenation–esterification reaction of FUR with acetic acid to form furfuryl acetate in the liquid phase under 20 MPa H$_2$ at 150 °C. In these studies, several supported Pd, Pt, Cu, and Ni catalysts was tested.[50, 51] Unfortunately, the best yield of furfuryl acetate is obtained is 13% suing 5 wt% Pd supported on Al$_2$(SiO$_3$)$_3$ and Al-SBA-12 as catalyst, it still too low for real industrial applications and FAL was the major product (yield around 43%) where MFU was a minor by-product. The authors also pointed that acid sites near the hydrogenation active centers are the key fact to promote the esterification, but there are still serious drawback that must be resolved in further studies, such as the polymerization of furfuryl alcohols to form heavy compounds which is also driven by acid sites. Meanwhile in these studies there are no recycle tests to assess the reusability of the catalysts.

Using supercritical CO$_2$ has been demonstrated to be an alternative technique for process the hydrogenation of furfural into different furanic compounds. Some attempts were reported by M.Poliakoff *et.al*, in which the product selectivity can be controllable. It involved in the hydrogenation of furfural to form furfuryl alcohol, tetrahydrogen furan, methyl furan, 2-methyltetrahydrofuran and furan, all these products can be tuned by using two catalytic beds

with copper chromite and Pd/C in sequence under respective temperatures.[52] Thus, the best furfuryl alcohol yield was 98% by using only the first copper chromite reactor under conditions of 120 °C, 15 MPa $H_2$, 1 mL min$^{-1}$ $CO_2$, and 0.05 mL.min$^{-1}$ furfural.

### 1.1.4 Electrocatalytic Reduction of Furfural

Another interesting approach for the synthesis of FAL is the aqueous electro-catalytic hydrogenation of FUR using a sacrificial Ni or Ni/Fe alloy anode.[53] The generation of atomic hydrogen is performed in situ through the reduction of hydronium ions on the cathode surface using external electrons. A FAL yield of 63%, with a yield of MFU lower than 5%, were obtained by modulating the current density and the nature of both the electrolyte solution and electrodes. Similarly, Huber et al. employed a continuous-flow electro-catalytic membrane reactor for the reduction of an aqueous solution of FUR.[54] Different catalysts have been tested as the cathode materials, but the best results were accomplished by using Pd/C cathode, with a selectivity of FAL range from 54% to 100% at 130°C–150°C.[55] Moreover, furfuryl alcohol (FAL), tetrahydrofurfuryl alcohol (THFA), Methyl furan (MFU), and 2-methyl tetrahydrofuran (MTHF) were also detected, and the product selectivity varied as a function of the applied voltage. The current efficiency reached 24–30%; the unaccounted for current was utilized in the production of $H_2$ rather than FUR hydrogenation.

## 1.2 General Strategies of Hydrogen Transfer Reduction

To facilitate discussion about the effect of catalysts, hydrogen donors, on catalytic transfer reduction (CTH) on product distributions in the following sections, we will first introduce several common mechanisms of CTH process. There are two main mechanisms for heterogeneous CTH reaction[56] depending on the type of metal used: the direct hydrogen transfer and the hydride route. In general, direct hydrogen transfer is proposed for main group elements, whereas the hydride route is considered to be the major pathway for transition metals. As regard to Meerwein–Ponndorf–Verley (MPV) reduction, Lewis acid site were believed to be the active sites for MPV reaction but only in Sn, Zr beta zeolite.[57] Pure gas phase hydrogen transfer reduction over MgO was believe to occur via $Mg^{2+}$ $O^{2-}$ pair formed six member ring[58].

### 1.2.1 Direct hydrogen transfer

In direct hydrogen transfer, the hydrogen is transferred directly from the donor to the acceptor without any involvement of metal hydrides. The mechanism is thought to proceed through a cyclic six-membered transition state. (**Figure 1.4**)[59] This mechanism was originally proposed for the Meerwein-Ponndorf-Verley reduction, typically, the complex Al(Oi-Pr)$_3$ was used as catalyst. The aluminium-catalyzed hydride shift from the a-carbon of an alcohol component to the carbonyl carbon of a second component, which proceeds via a six-membered transition state, is referred to as the Meerwein-Ponndorf-Verley reduction (MPV) or the Oppenauer Oxidation, depending on which component is the desired product. If the alcohol is the desired product, the reaction is viewed as the Meerwein-Ponndorf-Verley reduction. One of the main advantages in the use of MPV reaction for the reduction of carbonyl compounds, is its high selectivity for C=O double bond.
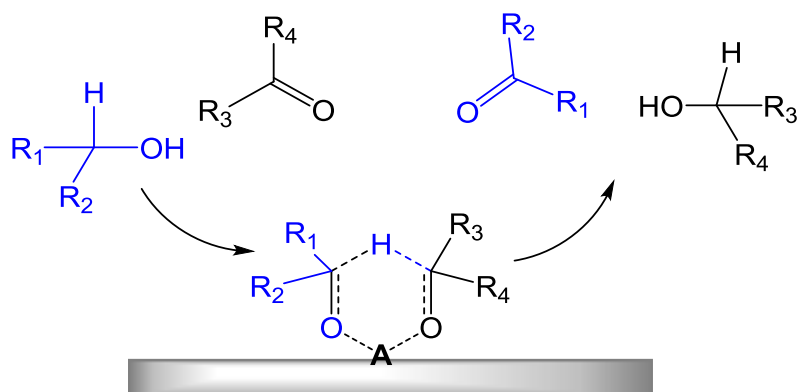


**Figure 1.4** Direct hydrogen transfer processes via six members ring intermediate via metal sites, A=Lewis acid

## 1.2.2 Hydride Route

The hydride route proceeds in a stepwise manner through surface hydride formation. Typically, the metal or Lewis base catalyst removes one hydrogen from the donor such as methanol, both through hydride elimination and deprotonation over alcohol OH group. (**Figure1.5**) The hydrogen is then transferred over the surface to the acceptor, *e.g.* ketone. Most of noble metal catalysts usually operate via this kind of mechanism. The surface dehydrogenation was supposed to the rate limited step. When surface was saturated with hydride, the reaction will be speed up.
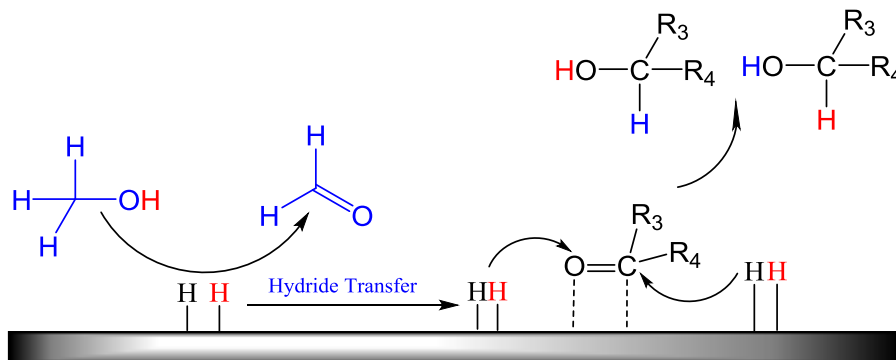
**Figure 1.5** Hydrogen transfer via metal hydride route.

## 1.3 Catalytic Hydrogen Transfer in Biomass Transformation

The current interests are mainly focused on the utilization of biomass as an alternative source for the production of fuels and chemicals. In order to upgrade biomass feedstock, it is necessary to set up an oxygen removal step, due to the high oxygen content which is typical for these compounds. In this section, we summarize the various catalytic systems and the latest research progress for the selective hydrogenation of biomass derived platform molecules using H-transfer reaction with different hydrogen donors. A list of most frequent employing heterogeneous catalytic system for hydrogen transfer processes in biomass transformation is reported in **Table 1.3**, in which hydrogen donor, biomass relevant substrate and catalysts were specified.

**Table 1.3** Heterogeneous catalyst used in H-transfer hydrogenation processes of biomass derived oxygenated compounds

| Substrate | Catalyst | H-donor | Ref. |
|-----------|----------|---------|------|
| **levulinic acid and levulinate(EL)** | ZrO2 | 2-propanol/isobutanol | [60] |
| | ZrO2 | Supercritical ethanol | [61] |
| | Zr(OH)x | Supercritical ethanol, 2-propanol | [62] |
| | Zr-Beta | Secondary alcohols | [63, 64] |
| | Zr-HBA | 2-propanol | [65] |
| | Ni Raney | 2-propanol | [66] |

| | | | |
|---|---|---|---|
| | Ru(OH)$_x$/TiO$_2$ | 2-propanol | [67] |
| | Supported Au | Formic acid or butyl formate | [68, 69], |
| **HMF** | Pd/C and H$_2$SO$_4$ | Formic acid | [70] |
| | Pd/C | Formic acid | [71] |
| | Pd/C Ru/C over ionic liquid | Formic acid | [72] |
| | Pd/ZrPO$_4$ | Formic acid | [73] |
| | Cu-PMO | Supercritical methanol | [74] |
| | MgO | Methanol | [75] |
| | Ru/C | 2-propanol | [74, 76] |
| | Pd/C, Rh/C with ZrCl$_2$ | Methanol | [77] |
| | Pd/Fe$_2$O$_3$ | 2-propanol | [78] |
| | Ru/hydrotalcites | 2-propanol | [79] |
| **Furfural** | MgO | Methanol | [75] |
| | Pd/Fe$_2$O$_3$ | 2-propanol | [78] |
| | Cu/Mg/Al/O | Ethanol, propanol and 2-propanol | [80] |
| | Ru/RuO$_2$/C | Primary and secondary alcohols | [81] |
| | Ru/Carbon | 2-propanol | [82] |
| | Al/Mg hydrotalcites doped with La, Cu, Cr, Mn, Zr | Supercritical methanol | [83] |
| **Lignin** | Ni Raney | 2-propanol | [84, 85] |

| | | | |
|---|---|---|---|
| **Vanillin** | Pd supported catalyst | Formic acid | [86] |
| **Sorbitol/Mannitol** | Ru/C | 2-propanol | [87] |
| **Sugars** | Cu/Ni/Al oxide | ethanol | [88] |
| **Glycerol** | Iron oxide and iron phosphate | $C_3$ alcohols | [89] |
| | FeOx-ZrO$_2$ | Formic acid | [90, 91] |
| | Pd supported catalysts | 2-propanol | [92] |

.

Obviously, from **Table 3.1**, the main work was focused on (hydroxymethyl furfural) HMF, levulinic acid (LA) and furfural (FU) reduction. One of the key challenges for upgrading furans based compounds is product selectivity; a mixture of side chain ring-hydrogenated and ring-opened products is often formed.

Catalytic hydrogen transfer reduction via the Meerwein–Ponndorf–Verley (MPV) reaction between FUR and secondary alcohols has produced remarkable results. Indeed, selective conversion of FUR to FAL only has recently been reported with a Cu-based catalyst obtained by reducing a spinel-like Cu/Al/Mg mixed oxide and using isopropanol as the hydrogen donor,[80] but there is absence of catalyst recycling studies to evaluate catalytic stability. Similarly, around 95% FAL yield was obtained with a bimetallic Ni-Cu/Al$_2$O$_3$ catalyst where the same hydrogen donor was used and reaction conditionals were at 200 °C under 4.5 MPa N$_2$.[93]

It must be mentioned that catalytic transfer hydrogenation in the gas phase has also been attempted. This reaction is based on the MPV reduction principle: selective reduce carbonyl group.[94, 95] Moreover, this CHT process minimizes the formation of by-products (MF, THFA, and furan) that are frequently generated in the conventional gas-phase H$_2$ reaction. The alcohol can be chosen to produce an aldehyde or a ketone with industrial applicability. Thus an 85% FAL yield was obtained by gas-phase MPV reduction of FUR coupled with oxidation of cyclohexanol to cyclohexanone with Cu–MgO–Cr$_2$O$_3$.[96, 97] Cyclohexanone is used as an intermediate in the production of nylon-6 and nylon-6,6. Unfortunately no information regarding

the deactivation was provided, which is a key consideration for correct assessment of the technical viability of this process.

Beside reduction of aldehyde groups, some attempts were made to reduce and open the furan ring in order to produce linear diols such as 1,6-hexanediol which is extensively used in the production of polyesters for polyurethane elastomers, coatings adhesives and polymeric plasticizers. Ebitani and co-workers[73] reported the direct synthesis of 1,6-hexanediol from HMF over $Pd/ZrPO_4$ using formic acid as H-donor. Their results indicated that the surface acidity, due the Brönsted acid sites, is responsible for furan ring opening (C-O bond cleavage), while palladium catalyzes C=O hydrogenation. One more case should be mentioned here, sugar reduction, including fructose, mannose, arabinose and xylose to their corresponded polyols was performed by J.Pérez-Ramírez *et.al*. in which, ethanol was used as hydrogen donor.[88]

### 1.3.1 Alcohols as Hydrogen Donor

Alcohols are widely used hydrogen donors for metal-catalyzed catalytic transfer (CTH) reduction (**Table 1.3**), with many parallels with acid–base chemistry discussed in previous **section 1.2**. Secondary alcohols generally show higher activity than primary alcohols in dehydrogenation over metal surfaces, facilitating hydrogen transfer to object substrate. This can be readily attributed to the enhanced stabilizing effect of two, rather than one, alkyl groups via inductive electron donation to the α-C of the alcohol in the dehydrogenation process.[66, 78, 81, 98] In particular, Vlachos and co-workers studied the effect of the structure of alcohols on the conversion of furfural to 2-methylfuran (2-MF) over Ru/C.[81] It pointed that the secondary alcohols was active than primary alcohols, this work shows that a longer alkyl chain in the alcohol is beneficial for CTH activity, which holds for both primary and secondary alcohols. However, this effect diminishes when the side chain contains more than two carbon atoms: i.e., the CTH activity of alcohols increases in the sequence ethanol < 1-propanol ≈ 1-butanol < 2-propanol < 2-butanol ≈ 2-pentanol. The reduced enhancement effect for longer side chains could be attributed to the diminished added stabilizing effect, site blocking caused by the larger footprint of the adsorbed alcohol, or a combination of the two. Interestingly, methanol has been employed as a hydrogen donor in the hydrogenolysis of glycerol.[99] When methanol dehydrogenates into formaldehyde and $H_2$, the formaldehyde can react with water to form formic

acid. The decomposition of formic acid to $CO_2$ and H is more energetically favorable than methanol dehydrogenation; thus, $CO_2$ was the only product aside from hydrogen when methanol was used as the hydrogen donor on Ni–Cu/$Al_2O_3$ at 220 °C. Thus, two molecules of hydrogen are produced for each methanol molecule, twice as much as that from 2-propanol. Comparable glycerol conversions and product distributions were observed with 2-propanol and methanol as the hydrogen donors.[99] Moreover, supercritical methanol has been demonstrated as an effective environment for conversion of HMF to DMF.[74] it indicated that the influence from solvent should also be considered as important fact.

The use of isopropyl alcohol, as hydrogen donor as well as reaction medium, was alternatively studied by Vlachos and coworkers[76] for HMF reduction. When the reaction was conducted over the Ru/C based catalyst, 100% conversion of HMF and a 81% of yield in DMF were achieved at 190°C after 6 h. Unfortunately, when the recovered Ru/C was reused in the second cycle, HMF conversion and DMF yield were significantly decreased to 47% and 13% respectively,, showing a considerable deactivation of Ru/C even after its first use, which might be due to the formation of high molecular weight by-products on ruthenium surfaces. More recently, Pd and Rh supported onto carbon were used for HMF hydrogenation in the presence of MeOH at 150°C and 20 bar of $H_2$ pressures.[77] $ZrCl_2$ was used as co-catalyst because it was supposed to improve DMF selectivity due to the presence of a strong synergistic effect between Pd and Zr; the addition of Zr salt to the reaction mixture has also been function when Ru/C was used as catalyst. DMF yield reached to 39%, HMF conversion was around 75%, after 2 hours reaction. However, in the presence of methanol HMF etherification occurred, forming 5-methoxymethylfurfural; this reaction was catalyzed by Lewis acid sites which were belonged to the used catalyst. On the contrary, the use of THF as solvent led to 85% yield of DMF after 8h reaction with fully conversion of HMF, it revealed the inability of these catalytic systems for high selective transform HMF into DMF when it was absence of alcohol.

Another Pd based catalys was reported by Hermans and coworkers[78] in which Pd was supported on $Fe_2O_3$ and 2-proponal was used as hydrogen donor. The yield of DMF reached to 72% when a continuous-flow reactor was employed, reacted at 180 °C. Compared with HMF, furfural presence similar structure but limited functional group, so it was easily selective reduction of carbonyl group *via* H-transfer. In fact, in the same paper, it also investigate hydrogen transfer reduction over $Fe_2O_3$-supported Cu, Ni and Pd catalysts, and all the catalytic

systems can process the sequential transfer hydrogenation/hydrogenolysis of furfural to 2-methylfuran. An optimal yield of 57% of furfuryl alcohol and the formation of 10% of MFU were observed in a batch reactor at 180°C after 7.5 hours of reaction with $Pd/Fe_2O_3$. The remarkable activity of $Pd/Fe_2O_3$ in both transfer hydrogenation and hydrogenolysis is attributed to a strong interaction between metal and support and it indicated that the noble metal catalyst, behavior in catalytic transfer reduce is similar like act as dehydrogenation catalysts. Recently, Chilukuri and co-workers reported a Ru-containing hydrotalcites catalyst for HMF conversion to DMF in 2-propanol.[79] It pointed that 2-propanol was play as solvent and H-donor. Unfortunately, acetone was formed as byproduct and it has to be separated from the final mixture, increasing the cost of the whole process.

Further, other alcohols can also be used as H-donor in HMF reduction. A new approach was reported by Riisager *et al.*[74] process the selective hydrogenation of HMF via hydrogen transfer, in which supercritical methanol was used both as a hydrogen donor and as reaction medium in the presence of a Cu-doped porous metal oxide. The author emphasized that the production cost can be reduced and the operation security can be improved to a certain extent when methanol is used as a hydrogen donor instead of $H_2$. However, in the reaction process, the critical temperature of methanol is very high (as high as 300°C) and the selectivity of DMF is very low. Indeed, only 34% DMF yield can be obtained with 100% HMF conversion at 300°C after 0.75 hour of reaction.

Using methanol as hydrogen resource was also investigated by Cavani and coworkers.[75] In their work, HMF can be selectively reduced into BHMF (99% yield) over bulk MgO without additional solvent, under mild condition (160°C). In the same reaction conditions, furfuryl alcohol yield was reached to 97%. It revealed that bulk MgO was to be an excellent catalyst due to the capacity of methanol activation at low temperature, which is was believed to be the speed control step.

From above review, it concluded that, most of alcohol could be easily adopted as hydrogen donor in furan based compounds upgrading, and most of reaction was focus on selective carbonyl group reduction to corresponded alcohol. Acting as hydrogen resource, alcohol could be easy handling and scale up.

### 1.3.2 Formic Acid and Formate as Hydrogen Donors

Formic acid (FA) could be sustainable synthesized from biomass compounds. it can be formed renewably from lignocellulosic biomass such as rehydration of HMF to levulnic acid and formic acid[100] or from electrochemical reduction of $CO_2$,[101] which makes FA an environmentally friendly source for both high-purity hydrogen production[102-104] and a hydrogen donor for CTH reactions. Two surface species have been proposed to directly participate in hydrogen transfer (**Figure 1.6**): (A) surface hydrogen (hydride) and (B) adsorbed formate species. Adsorbed atomic hydrogen formed via stepwise hydrogen transfer from FA to the metal surface[105] appears to be a natural choice; however, it fails to explain some results obtained from isotopic labeling studies on Pd/C,[106, 107] one of the most widely used CTH catalysts with FA. Formate with larger metal cations showed higher activity for the hydrogenolysis of benzyl acetate, which was attributed to the ease of separating the ions due to the longer initial distance of the charge centers.[108] However, FA exhibits higher activity than formate salts in the CTH of α-methylbenzyl alcohol on Pd/C, which could be attributed to the role the proton plays in the dehydration step. It seems that formate species is more easy to process hydrogenenolysis of alcohol.[109] With plenty of methanol feeding the surface surfer mass formate species which also believed to be the active hydrogen donor in MgO based system. Further the fact that the additions of bases will accelerate the formate hydrogen transfer. Three distinct roles of formic acid in this process were identified: (1) hydrogen donor, (2) acid catalyst, and (3) deoxygenation agent for furfuryl alcohol.
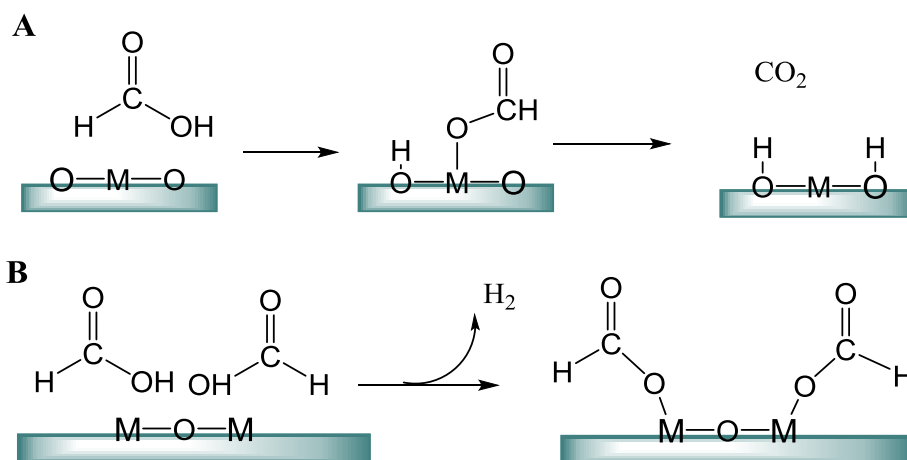


**Figure 1.6** Possible Surface Adsorbed Hydrogen Donor in catalytic transfer reaction with formic acid: (a) Adsorbed Hydrogen Atom; (b) Adsorbed Formate M=metal

In 2010, Rauchfuss and co-workers invented a novel catalytic system, in which formic acid (FA) was first used as a hydrogen donor for the selective hydrogenation of HMF.[70] When the reaction was carried out in THF over the Pd/C catalyst, more than 95% DMF yield with 100% HMF conversion was observed at 70°C after 15 h. Furthermore, a one-pot process for synthesis of DMF from fructose was also investigated. In the presence of FA, $H_2SO_4$, Pd/C and THF, fructose was initially dehydrated at 150°C for 2 h, and the generated HMF was subsequently hydrogenated at 70°C for 15 h, obtaining 51% DMF yield. It is worth noting that using FA as catalyst it is possible to perform three different reactions, thanks to its peculiar characteristics: it is an acid catalyst for the dehydration of fructose into HMF and a reagent for the deoxygenation of furfuryl alcohol as well as a hydrogen donor for the hydrogenation of HMF into DHMF. The use of formic acid for hydrogenation is very attractive from industrial view, because formic acid also could be produced from derived from biomass such as the HMF hydration, equivalent formic acid is produced company with levulinic acid (LA) and formic acid also can be regenerated by hydrogenation of formed $CO_2$. In 2012, a similar catalytic system using formic acid as hydrogen resource was reported by De *et.al*.[72] In this study, microwave was chosen as the heating system. Details investigate indicated that the conversion of fructose into DMF via HMF intermediate was catalyzed by formic acid due to the acidity. The author also concluded that the first step, dehydration of fructose to produce HMF was also benefit the coexistence of formic acid (FA) and ionic liquid $[DMA]^+[CH_3SO_3]^-$ (DMA=*N,N*-dimethylacetamide). In the following steps, HMF was transformed into DMF by sequential hydrogenation and hydrogenolysis in which FA act as H-donor and when Ru/C was used as catalyst, the maximum yield of DMF was reached (32% yield from fructose and 27% yield from agar respectively). After all, using FA will increase environmental hazards pollutions risk so it limit its large scale-up using. Meanwhile, a series of special corrosion-resistant equipment are needed, and then the corresponding costs will be increased, which restrain a wide range of external application.

## 1.4 Methanol Transformations as Hydrogen Donor

Methanol was synthesis mainly from syngas, but recently, part of syngas could be produced from biomass feedstocks, so in some view, methanol could be sustainably synthesized. Meanwhile as hydrogen resource, after reaction only light compound such as CO, $CO_2$, $H_2$ and $CH_4$ which is easy to eliminate from reactor, so purification of product could be easy handle. In

order to high utilization of methanol transformation as hydrogen donor inhibited byproduct producing. Some researches were carried out to investigate the intermediate via methanol reaction without oxygen.[110-113] Possible species of methanol transformation was lined in the order: Methanol ---- methoxy---- formaldehyde---- formic acid, formate or methyl formate---- carbonate (bicarbonate). **Figure 1.7**

$$CH_3OH \longrightarrow H_2CO \longrightarrow HCOOH \begin{array}{c} \nearrow HCOO^- \quad \text{Formate} \\ \searrow HCOOCH_3 \quad \text{Methylformate} \end{array}$$
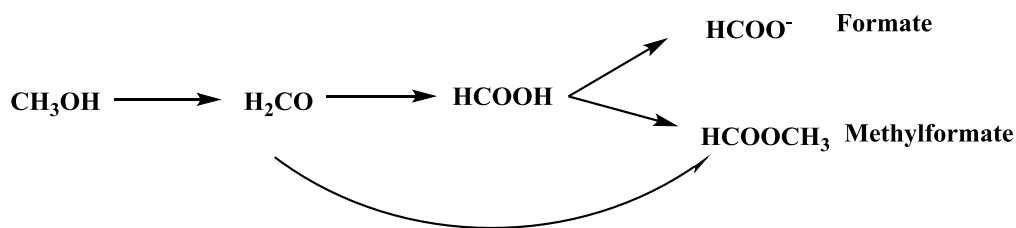
**Figure 1.7** Possible species of methanol transformation over MgO surface in gas phase reaction

All the processes would benefit from exact understanding of the reaction mechanism. We explored methanol dehydrogenation over basicity sites as possible alternatives to activate methanol. We examined trends in methanol dehydrogenation. It is well established that MgO catalyzes the dehydrogenation of methanol. High temperature could form $CH_4$ Alternatively, adsorbed methoxy and formate species may yield methylformate (Tishchenko reaction) which is easy to decompose at high temperatures to methane and $CO_2$. Therefore, the data indicate the initial formation of formates followed by the slower formation of carbonates. Methanol has been used as a hydrogen source in directly methanol fuel cells. Formic acid can be reformed to release hydrogen and formic acid can decompose on metal surfaces through either dehydrogenation to produce $CO_2$ and $H_2$ or dehydration to produce CO and $H_2O$. Formic acid and formaldehyde as hydrogen donor.[114] The Ru based catalyst could be used in activation methanol transfer, the product $HCOOCH_3$ was observed as the product of methanol oxidation[115]. During the reaction, Ru as hydride accepter whiles the methanol was activated. If the product of methanol is stable the equilibration will not shift to the furfural reduction steps. In high temperature it is believe that formic aldehyde was the active species from methanol[116] it demonstrate methylation was happen via formic aldehyde $CH_2O$. According to the literature, the activation of methanol could include methanol dehydrogenation and high temperature disproportionation. While methanol activation, methanol may generate a wide range of products, such as formaldehyde ($CH_2O$), dimethyl ether ($CH_3$-O-$H_3C$), methyl formate ($HCOCH_3$),

dimethoxymethane (CH₃OCH₂OCH₃), formic acid(HCOOH). It was believed that formaldehyde competes with formate at low temperature. Thus the activation species such as formaldehyde, formate, and methyl formate could not be exclusive when methanol was treated as hydrogen resource at high temperature.

## 1.5 Furfural Hydrodeoxygnation Investigations

### 1.5.1 Furfural and Furfuryl Alcohol Activation

In the gas phase, The report from R.F.Lobo *et al*.[57] and A.Corma *et al*.[117] indicate that tetravalent metals (Ti, Sn, Zr) substitution of Beta zeolite could run furfural reduction via similar Meerwein Ponndorf Verley Oppenauer (MPV) mechanism, thus there are no furfuryl alcohol hydrogenolysis product formed. Similarly, when supported transition metal Cu/ZnO catalytic system was employed for furfural reduction,[118] only furfuryl alcohol was produced. There are few research work in which furfural or furfuryl alcohol hydrodeoxygnation could process. In liquid phase reaction, the report from G.Vlachos *et al.* specified that surface formed RuOx cluster was believed to be the active site for furfural hydrodeoxygnation, the high selectivity methyl furan is from beneficial effects of Lewis acid derived from RuOx.[81, 119] Further, the combination strategy was verified to emphasis the synergy effects between Ru/C and homogeneous metal chloride.[120] DFT calculations suggest that methyl furan formation involves directly hydrogenation of furfural via η² (C=O) binding model to process deoxygenated and hydrogenation to methyl furan and the route involved two steps: adsorbed furfuryl alcohol dehydration and subsequent hydrogenation to methyl furan. There are few reports could process furfural furfuryl alcohol hydrodeoxygnation so based the above literature review, the furfural and furfuryl alcohol activation should also be considering an important role towards product distribution, specifically in methyl furan selectivity.

The first report of furfural reduction to product of methyl furfuran was usd Fe-Pt dual metal supported catalyst in which 5% iron was doped into the catalyst. Similarly, according to T.Rajia *et al.* Fe metallic nanoparticle was employed as the catalyst and the promotion of Fe for methyl furan selectivity was investigated. They pointed that presence of oxygen vacancies in the Fe oxide system promoted furfural activation.[121] B.M.Nagaraja *et al*. reported a superior activity of Cu/MgO and Cu–MgO–Cr₂O₃ catalysts in FAL hydrogenation.[19, 122] The incorporation of

inexpensive Fe on Cu-based heterogeneous catalysts for various catalytic transformations has been studied in many reports. Among these catalytic systems, most of them were just produce furfuryl alcohol and reports mainly focus on the basic hydrotalcite mixed metal oxide. Such as double hydroxides.[123] Meanwhile noble metal catalysts was reported as catalyst[124] here Cu was recongniated to the base metal and molybdenum carbide was also used as catalyst for furfuran reduction in gas phase.[125] Comparably, carbonyl was adsorbed over Cu surface e was reported by J.A.Dumesic *et al*.[126] in which surface metal was supposed to participate furan ring activation. DFT calculation reveal the furfural adsorption geometric state[127] was alternative factor could influence furfural reduction kinetic. Further research was focus on furan ring activation over Rd(111) face.[128] Since the active sites of Cu-based catalysts in the vapor phase involve $Cu^0$ or $Cu^+$ species remains controversial,[15, 16, 21] but from the view of reaction kinetics, it had been shown that the Langmuir–Hinshelwood model fits the reaction rate data.[14, 18]

Beside comparison of experiments, Density functional theory (DFT) calculations, and infrared (IR) spectroscopic techniques, were employed here to investigate furfural hydrogenolyis mechanism. It provided a model for surface intermediates adsorption behaviors as well as plausible reaction pathways. Two different routes have been proposed for furfural activation: first category was Cu-based catalysts[18] and others are for group VIII metals[22, 129-131] In the first category, according to Resasco *et al*., the adsorption of FUR occurs preferentially *via* the lone pair of electrons from carbonyl group oxygen, it formed a surface $\eta^1(O)$-aldehyde binding mode in **Figure 1.7 A** [18] The FUR molecule lies straightly to the catalyst surface meanwhile the aromatic ring get net repulsion because the surface Cu atom overlap of the 3d band with the aromatic furan ring. Thus, the reaction can proceed either through an alkoxide (H addition to the C atom of the carbonyl group) or a hydroxyalkyl (H attack on the O atom of the carbonyl group) intermediate. In the second intermediate pathway was more plausible, due to its lower activation energy barrier. It could be explained from the stabilizing effect of the aromatic furan ring on the hydroxyalkyl intermediate.

A) Cu catalysts

H addition to C atom

Alkoxide species

$\eta^1$(O)-furfural

H addition to O atom

Hydroxyalkyl species

$H_2$

Furfuryl alcohol

B) Group VIII catalysts

H addition to O atom

2-Methyl furan

$+ H_2O$

$\eta^2$(C-O)-furfural

$\eta^1$(C)-acyl

Furan

$+ CO$

T

H addition to O atom

Hydroxyalkyl species
$\eta^2$(C-O)-furfural

$H_2$

Furfuryl alcohol

Indirect route
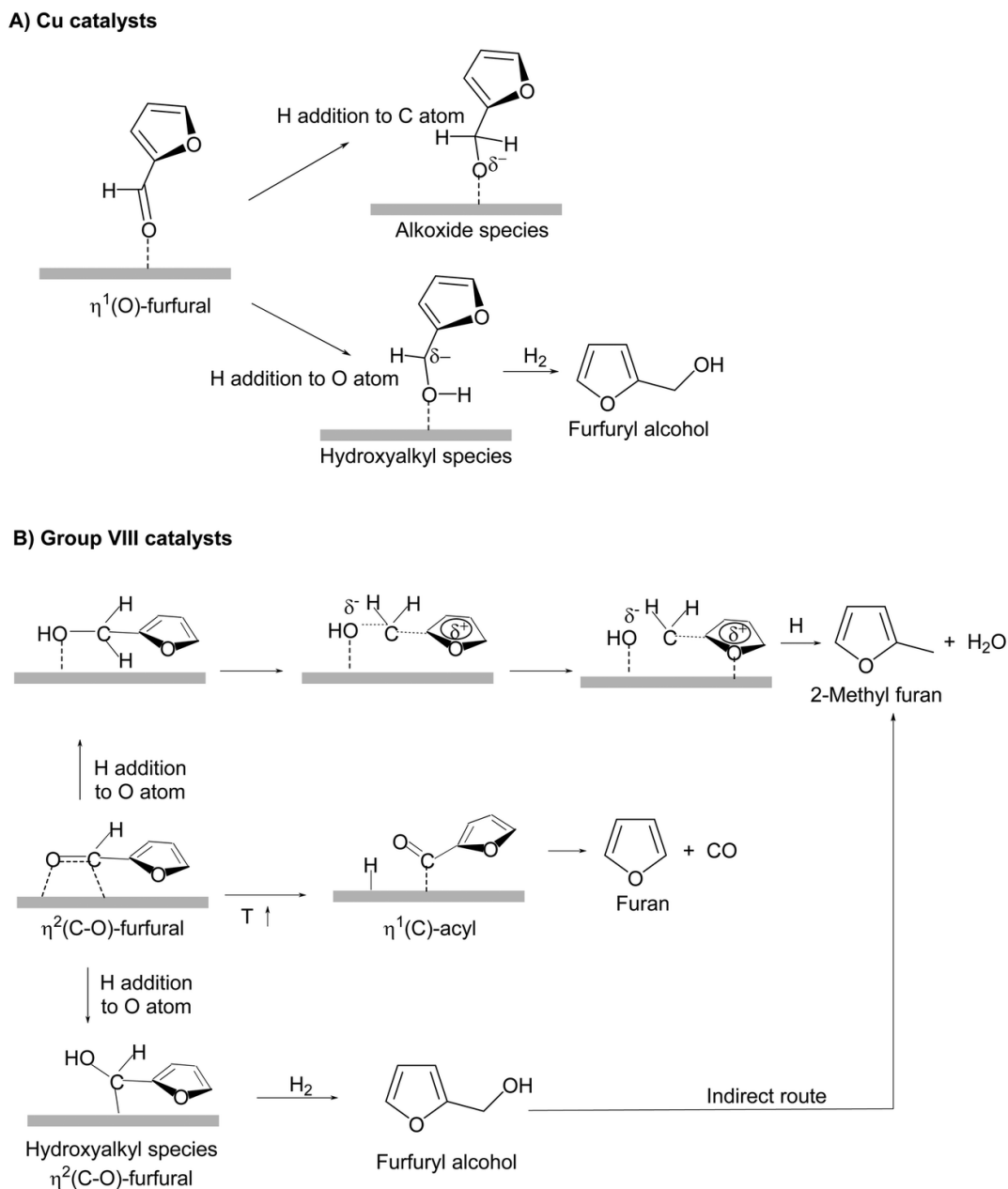
**Figure 1.7** Mechanism of furfural hydrogenation with Cu and Group VIII metals reposted from ref. [18, 22]

In contrast, for Group VIII B metals (Pd, Ni, or Pt), the interaction between the furan ring and the metal surface is presence thus a flat $\eta^2$(C=O) geometric mode is formed.[129-131] The preferred pathways toward FAL production also process through two steps: hydrogenation of the surface $\eta^2$(C=O) adsorbed carbonyl group, one hydrogen to attack O atom and then to generate a hydroxyalkyl intermediate, followed by hydrogenation of the carbon to generate adsorbed FAL. Since furfural decarbonylation was also inevitable. It indicated that the energetic barrier of the

hydroxyalkyl species intermediate transformation is smaller than that of transformation of FUR to furan via the formation of a $\eta^2$(C)-acyl intermediate and further process decarbonylation. Therefore, through decarbonylation towards furan generation is thermodynamically favor but hydrogenation to furfuryl alcohol is kinetically preferred, more FAL could be obtained via furfural $\eta^2$(C=O) geometric mode over iron metal. DFT calculations also indicated that MF formation involves a direct pathway involving the hydrogenation of adsorbed FUR to an alkoxy intermediate that is subsequently deoxygenated and hydrogenated to MFU and an indirect route from FAL involving dehydration of the adsorbed FAL and subsequent hydrogenation to MFU, both with higher energetic barriers than the FAL synthesis.[131] The author also pointed that at low $H_2$ pressure, where surface not fully coverage with hydride, the increase of H coverage can change the preference for reaction pathway. The relatively small differences could change in the activation energies.

Base on previous literature review, VIII elements, especially iron are suitable metal for furfural activation. It is evident that iron addition increased the methyl furan selectivity. The conversion of furfural in hydrogen over $SiO_2$ supported transition metal catalyst have been investigated at 1 bar and it is clear to show that furfuryl alcohol was the primary product when mono Ni was employed to be the catalyst, in contrast, when Fe was doping the Ni, the yield of methyl furan was greatly increased. The addition of Fe suppress the decarbonization and promoting the C=O hydrogenation at low temperature and the C-OH hydrogenolysis at high temperature. The authors reported that the difference between Fe interaction with furan ring in theoretical level.[132]. They indicated that there is a bond between furan ring and iron initially and the interaction was transfer from the delocalization region of furan ring to iron surface. The similar behavior was reported in Cu-Fe bimetal system, it found that Fe-containing Cu-based catalysts show much higher reactivity and very high selectivity towards 2-methylfuran. It reveals that partial reduce $Fe^{2+}$ was supposed to the promoter.[133] Similar report was summarized below Fe-Pt bimetallic supported catalyst surface furan adsorption desorption analysis[134]. Pd-Cu selective form furfuryl alcohol[129], Ni-Fe selective form methyl furan, [22] where Fe is especially efficient for furfuryl alcohol conversion into methyl furan. Iron oxide was predicted to have one of lowest selectivity. Such as the catalyst system $Pd/Fe_2O_3$ catalyst was reported to be high selective to furfural sequent reduce to methyl furan in which the metal support interaction is believed to the main effects it provide alternative strategy for C–O bond activation utilizes

reducible transition metal oxides. In the "reverse Mars–van Krevelen mechanism[135] bridge oxygen vacancy was supposed to be the active site which was confirmed by Vlachos and co-workers[136]. Furthermore VIII volume metal was believed to be good candidate for side chain C-O bond hydrogenolysis catalyst. It was also demonstrated by DFT calculation from researchers Michel and Gallezot, [137] in which it show that the strong interaction between Ru and water due to the redox capacity favor surface adsorbed water to act as hydrogen resources, and the consumption of hydrogen from water could recharged by molecular hydrogen. In this way, ruthenium is suitable to be a promise catalyst for the hydrogenation of carbonyl compounds, especially in aqueous system.

## 1.6 Aim of This Work

In the growing field of furfural hydrogen transfer reduction, there is a lack of fundamental knowledge of the reaction mechanism and the elementary steps, which are central information for the rational design of improved catalysts. In this thesis, several efficient approaches have been disclosed for mechanism investigation of furfural reduction and hydrogen transfer process. However, there is still a lack of understanding on the hydrogen transfer reduction of furfural in gas phase. Thus, this work is focused on the gas phase hydrogenation of furfural over iron and magnesium oxides. Numerous catalysts with different iron and magnesium molar ratios were prepared by co-precipitation or impregnation methods and were tested for the reduction of furfural using methanol as hydrogen donor. The way FeOx influences the product distribution and reaction pathway was discussed.

Infrared spectroscopy has proved to be a convenient tool for the identification of adsorbed species and the elucidation of reaction pathways on oxides surfaces. In order to investigate the methanol hydrogen transfer and how furfural is activated towards hydrogenolysis, in situ DRIFT and infra spectra were recorded. This understanding will help in the design of more competitive catalysts. Furthermore, focusing on the mechanistic interpretation, labeled methanol reactions were also carried out to reveal the reaction pathways.

# Chapter II Iron Based Catalytic System for Furfural Reduction

## 2.1 Introduction

The use of biomass, particularly utilization of lignocellulosic materials for fuels and chemicals production has been increased with the aim of reducing the exploitation of non-renewable resources. This renewable feedstock contains highly functionalised carbohydrates and the actual industrial challenge is to develop new processes for converting biomass into platform molecules and reducing their oxygen content.[138] Among these platforms, furan derivatives are considered to be important intermediates because of their rich chemistry. For this reason, many efforts have been made in the conversion of furfural (FU), which can be large scale produced from hemi-cellulose, into furan based compounds in the form of furfuryl alcohol (FAL) and 2-methylfuran (MFU)[78]. Here, MFU is an article of commerce compound (chemical intermediate) which is normally manufactured by catalytic hydrogenolysis of furfural alcohol or via a hydrogenation-hydrogenolysis sequence from furfural.[139] It had the real application to investigate the combustion properties of blend methyl furan with gasoline.[140, 141]

Many of hydrogenation process involve molecular hydrogen but one promising alternative can be H-transfer process, where borrowing hydrogen from an hydrogen donor(e.g. an alcohol) [142]. Avoiding the use of $H_2$ for substrate reduction, both the safety of the process and the selectivity could be increased. As a matter of fact, the lower hydrogenating capability of most hydrogen donors promotes a higher degree of control especially when partially hydrogenated molecules are needed;[143] one of the advantages of this process is that hydrodeoxygenation (HDO) catalysts are generally those that can selectively break the C−O bond leaving the nearby C=C and C−C bonds unchanged.

FAL can be obtained from selective hydrogenation of FU carbonyl group. MFU is often produced through the further hydrogenolysis of FAL[144-146] and has drawn the attention of researchers as gasoline alternative due to its very attractive combustion performance in engines.[147]

It is generally assumed that the mechanistic pathways of HDO processes with $H_2$ and organic hydrogen donors converge after adsorbed atomic hydrogen is formed. Catalytic transfer HDO of furfural has been investigated over heterogeneous catalysts using different hydrogen donor [80,

81, 83, 148]. Gas-phase reduction of FU into FAL has been carried out using methanol as hydrogen donor and MgO as heterogeneous basic catalyst; furfural was completely reduced into its corresponding alcohol through a Meerwein–Ponndorf–Verley (MPV) process.[75] More recently, Hermans *et al*. obtained 62% yield of 2-methylfuran over $Pd/Fe_2O_3$ using 2-propanol as H-donor.[78] Vlachos *et al*. indicated that surface RuOx species may also be involved in hydrogenation process and the mechanism was interpreted by a synergic effect between Lewis acid RuOx and metallic Ru cluster. In this work, the authors suggested that Lewis acid sites derived from RuOx play an important role in furfuryl alcohol activation; however, a deep understanding of the role of acid and basic sites in the reaction mechanism is currently lacking. [82, 119]

Recently, 90 % MF yield was observed through catalytic transfer hydrogenation (CTH) of furfural using methanol as hydrogen donor over iron-magnesium mixed oxide  catalyst (Fe/Mg/O)[149]; the introduction of $Fe^{3+}$ cation into the magnesia structure led to the formation of higher quantity of MFU, derived from FAL hydrogenolysis. Since iron is known to have both redox and acid-base properties,[150] it is worthy to study in detail the system with the aim of understanding which property can influence more products distribution. Therefore, in this chapter, catalysts with different iron content were prepared in order to study the role of acid-base and redox properties in MFU formation. Moreover, Fe/Mg catalysts with different synthetic procedure (co-precipitation and incipient wetness impregnation) were prepared to understand how products distribution is affected by the presence of different iron species. The synthesised materials were characterised with different techniques and redox, acid-base properties and crystalline phase of the samples have been compared.

## 2.2 Results and Discussion

### 2.2.1 Reaction Temperature Optimization

MgO has been found to be an excellent catalyst for reduction of furfural (FU) into furfurly alcohol (FAL) using methanol as H donor. At low temperature, in liquid phase, FAL was the only product detected, with high selectivity[75]. Similarly, in gas phase, over bulk MgO only FAL could be formed, in contrast, when iron was introduced into MgO system, product distribution was dramatically shift to methyl furan formation. **Figure 2.1** summarizes the

catalytic performance obtained over Mg-based catalysts and co-precipitated Fe/Mg/O mixed oxide catalyst under different reaction temperature. Comparing with bulk MgO, the co-precipitated Fe/Mg/O_1_2 mixed oxide showed higher selectivity (79%) to methyl furan (MFU) at 380 °C whereas MgO presented higher selectivity (95%) towards FAL at 250°C. For both catalysts, the carbon loss was increased when reaction was performed at very high temperature (500°C). At low temperature (250 °C), MgO exhibit maximum FAL formation, and the optimal temperature for methyl formation was 380 °C over Fe/Mg/O_1_2 catalyst.
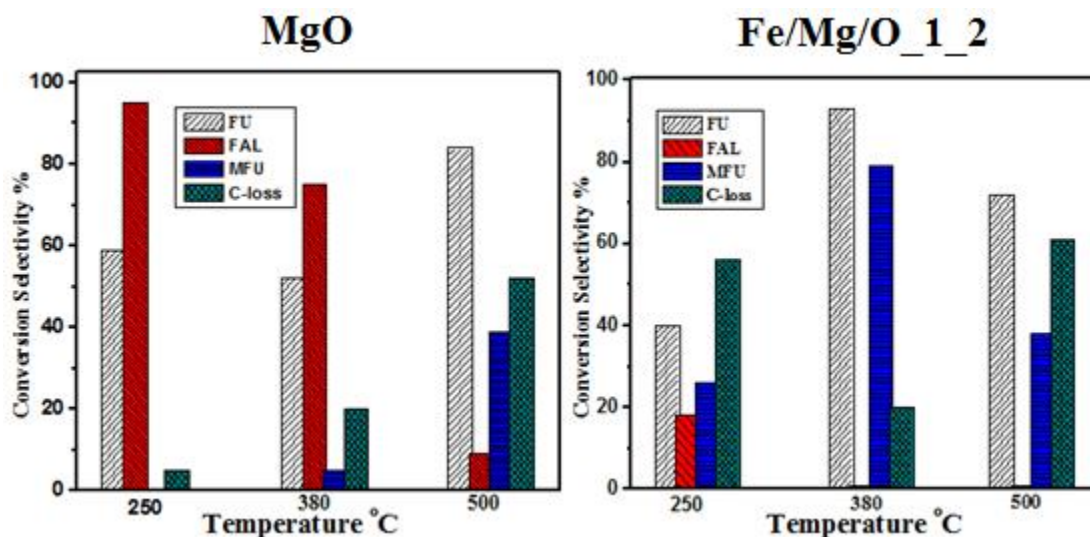


**Figure 2.1** effect of temperature on catalytic performance in gas phase furfural reduction. MgO (Left), Fe/Mg/O_1_2 (Right). Reaction conditions: 380°C atmosphere pressure. Methanol/furfural ratio: 10/1, space time 1.1

In conclusion, it reveals that iron oxide promoted methyl furan formation. The optimal reaction temperature was set up at 380 °C over Fe/Mg/O mixed oxide. High carbon loss was not prevented both in low temperature and high temperature. Iron oxide plays a direct role in the processes of furfuryl alcohol hydrodeoxygantion.

How does iron influence products distribution, it is still unclear. In this chapter, focusing on this question, various iron content MgO catalysts were synthesized including co-precipitation and witness impregnation strategy within different Fe/Mg ratio. Systematic comparison of catalytic performance and characterization of catalysts were carried out to the effect of iron addition on MgO properties and the influence of acid-base properties and redox capacity in MFU formation. Therefore, in order to compare, the reaction temperature was fixed at 380 °C.

## 2.2.2 Fe/Mg/O catalysts prepared by co-precipitation

Catalysts with different amount of Fe obtained by different synthetic procedures (Fe co-precipitation vs. Fe addition by incipient wetness impregnation) were prepared and compared. Several Fe/Mg/O catalysts containing different Fe/Mg ratios were prepared mixing Fe (III) and Mg (II) nitrates in aqueous solution and co-precipitating them by basification with NaOH. **Table 2.1** reports some results concerning morphology, structure and acid-base properties of the prepared Fe/Mg oxides, calcined at 450°C, compared with the analogous data for the pure oxides, MgO and $Fe_2O_3$. $Fe_2O_3$ is a base but it is not an alkaline. The data reported in **Table 2.1** indicated that the addition of Fe generally caused a decrease in surface area of mixed oxides. Pristine MgO was obtained with high surface area (172 $m^2$/g) while $Fe_2O_3$ shows the smallest value compared to all the prepared samples.

**Table 2.1** Physicochemical properties (specific surface area, crystalline phase, Lewis acidity, Brönsted acidity and basicity) of MgO, $Fe_2O_3$ and Fe/Mg/O co-precipitated samples

| Catalyst | Surface area ($m^2$/g) | Crystalline Phase (XRD) | Lewis acidity (mmol.g-1)* | Brönsted acidity (mmol.g-1)* | Basicity (mmol/g)** |
|---|---|---|---|---|---|
| MgO | 172 | Periclase MgO | 0 | | 7.51 |
| Fe/Mg/O_1_10 | 102 | MgO-like mixed oxide | 0 | -(a) | 2.62 |
| Fe/Mg/O_1_2 | 140 | MgO-like mixed oxide | 0.43 | -(a) | 2.34 |
| Fe/Mg/O_1_1 | 74 | MgO-like mixed oxide | 0.62 | -(a) | 1.09 |
| $Fe_2O_3$ | 51 | Hematite | - | - | 1.38 |

*Quantification of Lewis and Brönsted acid sites was obtained from Pyridine-FTIR analysis.
**Basicity measurements were performed by TPD analysis using $CO_2$ as probe molecule (a) Not detected by Pyridine-FTIR analysis.

Detailed XRD patterns of Fe/Mg/O samples are given in **Figure 2.2**. Iron oxide was present as hematite, while MgO shows the periclase structure. Fe/Mg/O_1_2 catalyst showed the broadening of the XRD peaks that can be related to the decrease of the crystallinity of the

precipitated periclase. This suggests that the crystal structure is slightly distorted, thus indicating the insertion of Fe in the MgO lattice. The results well agreed with those reported in the literature. In fact, the incorporation with trivalent $Fe^{3+}$ cation in the periclase lattice generates cationic defects and produces a low crystalline degree.[151-153]  No appreciable shifts for XRD lines were observed, because the ionic radius of $Fe^{3+}$ (0.69 Å) is very similar to the radius of $Mg^{2+}$ (0.65 Å); moreover, no evidences were found for the formation of segregated iron oxides. Sample Fe/Mg/O_1_1 containing a higher amount of Fe, was even more amorphous, thus indicating a higher quantity of Fe intercalated into the MgO structure. On the contrary, decreasing the iron content (Fe/Mg/O_1_10), an increase in the system crystallinity was observed.
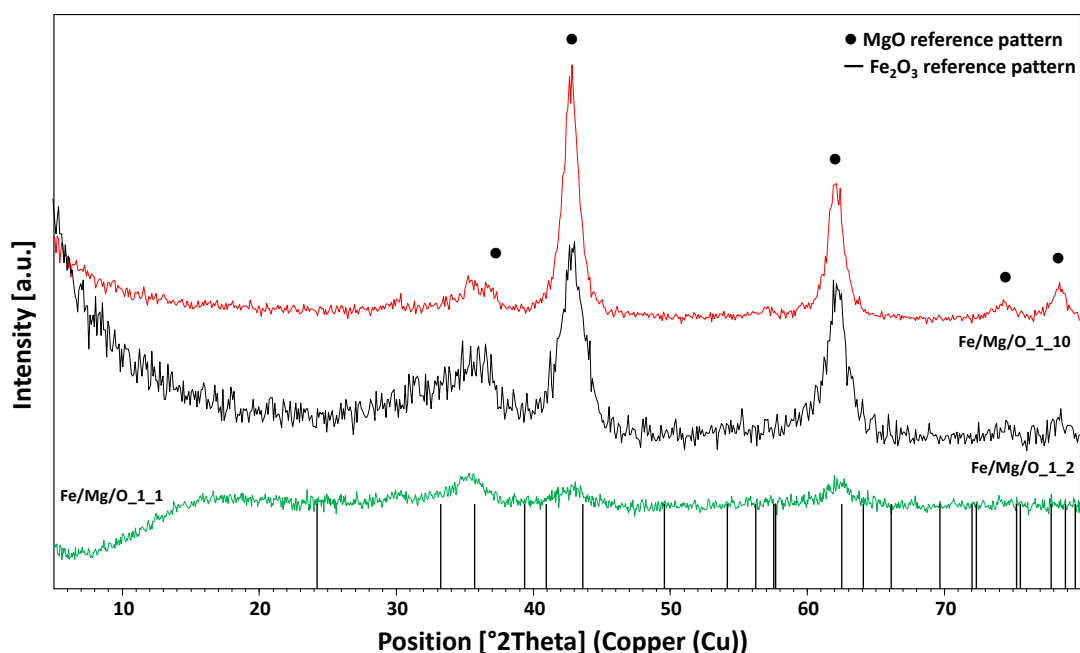


**Figure 2.2** XRD patterns of co-precipitated Fe/Mg/O catalysts. Legend: (-) Fe/Mg/O_1_10, (-) Fe/Mg/O_1_2, (-) Fe/Mg/O_1_1.

Addition of iron oxide led to introduce both acid and redox properties in the mixed oxide[150]. Therefore, the synthesised catalytic systems were further investigated through acidity and basicity measurements (pyridine adsorption and desorption FTIR, $NH_3$ and $CO_2$ -TPD) as well as $H_2$-TPR studies.

In order to study the different types of acid sites, the pyridine adsorption desorption FTIR (Py-FTIR) spectra were recorded. **Figure 2.3** (a) and (b) shows the IR spectra of adsorbed pyridine over Fe/Mg/O_1_1 and Fe/Mg/O_1_2 at different desorption temperatures. The acidity

distribution were summarized in **Table 2.2** The absence of band at 1540 cm$^{-1}$ which is the characteristic band of Brönsted acid and the presence of a band at 1444 cm$^{-1}$, corresponding to the adsorption of Pyridine at the Lewis acid sites (PyL), showed that only Lewis acid sites were present in Fe/Mg/O_1_2 and Fe/Mg/O_1_1, while Fe/Mg/O_1_10 was not characterised by neither Lewis nor Brönsted acidity. In order to evaluate the strengths of the Lewis acid sites, the spectrum was collected after evacuation at different temperatures. Analysis of the spectra at different temperatures allows to estimate the strength of the acidic sites[154]: the weak sites are defined as the ones from which pyridine is removed by evacuation at 200°C; the medium strength corresponds to evacuation between 200 and 400 °C and in the strong sites pyridine remain adsorbed after evacuation at 400 °C.
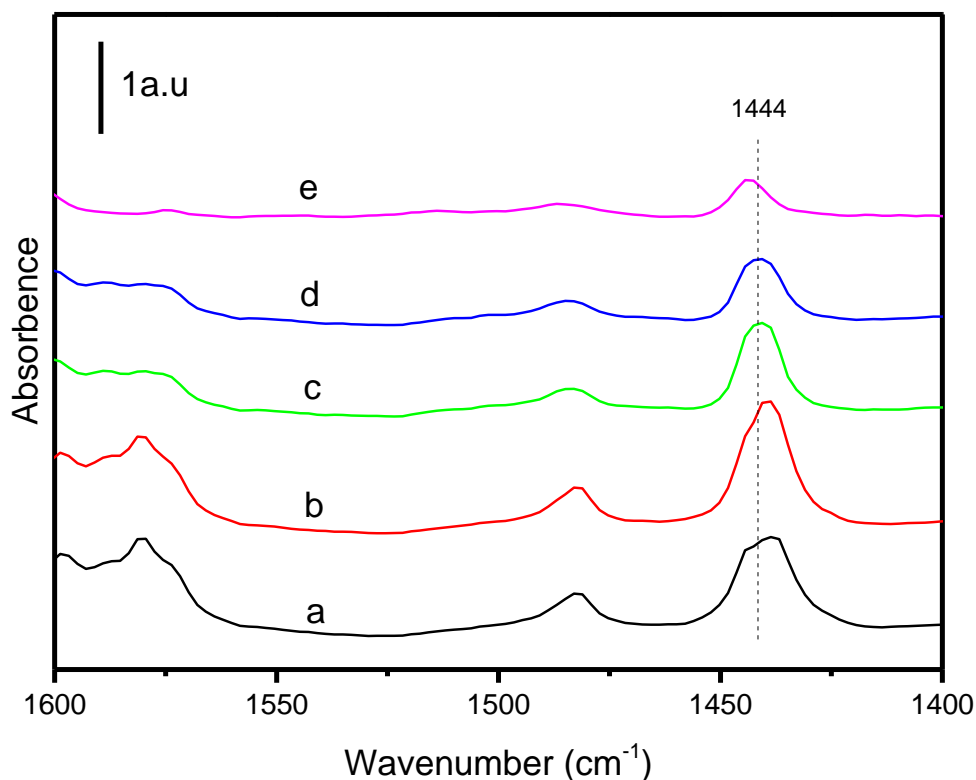


**Figure 2.3 (a)** Pyridine-FTIR spectra of Fe/Mg/O_1_1 obtained after evacuation at different temperatures. (a) room temperature (b) 100 °C; (c) 200 °C; (d) 300 °C and (e) 400 °C.
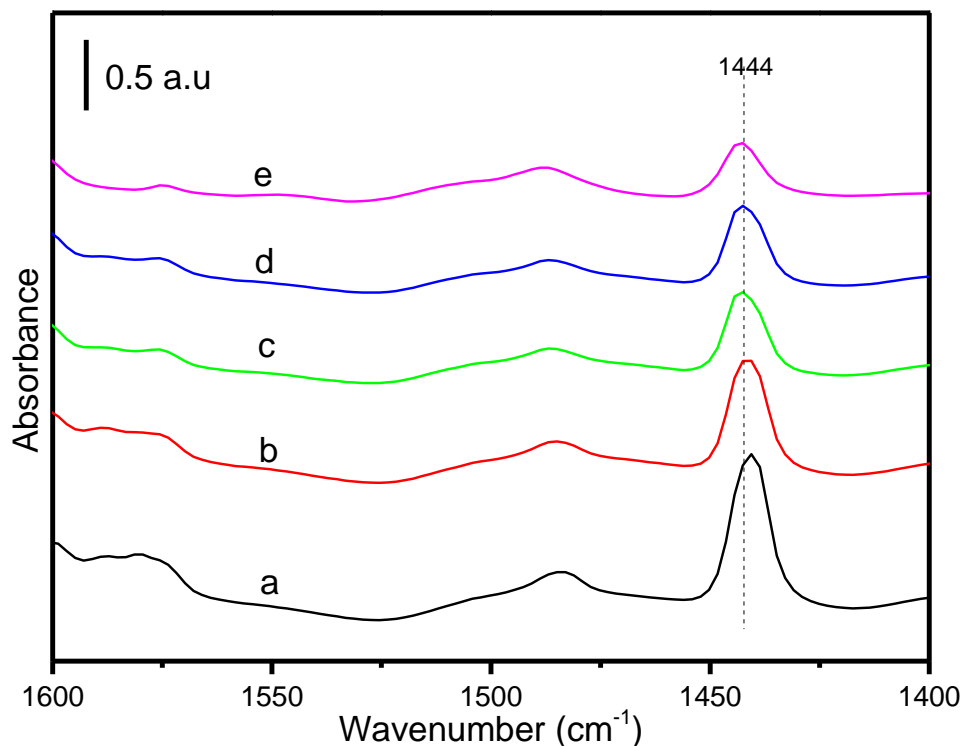
**Figure 2.3 (b)** Pyridine-FTIR spectra of Fe/Mg/O_1_2 obtained after evacuation at different temperatures. (a) room temperature (b) 100 °C; (c) 200 °C; (d) 300 °C and (e) 400 °C.

In **Table 2.2**, the amount of weak, medium and strong basic site is reported. Obtained results highlighted the increase in total amount of acidity when a greater amount of iron is inserted into the catalyst. The main difference between Fe/Mg/O_1_2 and Fe/Mg/O_1_1 is due to the substantial presence of medium-strength sites for the latter while the former has very few such sites, while both contain comparable amounts of weak and strong acidic sites. Semi-quantitative evaluation of the acid site surface concentration was obtained by peak integration.

**Table 2.2** Surface acidity quantification and distribution based on the infrared spectra

| Catalyst | Lewis acid mmol.g$^{-1}$ | | | | Brönsted acid mmol.g$^{-1}$ |
| | Weak[a] | Medium[b] | Strong[c] | | |
| | RT-200°C | 200-400°C | 400°C- | Total | Total |
|---|---|---|---|---|---|
| **Fe/Mg/O_1_10** | 0 | 0 | 0 | 0 | No |
| **Fe/Mg/O_1_2** | 0.20 | 0.07 | 0.16 | 0.43 | No |
| **Fe/Mg/O_1_1** | 0.25 | 0.24 | 0.13 | 0.62 | No |

(a) Total concentration measured at higher than Room Temperature and less at 200°C. (b) Total concentration measured higher than 200°C less at 400°C. (c) Total concentration measured higher than 400°C. d Total concentration is based on the spectra measure at Room Temperature.

The general activity both in terms of amount and acidity distribution follows the order: Fe/Mg/O_1_1 > Fe/Mg/O_1_2>> Fe/Mg/O_1_10 (no sites detected for Fe/Mg/O_1_10 samples), confirming the iron presence introduces in the systems Lewis acid sites and underlining that the catalyst acidity can be modulated by changing the iron content.

Pyridine absorption measurements were accompanied with NH$_3$-TPD analysis Results reported in **Figure 2.4** confirm that the sample Fe/Mg/O_1_10, with the lower iron content was not characterized by any acidic properties while Fe/Mg/O_1_2 showed the presence of a significant number of acid sites.
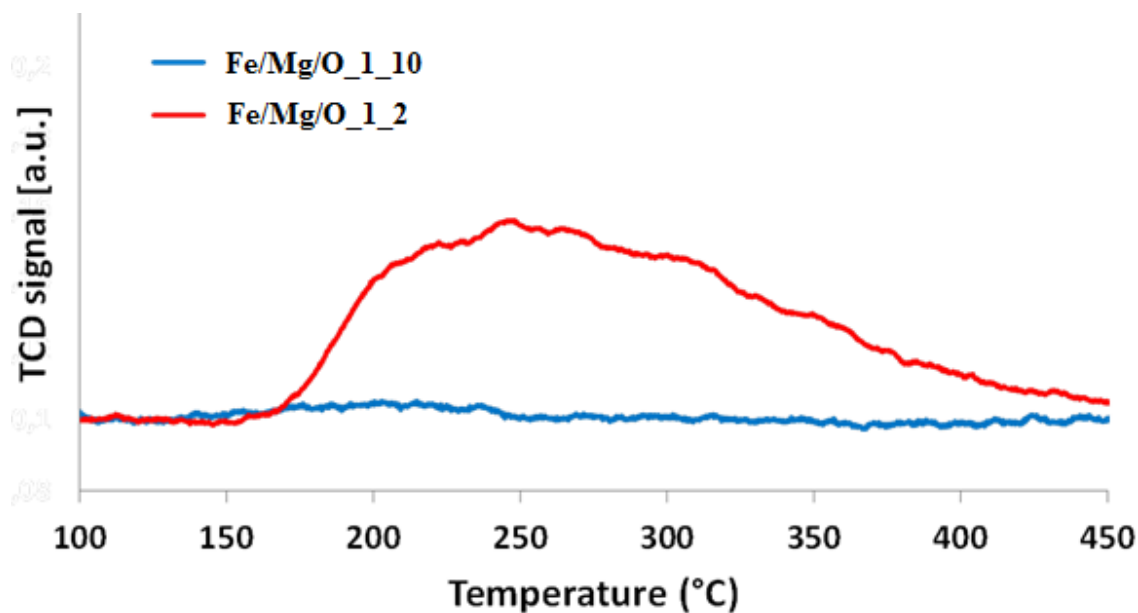
**Figure 2.4**. NH$_3$-TPD curves of co-precipitated Fe/Mg/O samples. Legend: Fe/Mg/O 1_2 (-), Fe/Mg/O 1_10 (-).

To characterize the basicity of the different catalyst, TPD analysis using CO$_2$ as probe molecule was performed. (Details results were summarize in **Table 2.1** and **Figure 2.5**). In principle, CO$_2$, as acidic probe, adsorbs specifically on basic sites and could form different types of carbonates depending on the basicity of the surface oxygen atoms. Desorption below 120 °C correspond to relatively weak basic sites while desorption higher than 280 °C was related to strong basic sites. The related between 120°C and 280 °C was medium sites.[155-157]

All MgO based samples show basicity. The density decreased in the following order: MgO>> Fe/Mg/O_1_10 > Fe/Mg/O_1_2 > Fe/Mg/O_1_1. Catalysts with higher Fe/Mg ratio showed lower basicity values because of the higher electronegativity which characterizes Fe$^{3+}$ atom with respect to Mg$^{2+}$. This decreases the charge density and makes the O$^{2-}$ less electrophilic than in pure MgO [158]. Pure Fe$_2$O$_3$ oxide exhibited low concentration of weak basic sites essentially due to surface oxygen lone pairs of the ferrites which correlate to the literature.[159, 160]
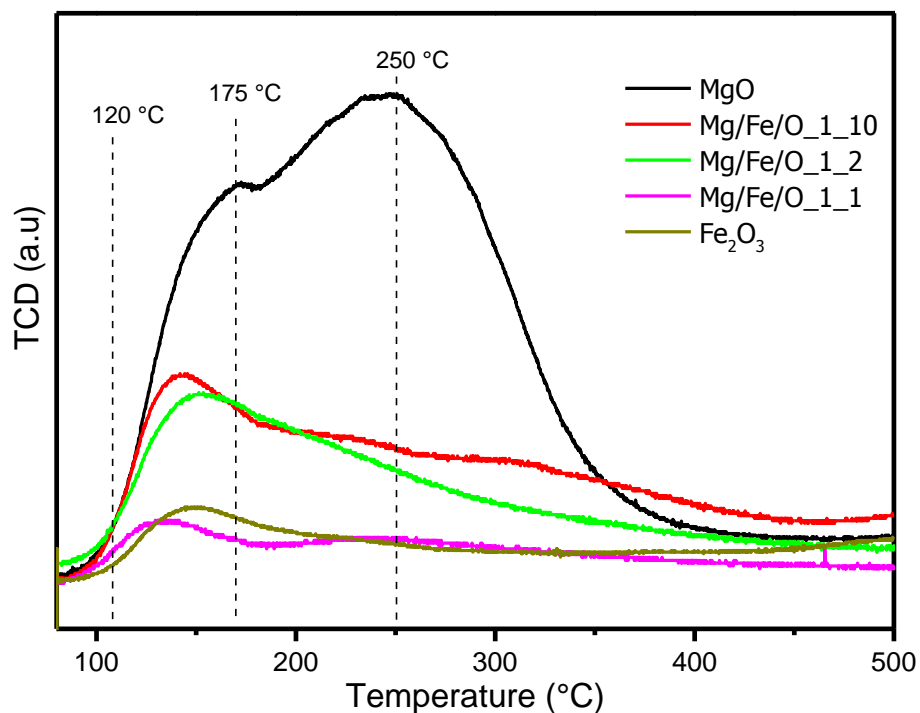
**Figure 2.5.** $CO_2$-TPD curves of co-precipitated Fe/Mg/O samples, MgO and $Fe_2O_3$

### 2.2.2 FeOx/MgO catalysts prepared by impregnation

Several FeOx/MgO catalysts containing different Fe:Mg ratios were prepared by incipient wetness impregnation of Fe(III) nitrate dissolved in aqueous solution on MgO, prepared with the co-precipitated method. Four samples with 1:100, 1:20, 1:10 and 1:2 final metal ratios, labelled FeOx/MgO_1_100, FeOx/MgO_1_20, FeOx/MgO_1_10, FeOx/MgO_1_2, respectively, were obtained. These samples differ in surface area and in crystalline phase. (see **Table 2.3** and **Figure 2.6** for XRD patterns) The trend which characterises surface area measurements is clear: the impregnation of iron precursor led to a significant decrease of the surface area. Pure MgO had a surface area of 172 $m^2$/g but when a small quantity of Fe wass impregnated on the solid (FeOx/MgO_1_100) the surface area value dropped to 150 $m^2$/g and then to 129 $m^2$/g with further increase. As a matter of fact, the lowest surface area was reached when Fe:Mg is equal to 1:2.

**Table 2.3.** Texture Properties (Specific surface area and crystalline phase) of FeOx/MgO impregnated samples.

| Catalyst | Surface area ($m^2$/g) | Crystalline Phase (XRD) |
|---|---|---|
| FeOx/MgO_1_100 | 150 | MgO-like mixed oxide |
| FeOx/MgO_1_20 | 129 | MgO-like mixed oxide |
| FeOx/MgO_1_10 | 94 | MgO-like mixed oxide |
| FeOx/MgO_1_2 | 33 | Periclase MgO, $Fe_2O_3$ |

In **Figure 2.6**, X-ray diffraction pattern of the impregnated samples and that of the pure oxides were reported. Samples with Fe:Mg 1:100, 1:20, 1:10 molar ratio showed the presence of the characteristic peaks of MgO periclase structure, while for sample with molar ratio 1:2 it was possible to reveal the presence of iron oxide (hematite) in addition to that of MgO. However, it could be hypothesized that for samples containing a lower amount of iron it was not possible to detect the presence of $Fe_2O_3$ due to its lower concentration. Thus, all these samples should be characterized by the presence of iron oxide on their surface.

**Table 2.4** Surface acidity Basicity quantification over different impregnated catalysts

| Catalyst | Lewis acid mmol.g$^{-1}$ | | | | Brönsted acid mmol.g$^{-1}$ | Basicity (mmol/g)** |
|---|---|---|---|---|---|---|
| | Weak[a] RT-200°C | Medium[b] 200-400°C | Strong[c] 400°C- | Total | Total | |
| **FeOx/MgO_1_10** | 0.05 | 0.06 | 0.04 | 0.15 | No | 2.67 |
| **FeOx/MgO_1_2** | 0.04 | 0.17 | 0.08 | 0.29 | No | 0.96 |

(a) Total concentration measured at higher than Room Temperature and less at 200°C. (b) Total concentration measured higher than 200°C less at 400°C. (c) Total concentration measured higher than 400°C. d Total concentration is based on the spectra measure at Room Temperature.
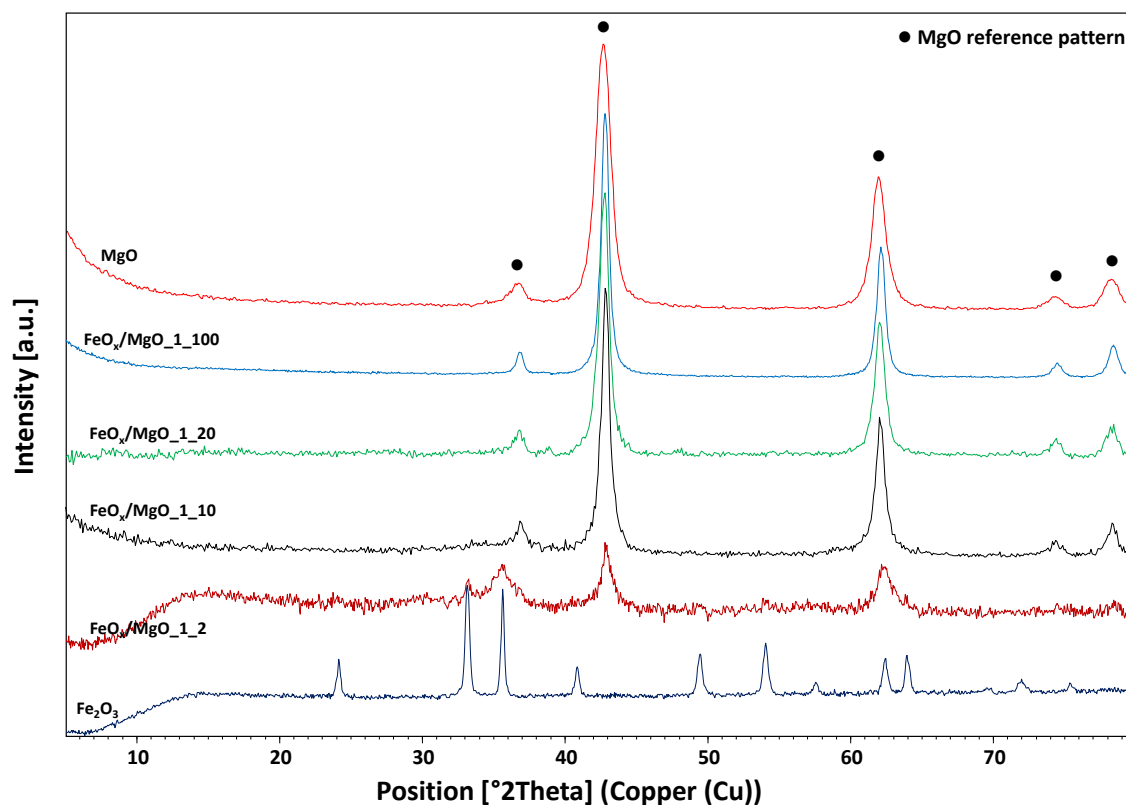
**Figure 2.6.** XRD pattern of different Fe/Mg ratios impregnated FeOx/MgO catalysts.

Sample FeOx/MgO_1_10 was characterized in order to study its acid-base and redox properties as a comparison with the co-precipitated sample with the same metal molar ratio. Pyridine FTIR absorption analysis showed that Brönsted acidity was not present and the total amount of Lewis acidity (0.15 mmol.g$^{-1}$ See **Table 2.4**) of the system was higher than that obtained with the system prepared with the same metal molar ratio with the co-precipitation method (see **Table 2.1**). This is mainly due to the fact that in co-precipitated sample $Fe^{3+}$ is intercalated within MgO lattice, while in impregnated systems it is deposited on the surface of the catalyst as iron oxide. The presence of the acidity in this system is the evidence of the formation of iron oxide on the surface. Indeed, iron oxide is characterized by acid properties as already reported in literature.[161, 162] and the formation of a FeOx layer on the surface of the basic magnesium oxide can change the physico-chemical properties of the final material.

In **Figure 2.7 (a) and (b)**, Py-FTIR spectra for FeOx/MgO_1_10 and FeOx/MgO_1_10 are reported at different temperature. This sample is characterized by a low acidity and low, medium and strong sites are basically present in the same amount (0.05, 0.06 and 0.04 mmol.g$^{-1}$

respectively See **Table 2.4**). Data show that this sample is characterized by acidic sites, while the co-precipitated catalyst with the same metal molar ratio did not show acid properties.
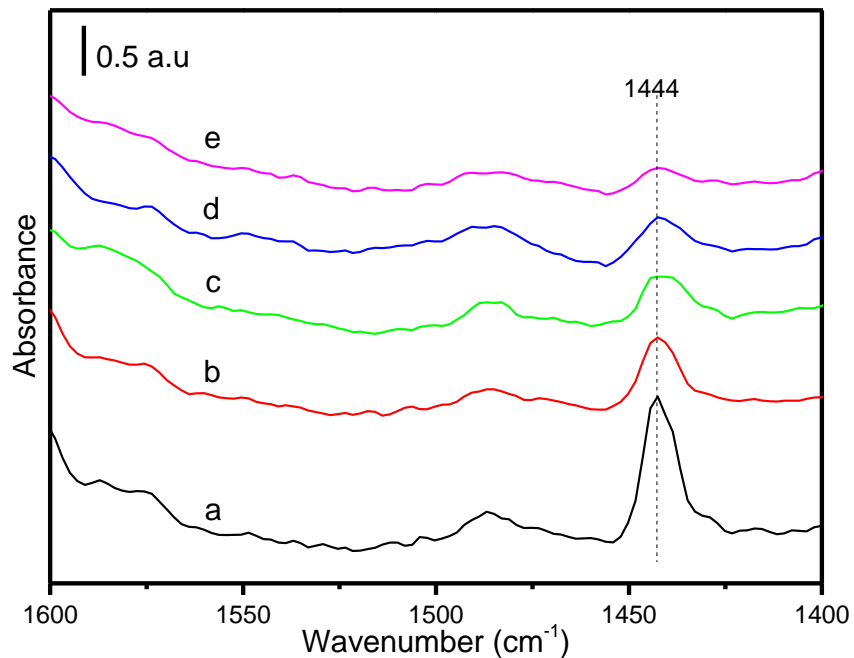


**Figure 2.7 (a)** Pyridine-FTIR spectra of FeOx/MgO_1_2 obtained after evacuation at different temperatures. (a) room temperature (b) 100 °C; (c) 200 °C; (d) 300 °C and (e) 400 °C.
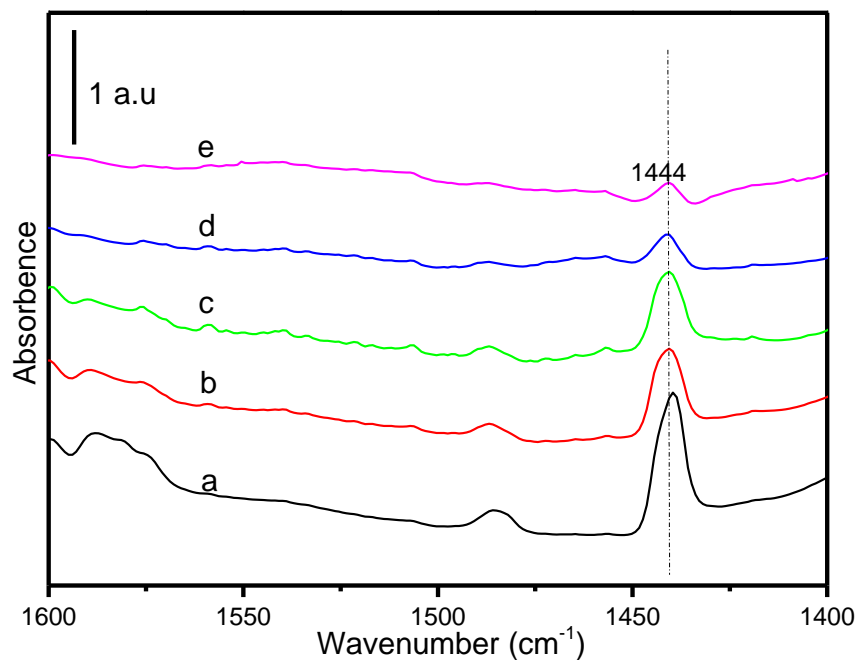


**Figure 2.7 (b)** Pyridine-FTIR spectra of FeOx/MgO_1_10 obtained after evacuation at different temperatures. a) room temperature (b) 100 °C; (c) 200 °C; (d) 300 °C and (e) 400 °C.

NH$_3$-TPD was performed on FeOx/MgO_1_10 (see **Figure 2.8**). This sample displayed a lower acid strength if compared to Fe/Mg/O_1_2, since ammonia desorption took place at a lower temperature, confirming what has been observed in Py-FTIR analysis. Moreover, comparing the behavior of co-precipitated and impregnated samples with the same metal molar ratio (Fe/Mg/O_1_10 and FeOx/MgO_1_10), it is evident how the synthesis played an important role in tuning acid properties. FeOx/MgO_1_10 is acid because of the presence of iron oxides on the surface, while the insertion of Fe$^{3+}$ in the same molar ratio with the co-precipitation method did not led to the formation of an acid catalyst since iron entered in MgO crystalline structure.
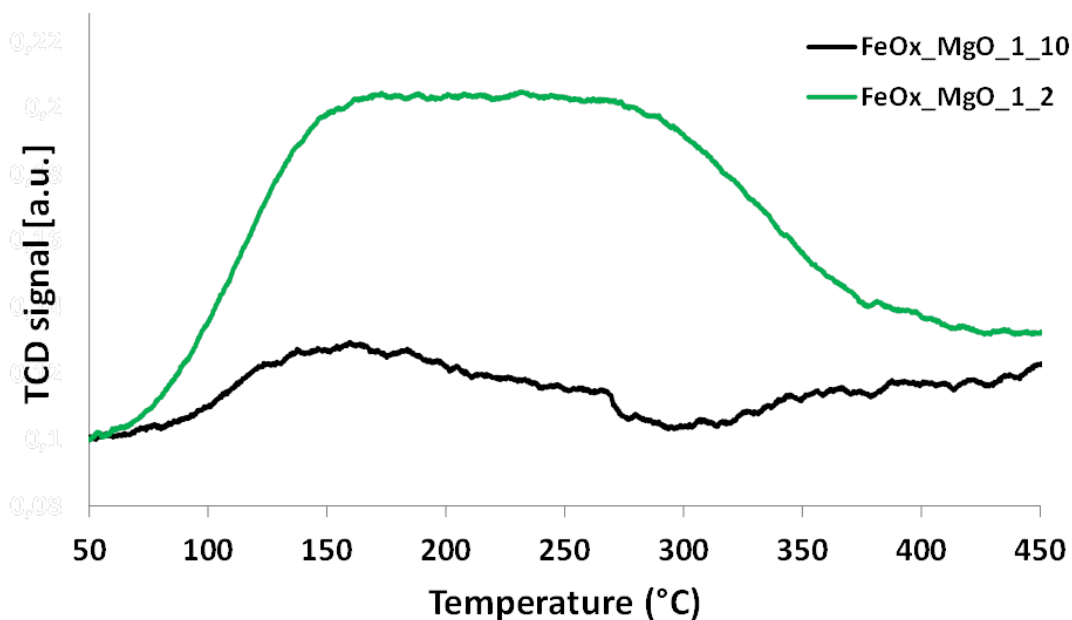


**Figure 2.8.** NH$_3$-TPD curves of FeOx/MgO_1_2 (–), FeOx/MgO_1_10 (–).

The comparison of CO$_2$-TPD profiles of the impregnated FeO$_X$/MgO catalysts was shown in **Figure 2.9**. Depending on the temperature of desorption of CO$_2$ the curve is usually classified into three categories: week adsorption (< 120 °C), medium adsorption (120 – 230°C), and strong adsorption (>230 °C) which are assigned to surface hydroxyl groups, oxygen in Mg$^{2+}$- O$^{2-}$ pairs and low coordination oxygen anions respectively.[155, 163] Results show that strong basicity decreased with in all the impregnated catalysts. The basicity of FeOx/MgO_1_10 (2.67 mmol.g$^{-1}$ See **Table 2.4**) was of the same order of magnitude as that of the co-precipitated sample with the same metal molar ratio. All studied samples show the presence of basic sites except the high iron content Fe/Mg/O_1_1, prepared by co-precipitation. For all the co-precipitated catalysts, the basicity follows the order: MgO>>FeOx/MgO_1_10≈Fe/Mg/O_1_10 >Fe/Mg/O_1_1>

FeOx/MgO_1_2 (See **Table 2.1** and **Table 2.4**), indicating that the basicity is not strongly affected by the synthetic procedure.
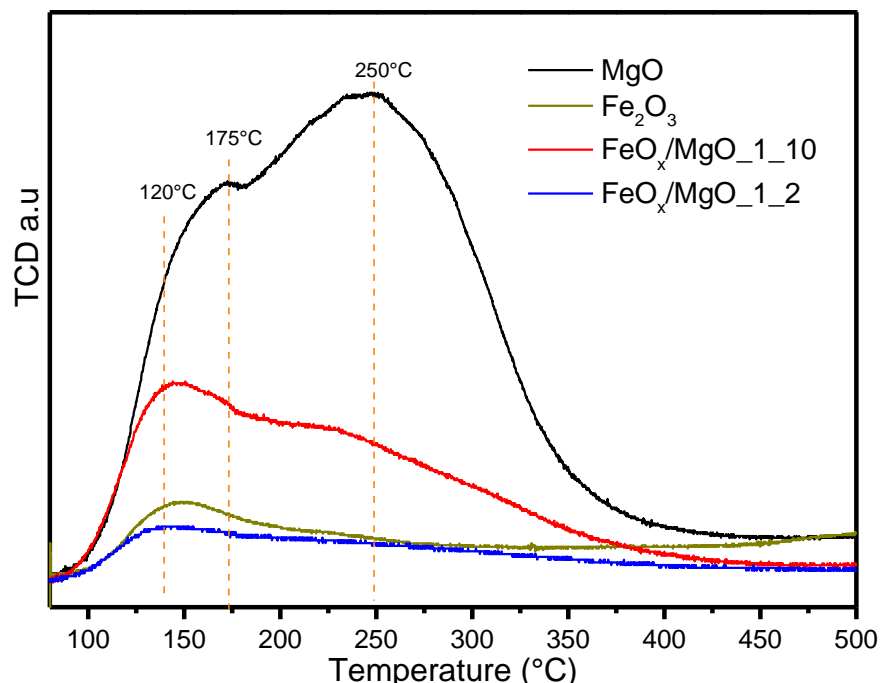


**Figure 2.9.** $CO_2$-TPD curves of impregnated FeOx/MgO samples, MgO and $Fe_2O_3$

### 2.2.3 Reactivity Tests of Fe/Mg/O Catalysts in Hydrodeoxygenation of Furfural

In our previous work, FU was converted to MF using methanol as hydrogen source trough a tandem MPV reaction involving hydrogenation and hydrogenolysis in sequence using MgO and Mg/Fe/O_1_2 catalysts (**Scheme 2.1**)
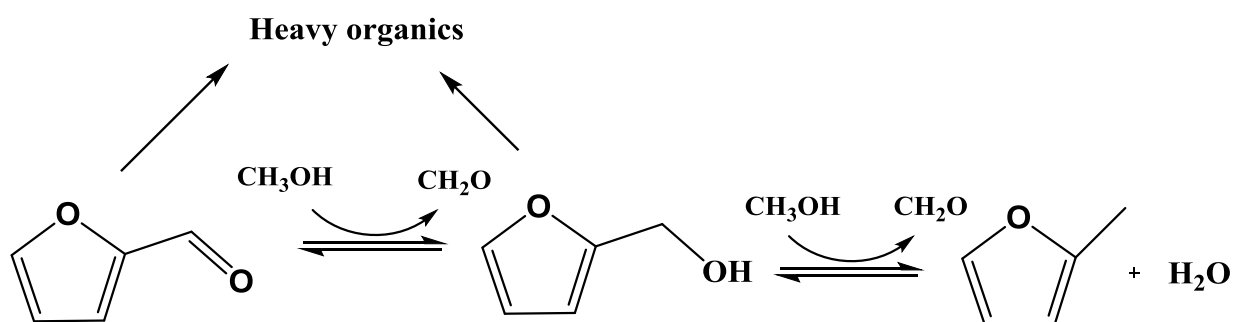


**Scheme 2.1** Reaction pathway for furfural hydrodeoxygenation over Fe/Mg/O catalyst

These systems were both active in FU conversion; however, their different chemical-physical properties led to different product selectivity. MgO was selective to FAL, while the mixed oxide produced preferentially MFU. Since interesting results were obtained with Mg/Fe catalysts, a

54

deep study on the mixed oxides systems was carried out to understand the role of iron in product distribution. In particular, the difference in the catalytic activity due to Fe content and preparation method were studied.

Primarily, the reaction was studied utilizing samples prepared by co-precipitation. The catalytic performances of co-precipitated Fe/Mg/O catalysts in furfuryl alcohol (FAL) and methyl furan (MFU) production from furfural (FU) are reported in **Figure 2.10**.
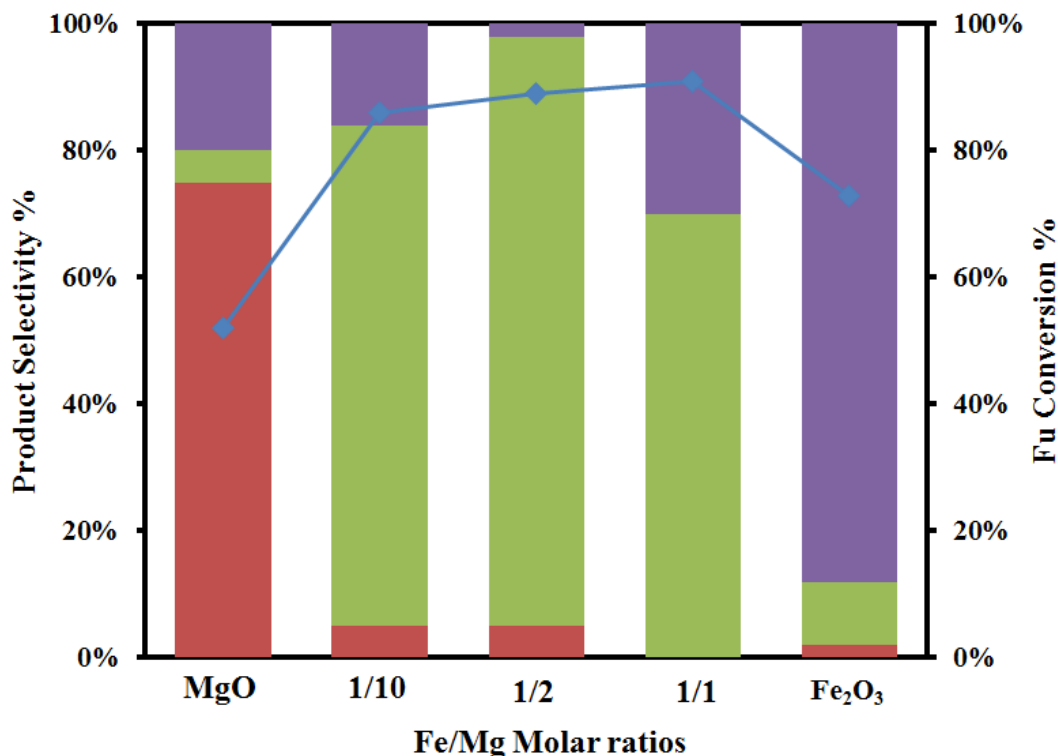


**Figure 2.10.** Profiles of co-precipitated Fe/Mg/O mixed oxide catalysts with different Fe content. Feed composition: 5% FU, 50% CH$_3$OH, 45% N$_2$, 1 atm, overall gas residence time 1.1s, and reaction time 1h, 380°C. Legend: ■ FAL ■ MFU ■ Carbon loss ◆ FU conversion

In the reaction with MgO, the H-transfer hydrogenation occurred selectively and FAL was mainly produced. However, in these conditions MgO exhibited limited activity in the further hydrogenolysis to MFU. The formation of some heavy products, consistent with the C- loss observed (20%), is present. Comparing with pure MgO (Fe/Mg ratio=0), the presence of iron improved furfural conversion and methyl furan selectivity. Notably, when low amount of iron oxide (Fe/Mg=1/10) was introduced, the selectivity of MFU was significantly increased from 5% to 51% while furfural conversion increased from 52% to 66%. The maximum conversion (93%)

and maximum MFU selectivity (79%) was achieved when Fe/Mg molar ratio reached 1/2. Further increase in iron content to the Fe/Mg ratio 1/1 significantly decreased the MFU formation and led to a poor carbon balance, probably due to higher heavy compounds deposition on the catalyst surface.[149]

Therefore, iron introduction favoured the formation of the targeted 2-methylfuran. FAL hydrogenolysis to form MFU was strongly influenced by the amount of Fe introduced in the catalyst and by the changes in its acid-base and redox properties. As a matter of fact, with the increase in the amount of iron in MgO structure, basicity decreases while the total number of acid sites increases along with redox capacity. Indeed, TPR analysis showed that Fe/Mg/O_1_2 is characterized by higher hydrogen consumption than Fe/Mg/O_1_10 and at the temperature of reaction (380°C), part of the catalyst can be reduced.

Since the basicity density dramatically decreased from MgO (7.51 mmol/g) to Fe/Mg/O_1_2 (2.34 mmol/g) and a clear enhancement in MFU yield was found, it is evident that MFU formation cannot be related to surface basicity.

Fe/Mg/O_1_2 is also characterized by the presence of acid properties but it has to be taken into account that the introduction of acid sites can lead to the selectivity towards MFU. As suggested by the high conversion but poor selectivity obtained with pure iron oxide, large iron oxide surfaces seem to promote side reactions (from FU and/or FAL).

Catalytic tests in the same reaction conditions were carried out using the impregnated samples (**Figure 2.11**). Also in this case, the formation of MFU was successful only in the presence of iron oxide. The increase of iron oxide loading, the selectivity to MFU strongly increased and a maximum MFU sel. (93%) could be obtained when the Fe/Mg ratio was 1/10. Notably, within the same Fe/Mg ratio in 1/10 the impregnated catalyst showed higher activity than co-precipitated one, revealing that the availability of FeOx on the MgO surface was supposed to be the additional factor and confirming once again the importance of the used synthetic procedure. The presence of a surface layer of iron oxide increased the acid properties of the material, while the basicity remained unaltered.
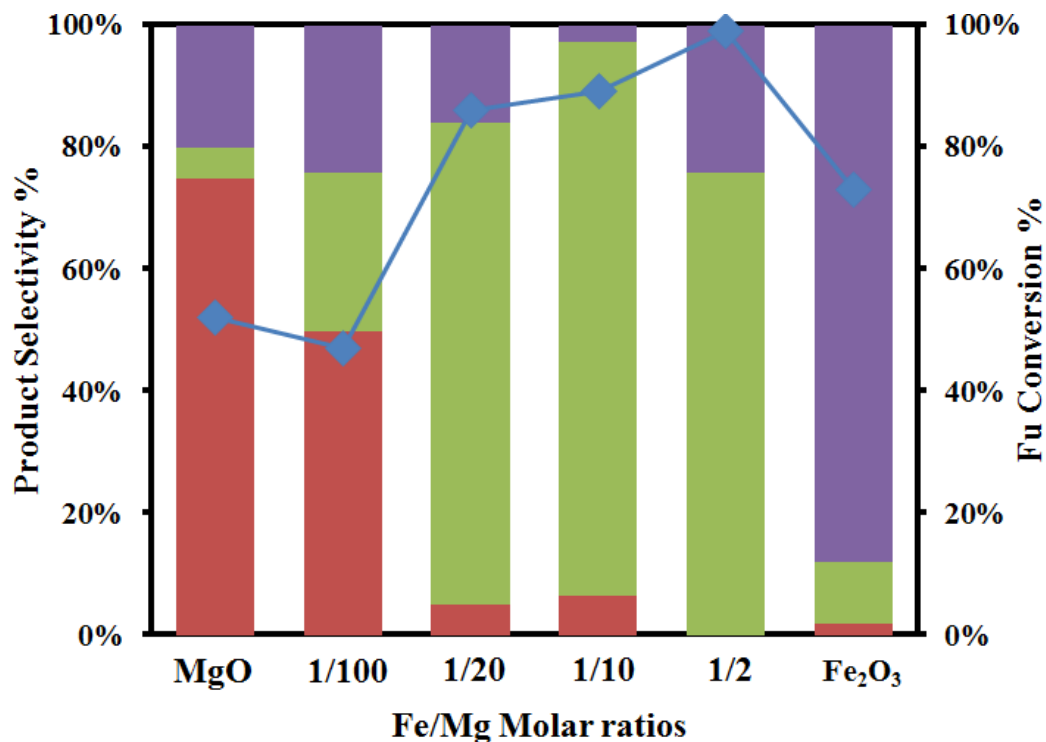
**Figure 2.11.** Reaction profiles of impregnated FeOx/MgO mixed oxide catalysts with different Fe content. Feed composition: 5% FU, 50% CH₃OH, 45% N₂, 1 atm, overall gas residence time 1.1s, reaction time 1h, 380°C. Legend: ■ FAL ■ MFU ■ Carbon loss ◆ FU conversion

### 2.2.4 Effect of Acidity on Reaction Product Distribution

In the literature, the hydrodeoxygenation capacity of a catalyst was generally associated with the Lewis sites present in the system; typical example are niobium oxide[164] and zeolite[165] which were used in liquid phase reaction. Indeed, the acid functionality catalyses the dehydration of alcohol to form intermediates which will be substituted by surface hydride. On metal oxides, it is reported that the electron rich oxygen anions show basic properties and electron donating character, while the electron deficient metal cations show acidic character. Basic and hydrogen-abstracting properties of MgO can be modulated with the introduction of host cations, typically trivalent metal cations. While Fe/Mg/O catalysts exhibited both Lewis properties and a very strong redox capacity, the Al/Mg/O system has no redox capacity.[150] In order to verify the contribution of the Lewis acid properties on the reaction, the $Al^{3+}$ was chosen as a dopant metal to modify MgO. Indeed, $Al^{3+}$ was reported to be a typical Lewis acid.[166] Therefore, in order to investigate the reaction pathways and product distribution influenced by Lewis acid properties the catalytic behaviour of co-precipitated Al/Mg/O_1_2 and impregnated AlOx/MgO_1_10 catalysts were studied in the same conditions of Fe/Mg/O system. The texture of Al containing

MgO samples was summarized in **Table 2.5**. It conducted that when AlOx was impregnate over MgO the surface area will dramatically decreased, in contrast co-precipitated sample Al/Mg/O_1_2 reserve high surface area.(132 $m^2$/g) Both sample present only periclase phase which assigned from MgO.

**Table 2.5** Surface area and catalyst crystalline phase from XRD analysis of MgO and Fe/Mg/O co-precipitated sample.

| Catalyst | Surface area ($m^2$/g) | Crystalline Phase (XRD) |
|---|---|---|
| Al/Mg/O_1_2 | 132 | periclase |
| AlOx/MgO_1_10 | 28 | periclase |

Further to confirm the surface acidity and basicity change. Further the acidity was analysis and the results were summarized in **Table 2.6** in which acidity from Fe/Mg/O_1_2 and FeOx/MgO_1_10 was also provided for comparing. The order in the sample Lewis acid density was the following: Al/Mg/O_1_2>AlOx/MgO_1_10> Fe/Mg/O_1_2 > FeOx/MgO_1_10 >> MgO (**Table 2.6**). Both in co-precipitated and impregnated systems, Al-containing MgO presented higher density of Lewis acidity rather than Fe containing MgO.

**Table 2.6.** Surface acidity quantification based on the pyridine infrared spectra analysis

| Catalyst | Lewis acid mmol.g$^{-1}$ | | | | Brönsted acid mmol.g$^{-1}$ | Basicity (mmol/g) |
|---|---|---|---|---|---|---|
| | Weak[a] RT-200°C | Medium[b] 200-400°C | Strong[c] 400°C- | Total | Total | |
| **Al/Mg/O_1_2** | 0.59 | 0.03 | 0.17 | 0.80 | No | 4.48 |
| **AlOx/MgO_1_10** | 0.40 | 0.13 | 0.06 | 0.59 | No | 2.54 |
| **FeOx/MgO_1_10** | 0.05 | 0.06 | 0.04 | 0.15 | No | 2.67 |
| **Fe/Mg/O_1_2** | 0.20 | 0.07 | 0.16 | 0.43 | No | 2.34 |
| **MgO** | - | - | - | 0 | No | 7.51 |

(a) Total concentration measured at higher than Room Temperature and less at 200°C. (b) Total concentration measured higher than 200°C less at 400°C. (c) Total concentration measured higher than 400°C. d Total concentration is based on the spectra measure at Room Temperature

Catalytic results are summarized in **Table 2.7**, where Al-based materials are compared to MgO and Fe-containing catalysts. Al/Mg/O_1_2 reached a conversion 63% with a 37% of carbon loss and a MFU selectivity of 22%. The comparison between Al/Mg/O_1_2 and Fe/Mg/O_1_2 indicated that Al containing catalyst converted less FU and showed a greater carbon loss, probably connected with an increased acidity. Indeed, Py-FTIR analysis (table 6) showed that the total amount of acidity in Al/Mg/O_1_2 is double respect to Fe/Mg/O_1_2. Moreover, the product distribution was totally different from Fe-based material since 41% of FAL was formed and MFU was obtained in lower amount (22%). This seems to indicate that the presence of Lewis acid is not the only feature leading to MFU formation. Moreover, the high acidity clearly increased by-product formation, as demonstrated by the higher carbon loss observed (37%).

**Table 2.7** Summary the catalytic performance over different Al, Fe doping MgO catalysts

| Catalyst | M/Mg Molar ratio | FU Conv (%) | FAL Sel (%) | MFU Sel. (%) | C-loss (%) |
|---|---|---|---|---|---|
| MgO | - | 52 | 75 | 5 | 20 |
| Al/Mg/O_1_2 | 1:2 | 63 | 41 | 22 | 37 |
| Fe/Mg/O_1_2 | 1:2 | 93 | 1 | 79 | 20 |
| AlOx/MgO_1_10 | 1:10 | 40 | 76 | 5 | 19 |
| FeOx/MgO_1_10 | 1:10 | 89 | 5 | 93 | 2 |

Feed composition: 5% FU, 50% $CH_3OH$, 45% $N_2$, 1 atm, overall gas space time 1.1s, reaction time 1h, 380°C.

Similar results were obtained with the impregnated systems. AlOx/MgO_1_10 exhibited slightly lower catalytic performance compared to MgO but the difference with FeOx/MgO_1_10 is really pronounced, since very few MFU is formed. Since the acidity was improved in a large amount, both in co-precipitation and impregnation, but the promotion of methyl furan selectivity was limited. This result reveals that Lewis acid is needed for the furfuryl alcohol side chain C-O

bond activation but it is not the dominant effect to increase furfural conversion and MFU selectivity. Additionally, the increase of Lewis acidity will lead high risk of degradation of products.

### 2.2.5 Effect of Basicity on Reaction Product Distribution

In order to illustrate the contribution of basicity in reaction system, the commercial silica was chosen as alternative support, and impregnated FeOx supported on Silica with Fe/Si ratio at 1/10 was prepared and tested.

**Table 2.8.** Summary the catalytic performance of silica supported iron oxide and comparing with bulk $Fe_2O_3$ and MgO.

| Entry | Catalyst | Fe/Si Molar ratio | FU Conv (%) | FAL Sel (%) | MFU Sel. (%) | C-loss (%) |
|-------|----------|-------------------|-------------|-------------|--------------|------------|
| 1 | MgO | - | 52 | 75 | 5 | 20 |
| 2 | $Fe_2O_3$ | - | 73 | 2 | 10 | 88 |
| 3 | Silica | - | 0 | 0 | 0 | 0 |
| 4 | FeOx/Silica_1_10 | 1:10 | 19 | 1 | 26 | 74 |

Feed composition: 5% FU, 50% $CH_3OH$, 45% $N_2$, 1 atm, overall gas residence time 1.1s, and reaction time 1h, 380°C.

A markedly difference was observed when FeOx/silica_1_10 was used as the catalyst **Table 2.8** Entry 4. Comparing with pure MgO, FeOx/silica_1_10 catalyst has low furfural conversion (19%) and very low furfural alcohol production while the major product (26%) was methyl furan. Nevertheless, very high carbon loss (74%) was observed in this test. However, when $Fe_2O_3$ is employed as catalysts, similar product distribution was observed but within high furfural conversion $Fe_2O_3$ (73%). This lead to two conclusions: first, that furfural conversion is related to the surface basicity and excess exposure acidity could also lead to furfural degradation. Second, the selectivity of methyl furan is not correlated to surface basicity but it was more feasible to form methyl furan when iron oxide presence. It predicts that iron oxide loading plays an important role in selectivity and the basicity was more favor for furfural conversion.

## 2.2.6 Conclusion of Acid and Base influence

In order to illustrate the influence of surface acidity and basicity toward product distribution, the relationship between basicity and acidity with FAL formation and carbon loss was summarized in **Figure 2.12** and **Figure 2.13**. This leads to different conclusions: i) furfural conversion to furfuryl alcohol is mainly related to the basic properties of the catalyst, since it promotes methanol activation. ii) the selectivity towards methyl furan is not correlated to surface basicity while it is clearly related the iron oxide presence; iii) the Lewis acidity favour MFU formation, nevertheless the redox properties of FeOx seems to play a significant role both on FU conversion and MFU selectivity.
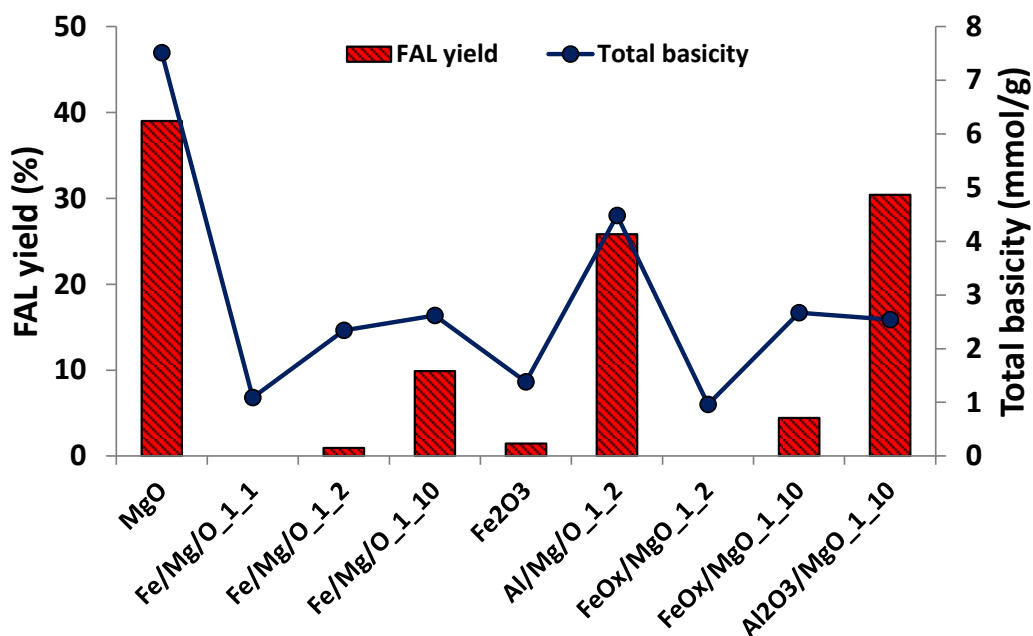


**Figure 2.12**. FAL yield obtained with the different catalysts as a function of the total basicity. Occasionally, Lewis acid increasing risk of heavy compounds formation. The presence of acid sites led to an increase in the formation of MFU but it also catalysed FU/FAL degradation/oligomerization
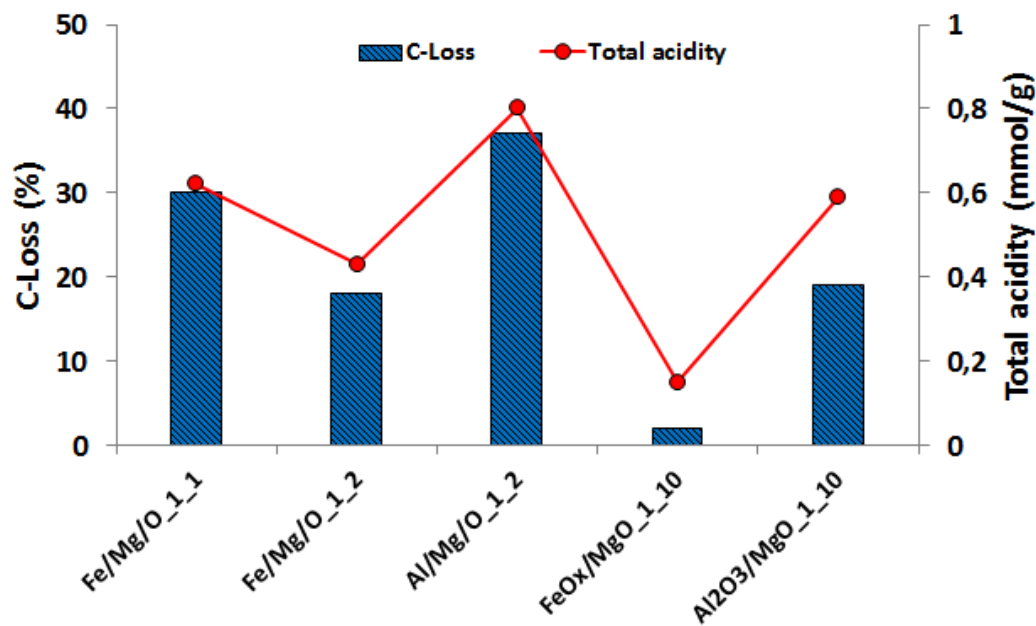
**Figure 2.13**. Carbon-loss obtained with the different catalysts as a function of the total acidity.

### 2.2.7 Effect of Iron oxide phase on FAL Hydrodeoxynation

In order to investigate the influence from the iron phase, physical mixed metal oxide, $Fe_2O_3/MgO$ and $Fe_3O_4/MgO$ in the same molar ratio (Fe/Mg=1/10) was also tested under the same reaction and the results were shown in **Table 2.9**. A notable increase in FU conversion and MFU selectivity was observed both in physical mixed $Fe_2O_3/MgO$ and $Fe_3O_4/MgO$ catalysts. Specifically, at in the same level of FU conversion (around 80%) but a clear improvement in the MFU selectivity was observed (52% and 69%). It well known that $Fe_3O_4$ is less acid than $Fe_2O_3$ and more easily re-oxidable.[167] Both $Fe_2O_3$ and $Fe_3O_4$ show high furfural conversion, but low selectivity of MFU products. Indeed, the two types of iron oxides showed high carbon loss, mainly ascribable to the polymerization of furfural based compounds promoted by the acidic properties of the materials.[119, 168] Nevertheless, MFU selectivity was higher on $Fe_3O_4$ compared with $Fe_2O_3$, suggesting that the redox feature is an important factor considering furfural activation. It is also evidence that the reaction performance is not just based on the nature of FeOx instead it mainly influenced by redox feather change where the interaction between Fe and MgO was play an important role. Based on these questions, next section we will continue to investigate the active phase over different catalysts.

**Table 2.9** Product distribution during furfural reduction over different iron oxide magnesium oxide physical mixture

| Entry | Catalyst | Fur con (%) | FAL sel (%) | MFU sel(%) | Carbon loss (%) |
|:-----:|:--------:|:-----------:|:-----------:|:----------:|:---------------:|
| 1 | MgO | 52 | 75 | 5 | 20 |
| 2 | $Fe_2O_3$/MgO_1_10 | 80 | 25 | 52 | 23 |
| 3 | $Fe_3O_4$/MgO_1_10 | 77 | 18 | 69 | 13 |

## 2.2.8 Catalyst Active Phase Investigation

Based on previous studies, it show that iron oxide phase play an important role towards methyl furan formation rather than surface basic acidic properties. Among co-precipitated and impregnated catalysts, when Fe/Mg ratio reach higher than optimal numbers, different Fe/Mg ratio there are similar methyl furan selectivity and the same level furfural conversion, so it means that over these catalyst, there should have some similar active sites presence, in order to investigate the surface active sites, Fe/Mg/O_1_2, FeOx/MgO_1_10 and bulk $Fe_2O_3$ was chosen for comparison.

## 2.2.8.1 Raman spectra Analysis over FeOx/MgO_1_10

Raman spectroscopy was applied to study the phase composition of iron oxide which was presented in **Figure 2.14**. Pure $Fe_2O_3$ synthesized via the same condition was also provided for comparing.
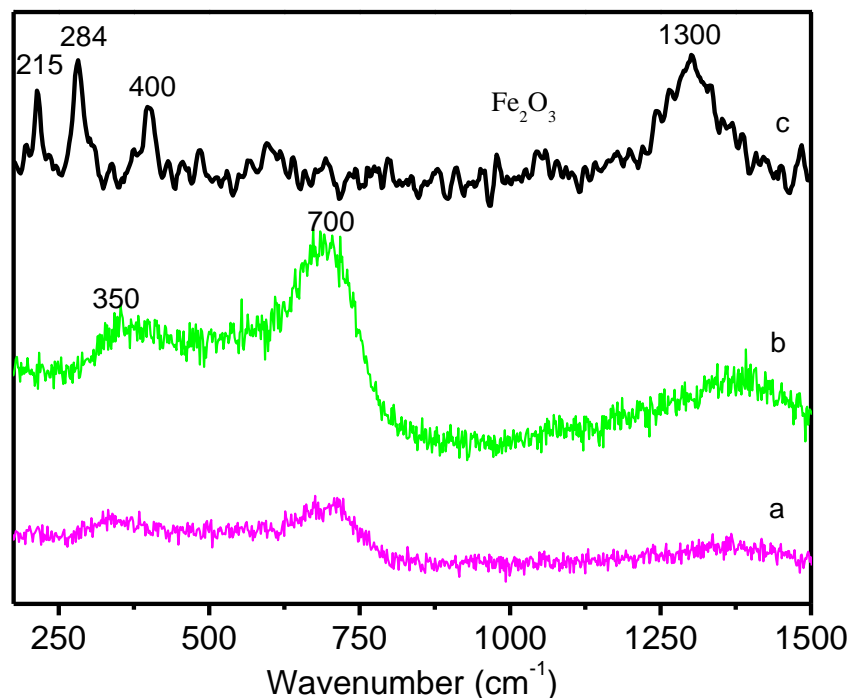
**Figure 2.14** Raman spectra of different prepared catalysts: a) impregnated FeOx/MgO_1_10, b) co precipitated Fe/Mg/O_1_2 , c) synthesized $Fe_2O_3$.

The Raman spectrum of the pure $Fe_2O_3$ catalyst possesses sharp bands at 215, 284, 400 $cm^{-1}$ that are characteristic of the hematite phase and the intense feature at 1300 $cm^{-1}$ is assigned to a two-magnon scattering which arises from the interaction of two magnons created on antiparallel close spin sites.[169, 170] (**Figure 2.14**, c). The Raman frequency of MgO was not detected in all the samples and both is absence of Raman bands from $\alpha$-$Fe_2O_3$ (hematite) phase. The broad features observed in the two samples (FeOx/MgO_1_10, (a) and Fe/Mg/O_1_2, (b), **Figure 2.14**) are characteristic of the phase mainly of $\gamma$-$Fe_2O_3$ (maghemite) [171-173]. Raman active phonon modes at 350 and 700 $cm^{-1}$ relate to the $T_{2g}$, and $A_{1g}$ optical transitions in iron ions, respectively but it is lack of peak in range 505–515 $cm^{-1}$ belonged to model $E_g$. A notable difference between the co-precipitation and impregnation samples is the intensity of the band which is observed at700 $cm^{-1}$ which due to the different iron oxide loading. Compared curve **a** and **b** it shows that the present iron oxide phase was similar which is the phase deriving from alfa $Fe_2O_3$ maghemite. It is truly conformed that no $\alpha$-$Fe_2O_3$ (hematite) phases existence from trivalent $Fe^{3+}$ nitrite precursor. The active iron oxide phase could be the intermediated state derived from $\gamma$-$Fe_2O_3$.

**2.2.8.2 TEM and Element Image Investigation**
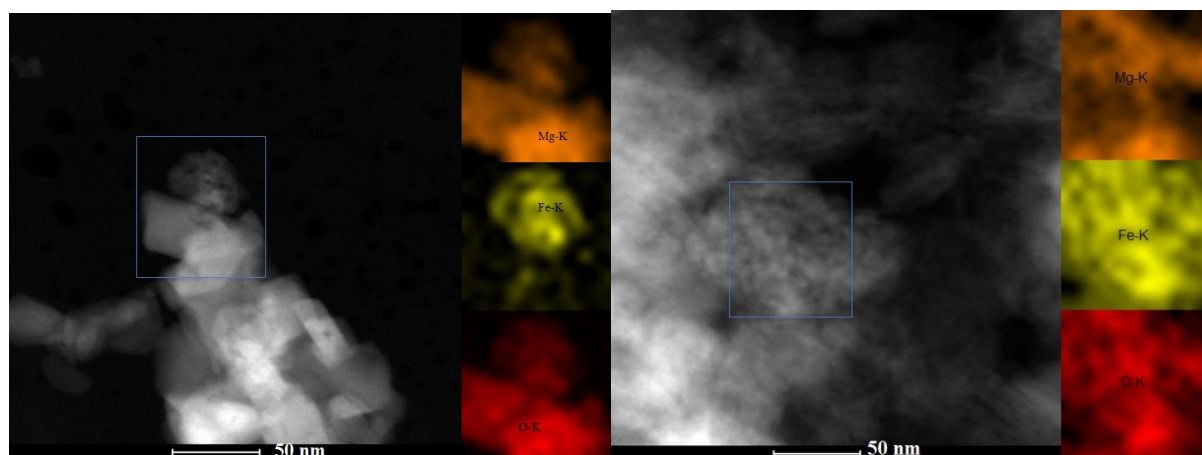
**Figure 2.15** The elemental mapping shows surface rich iron dispersion on the surface and phase separation. TEM image with the corresponding Fe-K, Mg-K and O-K element mapping for FeMgO catalysts FeOx/MgO_1_10 (left ) Fe/Mg/O_1_2 (right)

From TEM (see **Figure 2.15**) image, it reveal that uniform distribution of Fe, Mg elements in co-precipitated Fe/Mg/O_1_2 sample, in contrast FeOx/MgO_1_10 has iron phase rich part. Iron phase distributions and compositions for impregnated catalysts were studied using HRTEM bright field images and EDS line profiles and maps. The results was shown in **Figure 2.15** In order to investigate the iron phase distribution high resolution TEM and element mapping was carried out here, it is obvious that in cooperation system iron exhibited ultrafine dispersion, in contrast, impregnated sample FeOx/MgO_1_10 show some iron rich MgO part and separated MgO. It revealed that when impregnation the iron was reacted with surface Mg to form some iron rich MgO phase which was believed to the active phase. Meanwhile, more interaction between iron oxide and MgO phase show higher selectivity than the separated two phase system.

## 2.2.8.3  H₂ TPR Investigation
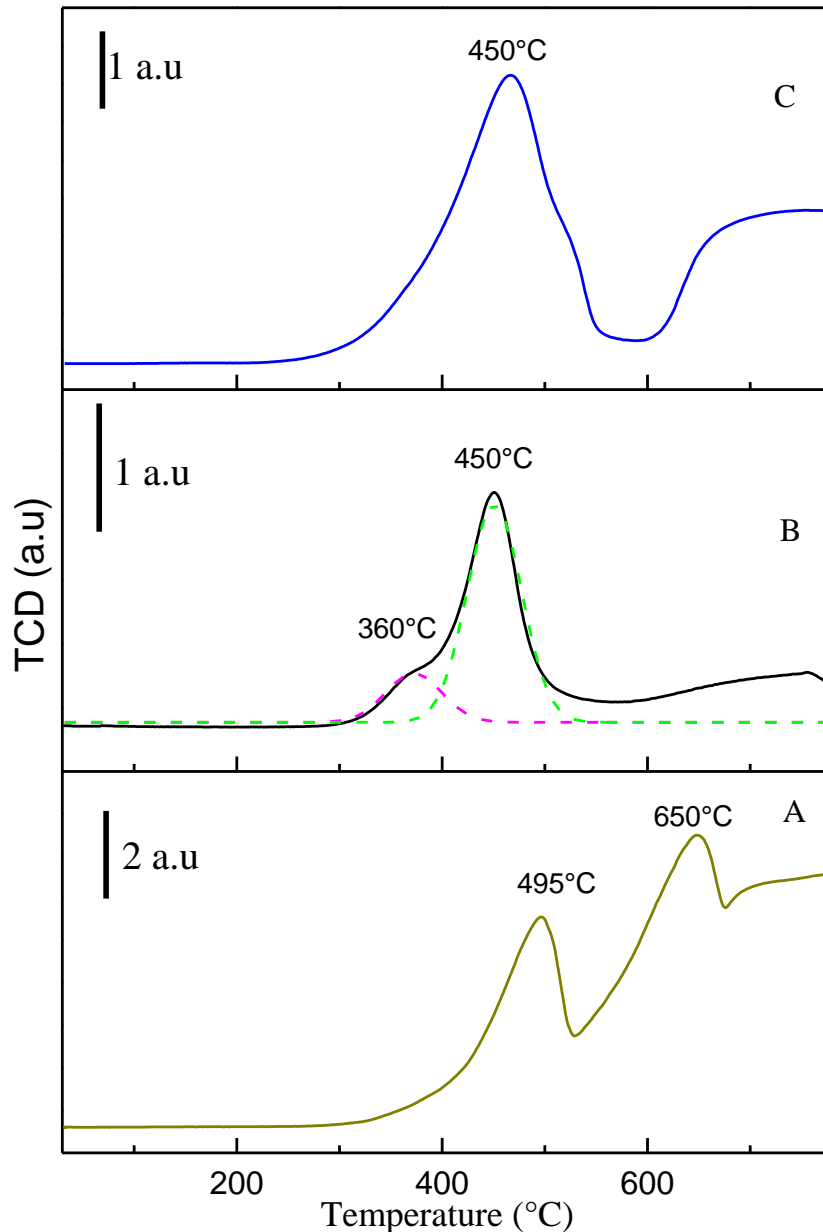


**Figure 2.16** Temperature programmed reduction (TPR) of: A) Fe₂O₃, B) FeOx/MgO_1_10, C) Fe/Mg/O_1_2

Temperature programmed reduction profiles (TPR) of the catalysts were performed and compared with $Fe_2O_3$ synthesized via the same procedures (**Figure 2.16 Curve A**) in an attempt to get information about the reducibility and discrimination iron oxide phase. It also provides insight on interaction between FeOx and MgO. According to the literature, the reduction of iron oxide: $Fe_2O_3$ (hematite) $\rightarrow$ $Fe_3O_4$ (magnetite) $\rightarrow$ FeO (wustite) $\rightarrow$ Fe[174-177]. Pure hematite

($Fe_2O_3$) presented three hydrogen consumption peaks at 495, 650 and higher than 800 °C typical for this iron phase. The low temperature peaks of FeOx/MgO_1_10 and Fe/Mg/O_1_2 shifted to 450 °C and 460°C respectively. On the other hand, FeOx/MgO_1_10 catalyst involved a shoulder peak of the reduction temperature to lower values as fitting (**Figure 2.16 curve B**). A comparison with the peaks of pure hematite indicated a displacement in the reduction temperatures of the iron phase in FeOx/MgO sample. Such displacement can be correlated to the interaction between the surface layer FeOx and MgO support. Similar behavior could be observed for Fe/Mg/O catalyst (**Figure 2.16 curve C**) the first broad peak 460°C shift to low reduction temperature relative to that of interaction between inserted FeOx and MgO structure. In addition, the $H_2$ consumption linearly increased with increase FeOx loading (see **Table 2.10**) increased since the catalyst was synthesized via different approach. It further demonstrated the similar catalytic performance due to the presence the Fe rich MgO species which present strong interaction between FeOx and MgO phase. Both Raman and TEM spectra were in complete agreement with $H_2$ TPR results.

**Table 2.10** Quantitative results of $H_2$ consumption for catalyst in $H_2$-TPR

| Samples | Peak | $H_2$ consumption(mmol/g) | Reduction phase |
|---|---|---|---|
| **Fe/Mg/O_1_2** | 460°C | 4.11 | $Fe^{3+}$ to $Fe^{2+}$ |
| **FeOxMgO_1_10** | 360°C | 0.37 | $Fe^{3+}$ to $Fe^{2+}$ |
| | 450°C | 1.11 | $Fe^{3+}$ to $Fe^{2+}$ |

## 2.3 Conclusion

In this study, we examined how the iron oxide phase influences the formation of 2-methylfuran via a catalytic transfer hydrogenation process. An optimum methyl furan yield of 83% was achieved using MgO supported FeOx catalyst. The activity especially in methyl furan selectivity has been attributed to coexistence of iron oxide and basic MgO phase. Specifically, the basicity favor furfural conversion and HDO of furfuryl alcohol intermediate was believed related to the nature of iron oxide. Finally, it reveals that the layer iron rich MgO species was responsible for

the promotion in the methyl furan selectivity due to enhanced the reducibility. It provides a new route to design solid base catalyst with high activities in catalytic transfer reduction reactions. Finally, it reveals that the top layer iron rich MgO species was responsible for the promotion in the methyl furan selectivity due to enhanced the reducibility.

## 2.4 Experimental Section

### 2.4.1 Materials

$Fe(NO_3)_3.9H_2O$, $MgNO_3.10H_2O$, $Al(NO_3)_3.6H_2O$, Magnetite ($Fe_3O_4$), furfural, furfuryl alcohol, methyl furan were purchased from Aldrich, all the chemical was used without purification except furfural. Furfural was purified by azeotropic distillation with water. Silica support was supplied by W.R. Grace & Co.

### 2.4.2 Catalyst preparation

Co-precipitated samples - The MgO and Fe/Mg/O catalysts were prepared by precipitation from an aqueous solution containing the corresponding metal nitrates. Fe/Mg/O with different Fe/Mg ratio was named as Fe/Mg/O_n_m where n_m refers to the Mg to Fe molar ratio. All prepared samples were dried at 120 °C for 2h and then calcined in air at 450 °Cfor 5h. Al/Mg/O sample was via the same procedures just change the precursor $Al(NO_3)_3.6H_2O$

Supported samples -FeOx supported over MgO (Silica) samples were prepared by incipient wet impregnation using $Fe(NO_3)_3.9H_2O$. The amount of nitrate required to obtain samples with a formal content of hematite phase was in the Fe/Mg molar range of 1:100 to 1:10. Samples with different Fe/Mg (Si) ratio were named as FeOx/MgO_n_m (FeOx/Silica_n_m) where n/m refers to the Mg to Fe (Si) molar ratio. All prepared samples were dried at 120°C for 2h and then calcined in air at 450°C for 5h. AlOx/MgO_n_m sample was via the same procedures just change the precursor $Al(NO_3)_3.6H_2O$. FeOx/silica was synthesized via the same procedures just changing the support. $Fe_2O_3$ was synthesised via the same procedure via precipitation like MgO

Physical mixed samples: physical mixture samples for comparing was synthesised by molt mixture with individually Fe/Mg ratio, here in this chapter, Fe/Mg ratio was set at 1/10

### 2.4.3 Characterization

**XRD** powder patterns of the catalysts were recorded with Ni-filtered Cu Kα radiation (λ = 1.54178 Å) on a Philips X'Pert vertical diffractometer equipped with a pulse height analyzer and a secondary curved graphite-crystal monochromato

**The BET surface** area of the catalysts was determined by $N_2$ absorption–desorption at liquid N2 temperature using a Sorpty 1750 Fison instrument. 0.3 g of the sample was typically used for the measurement, and the sample was outgassed at 150 °C before N2 absorption.

## $CO_2$ TPD

Chemisorption experiments were carried out on a BELSORB-max from BEL JAPAN. Ca. 100mg of catalyst was degassed at 450°C for 3h under under a 50 mL.min$^{-1}$ flow of pure helium. After cooling to 80°C, $CO_2$ was adsorbed by flowing the catalysts under 50% $CO_2$-He gas mixture for 30 mins (50ml.min$^{-1}$) followed by He treatment at 80°C for 15min to remove physisorbed molecules. The catalysts were then heated under He flow (50ml.min$^{-1}$) up to 500°C at a heating rate of 10 °C.min$^{-1}$.

## Pyridine IR

FTIR measurements were carried out in Perkin Elmer Spectrum spectrophotometer, between 4000 and 400 cm$^{-1}$. Self supported wafers of the samples containing around 35 mg (13 mm diameter) were evacuated at 10$^{-5}$ mbar and 450 °C for 1h, after cooling to room temperature, the spectrum was recorded as a background. The sample wafer was then exposed to pyridine vapors in room temperature for 30 mins until equilibrium was reached, and then a second spectrum was recorded, and then the wafer was subjected to evacuation for 10 min and then the spectrum was recorded named RT. Subsequent evacuations were performed at 100, 200, 300 and 400 °C for 10 min followed by spectral acquisitions. The spectra presented were obtained by subtracting the spectra recorded after pretreatment and before pyridine adsorption.

## $H_2$ TPR experiments

$H_2$ TPR experiments were carried out using Micromeritics ChemiSorb 2720 / 2750 equipped with a linear temperature control from 30°C to 1000°C. $H_2$-TPR was performed using 100mg of catalyst preliminary pretreated under Ar at 500°C for 60mins. A 13X zeolite was used to trap water that may be produced during the analysis working with a 5% $H_2$/Ar reduction mixture. The

samples were heated to 800 °C (rate: 10°C min$^{-1}$) and kept at this temperature for 30 min. The calibration for TPR curve was obtained by CuO (99%)

**NH$_3$ TPD**

NH$_3$-TPD analysis was performed using a Micromeritics AutoChem II chemisorption analyzer with a flow-through reactor connected to a thermal conductivity detector (TCD). The samples were activated at 500 °C for 1 h followed by the adsorption of NH$_3$ at 180 °C. The NH$_3$-adsorbed catalysts were purged in high purity helium flow gas for an extended 1 h to minimize the extent of physisorbed NH$_3$. Then, the TPD spectra were recorded by heating the samples from 180 to 550 °C at a rate of 10–20 °C/min in helium flow.

**Raman Spectra**

Raman spectra were recorded using a Renishaw spectrometer with a 514.5 nm Ar+ ion laser source equipped with a microscope (50 X lens was used). The power was 0.15 mW using 40 second exposure time and 6 accumulations per each spectrum

**2.4.4 Catalytic Test**

Catalytic tests were carried out in a continuous-flow fixed-bed micro-reactor (Pyrex, length 38 cm, internal diameter 1/3 inch). The catalyst (30-60 mesh particles) was placed in the reactor in order to have the contact time equal to 1.1 s, and then it was heated to 380°C under nitrogen flow (26 ml/min). The catalytic reaction was started by the vaporization of methanol and furfural (Sigma-Aldrich) in a 10/1 molar ratio using the nitrogen flow as the carrier gas (26 ml/min). Furfural was purified via distillation prior to being fed into the flowing gas stream. The total volumetric flow rate through the catalytic bed was held constant at 60 ml/min and the concentration of furfural, methanol, and nitrogen were respectively 5, 50, and 45%.

Analyses of reactant and products were carried out as follows: the outlet stream was scrubbed for 1h in cold acetonitrile, which was maintained at -26 °C by a F32 Julabo Thermostat. The condensed products were analysed by HPLC, using an Agilent Technologies 1260 Infinity instrument equipped with a DAD UV-Vis detector and an Agilent PORO shell 120 C-18 column.

# Chapter III In Situ IR Investigations on the Reaction Mechanism in the Catalytic Transfer Reduction of Furfural

## 3.1 Introduction

When dealing with hydrogen transfer processes, two main cycles should be considered: the activation of the hydrogen donor, methanol in our system, and the activation of the substrate, furfural or furfuryl alcohol. In literature, it is described that the transformation of methanol is the main factor to determine hydrogenolysis.[116, 158, 178, 179] Catalysts with basic sites tend to easily dehydrogenate methanol into formaldehyde, which after disproportionation can lead to formation of formate. At high temperatures, and over catalyst, all these compounds can also decompose, to yield CO, $CO_2$, $H_2$ and $CH_4$. Correspond, in the case of furfural or furfuryl alcohol activation although it has been shown that iron oxide is a promising catalyst for methyl furan formation in gas phase,[22, 180] but a fundamental understanding is still lacking.

In Chapter II we have shown that variations in iron content for iron magnesium mixed oxides lead to very different product distributions. One key factor influencing methylfuran selectivity was shown to be presence of iron oxide. This chapter aims at gaining some mechanistic insight for this selectivity through in situ infrared spectra investigations. In particular the three main components of reaction (scheme proposed in Chapter II see **Scheme 2.1**, namely methanol, furfural and furfuryl alcohol) were investigated separately on three different catalytic surfaces: MgO, $Fe_2O_3$ and most efficient mixed oxide obtained by impregnation, $FeO_x/MgO\_1\_10$. Noteworthy, the IR spectra of the different catalysts (MgO, $Fe_2O_3$ and FeOx/MgO_1_10) were acquired at different temperatures in the range from 25 °C to 400 °C. The spectra were subtracted with background collected at the corresponding temperature. Self supported catalyst was used as background to eliminate all signals arising from catalyst surface.

Analysis of the results (also through comparison with several available literature data) as well as comparative discussion is reported hereby.

## 3.2 Results and Discussion

### 3.2.1 Methanol Adsorption Desorption Techniques

In order to investigate the methanol activation over different surfaces, in situ DRIFTS strategy was employed. Exposure gas methanol over catalysts (MgO, $Fe_2O_3$ and FeOx/MgO_1_10) at room temperature and desorption at different temperature under dynamic vacuum gave information about how methanol reacts on the surfaces.

### 3.2.1.1 Literature Survey Vibration Frequency and Mode of Surface Species

Research activity on methanol has been vigorous because of its commercial importance as an alternative feedstock in fuel cells. When $CH_3OH$ is chemisorbed on a catalytic surface at ambient temperatures, it is usually present as a methoxy intermediate; the latter then undergoes extensive decomposition to yield a product distribution that depends upon the temperature. Methanol absorption on magnesia,[111, 113], iron oxide,[110] and relevant mixed oxides ( MgO and $Fe_2O_3$) have been already reported in the literature, and indicates that serval bonding modes of physisorbed methanol and activated methoxy species are possible.( see **Figure 3.1** )
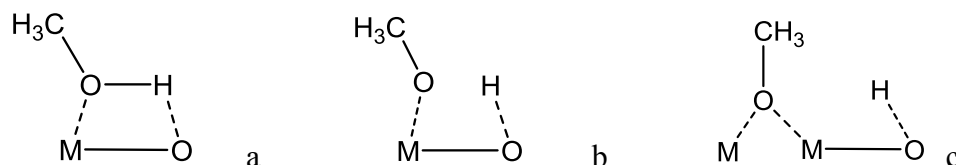


**Figure 3.1** Proposed modes of methanol adsorption over metal oxide the surface a) physical adsorbed, b) mono methoxy, c) bridging methoxy   M=Mg or Fe

Such studies also show that upon thermal treatment, several formates and carbonates species can be obtained major products of methanol activation at high temperatures.(see **Figure 3.2**)
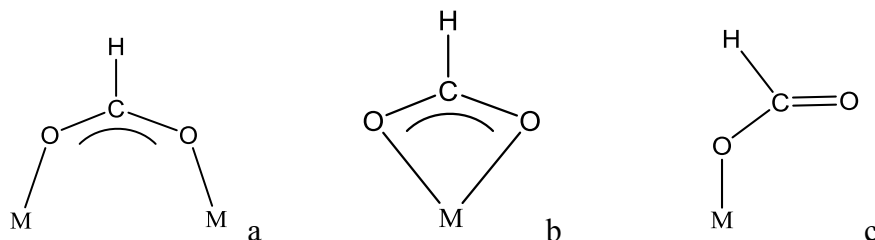


**Figure 3.2** Proposed modes of formate  adsorpted over metal oxide surface: a) bridging b) bidentate c)  monodentate  M=Mg or Fe
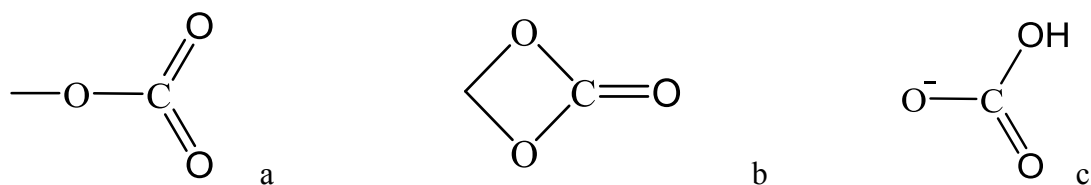
**Figure 3.3** Proposed modes of carbonate adopted over metal surface: a) unidentate carbonate

b) bidentate carbonate c) bi-carbonate or acid carbonate

Furthermore, Table 3.1 reports the summary of the different infrared modes bands, and their corresponding vibrational modes from literature.

**Table 3.1** Assignments for the bands in literature

| Surface Species | Mode Assignment | Catalyst | |
| --- | --- | --- | --- |
| | | MgO | Fe$_2$O$_3$ |
| Physisorbed Methanol $H_3C\diagdown OH$ | $v_s$(CH) | 2942[a] | 2925[d] |
| | $2\delta$(CH$_3$) | 2835[a] | 2824[d] |
| | $v_s$(CO) | 1058[a] | 1036[d] |
| Methoxy | | | |
| Methoxy Specie I $H_3C$ O—H M——O | $v_s$(CH) | 2917[a] | 2898[d] |
| | $2\delta$(CH$_3$) | 2809[a] | 2805[d] |
| | $v_s$(CO) | 1073[a] | 1070[d] |
| Methoxy Specie II $H_3C$ O H M——O | $v_s$(CH) | 2917[a] | – |
| | $2\delta$(CH$_3$) | 2809[a] | – |
| | $v_s$(CO) | 1073[a] | – |

| | | | |
|---|---|---|---|
| Methoxy Specie III  CH$_3$ | $v_{\mathrm{s}}$(CH) | 2917[(a)] | – |
| | $2\delta$(CH$_3$) | 2809[(a)] | – |
| M—O—M—O | $v_{\mathrm{s}}$(CO) | 1092[(a)] | – |
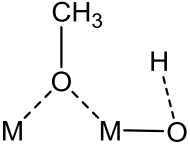
<div align="center">Formate</div>
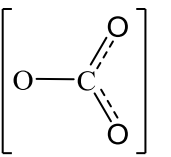
| Formate | $v_{\mathrm{s}}$(CH) | 2846[(b)] | 2880[(e)] |
|---|---|---|---|
| [O—C(=O)(=O)]$^-$ | $v_{\mathrm{s}}$(COO) | 1600-1620[(b)] | 1565[(e)] |
| | $v_{\mathrm{as}}$(COO) | 1330-1380[(b)] | 1350[(e)] |

Carbonate
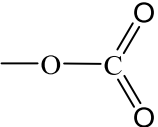
| Unidentate carbonate | $v_{\mathrm{s}}$(COO) | 1530-1470[(c)] | 1380-1395[(f)] |
|---|---|---|---|
| —O—C(=O)(=O) | $v_{\mathrm{as}}$(COO) | 1090-1020[(c)] | 1446-1590[(f)] |
| | $v_{\mathrm{s}}$(CO) | 1080-1040[(c)] | 1040[(f)] |
| Bidentate carbonate | $v_{\mathrm{s}}$(COO) | 1630-1590[(c)] | 1243-1355[(f)] |
| C=O | $v_{\mathrm{as}}$(COO) | | 1535-1670[(f)] |
| | $v_{\mathrm{s}}$(CO) | 1030-1020[(c)] | 1015[(f)] |
| Bicarbonate | $v_{\mathrm{s}}$(COO) | 1660-1620[(c)] | 1555-1720[(f)] |
| O$^-$—C(OH)(=O) | $v_{\mathrm{as}}$(COO) | – | 1396-1500[(f)] |
| | $v_{\mathrm{s}}$(CO) | 1050-990[(c)] | 1220-1226[(f)] |
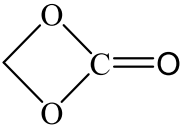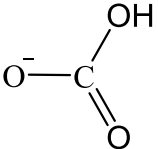
Note: (a) For methoxy over MgO see references [111, 181], (b) for formate over MgO see references [8], (c) carbonate over MgO see references [112], (d) methoxy over Fe$_2$O$_3$ see references [110, 182], (e) formate over Fe$_2$O$_3$ see references [110, 113, 183, 184], (f) carbonate over Fe$_2$O$_3$. [160]

These precedents show that substantial differences arise in DRTIFTS spectra with metal oxide surfaces, thus suggesting that DRIFTS is a valid spectroscopic tool to distinguish surface intermediate species for our work.

### 3.2.1.2 Over MgO

The spectra of methanol adsorbed on bulk MgO, after outgassing at different temperatures, are shown in **Figure 3.4**. At room temperature, two sets of peaks can be observed in the C-H region: one at 2944 and 2835 cm$^{-1}$, corresponding to physisorbed methanol, and the other at 2917 and 2798 cm$^{-1}$, assigned to mono-coordinated methoxy groups.[182] The $v_s$(C=O) bands corresponding to those species can be found at 1058 and 1108 cm$^{-1}$, respectively. [185] When the temperature was increased to 150 °C, new peaks appeared at 2809 and 1092 cm$^{-1}$, which were attributed to bridged methoxy species, based on the literature precedents reported in Table 3.1 . Further increase of the temperature causes a rapid formation of a species which we attribute to a formate isomer since it displays a $v_s$(CH) peak at 2846 cm$^{-1}$, a characteristic $v_{as}$(COO) at 1600-1610 cm$^{-1}$ and the $v_s$(COO) peaks in the 1379-1339 cm$^{-1}$ region, in agreement with data in **Table 3.1** .At 300 °C only formate and bridged methoxy species could be observed, and at 380 °C (the reaction temperature) only formate is present on the MgO surface. Formate species were not removed even when outgassing at 400°C, demonstrating the good stability of these species over MgO surface.
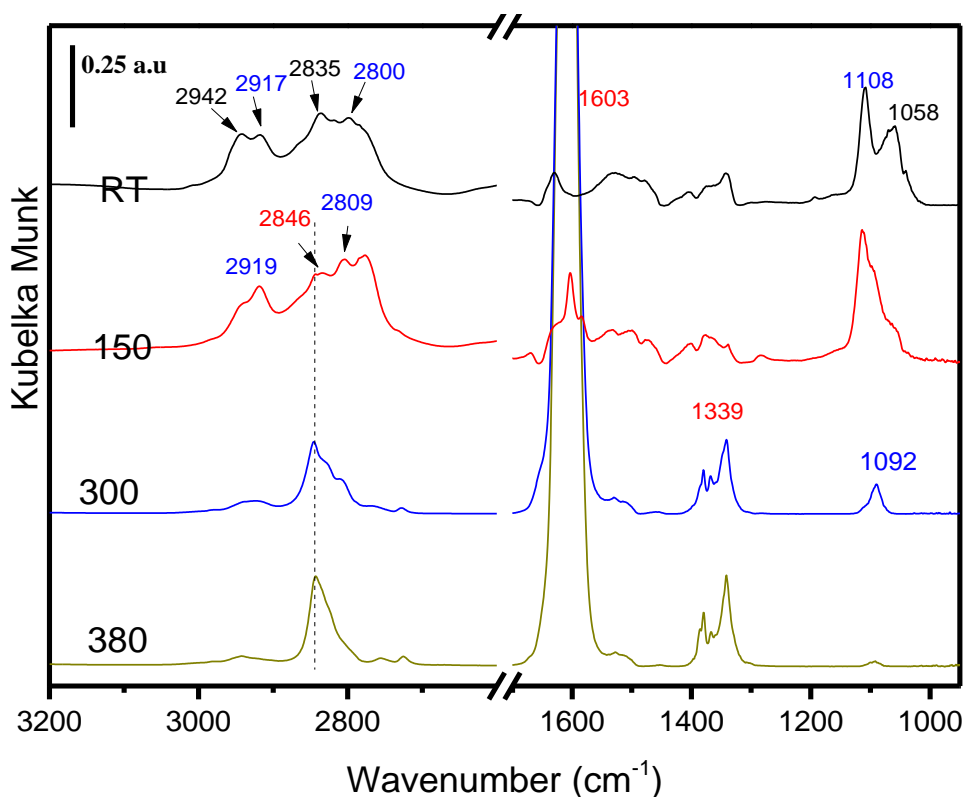
**Figure 3.5** Spectra of MgO with formic acid desorption using kinetic collecting mode from RT to 380°C

In order to further corroborate such assignment to a formate species, we independently exposed a pristine MgO surface to formic acid and recorded the DRIFTS spectra degassing upon thermal treatment. (see **Figure 3.5**.) As noted by Busca et al. the frequencies of formate ion may vary slightly if produced by formic acid adsorption or methanol oxidation and shift slightly upon heat treatment.[113] Peaks 1625 and 1605 cm$^{-1}$ was assignment for formate over MgO. The absence of a strong band close to 1740 cm$^{-1}$ (theoretic in gas phase formic acid) indicates that physical formic acid is not adsorbed on the surface of magnesia. When outgassing is performed higher than 300 °C the strongest band close to 1625 cm$^{-1}$ splits into three bonds, new peaks 1684, 1669 and 1605 cm$^{-1}$, suggesting that the surface formates are being decomposed, specifically, peak at 1669 cm$^{-1}$ collected at 300 °C is assigned to bidentate formate, similarly, the peak 1684 cm$^{-1}$

collected at 380°C is assigned to bi-carbonate, where the peak 1602 cm$^{-1}$ is belong to bridging formate species.

Indeed the formic acid exposure leads some common modes as the ones observed above with methanol; indicating that indeed one of the possible formate isomers is formed upon exposure of MgO to methanol and thermal treatment.

### 3.2.1.3 Over Fe₂O₃

Exposure α-Fe$_2$O$_3$ to methanol gas at room temperature gives rise to different IR absorption bands (**Figure 3.6**): similarly to what was observed over MgO surface, the peaks at 2942, 2832 cm$^{-1}$ are due to physical adsorbed methanol, and the ones at 2902, 2802 and 1071 cm$^{-1}$ correspond to methoxy species. At 300 °C the methoxy peaks have completely disappeared and a substantial amount of formate have been formed. This formate is activated in two different modes with $V_s$(CH) peaks at 2853 and 2804 cm$^{-1}$, $V_{as}$(COO) at 1644 and 1611 cm$^{-1}$ and the $V_s$(COO) around 1300 cm$^{-1}$. Outgassing at 380 °C causes the disappearance of the formate species (no CH vibrations observed) giving place to new species, presumably carbonates, suggested by the absence of C-H stretching bands at around 2800 cm$^{-1}$ while still observing $v_s$ and $v_{as}$(COO) bands. Additionally, correlation with temperature was shown in **Figure 3.7**, formate was formed after methoxy species saturated Fe$_2$O$_3$ surface. The formation of formate started at 175 °C and reached a maximum 320 °C. Meanwhile methoxy/methanol species disappeared rapidly at temperature higher than 200 °C.
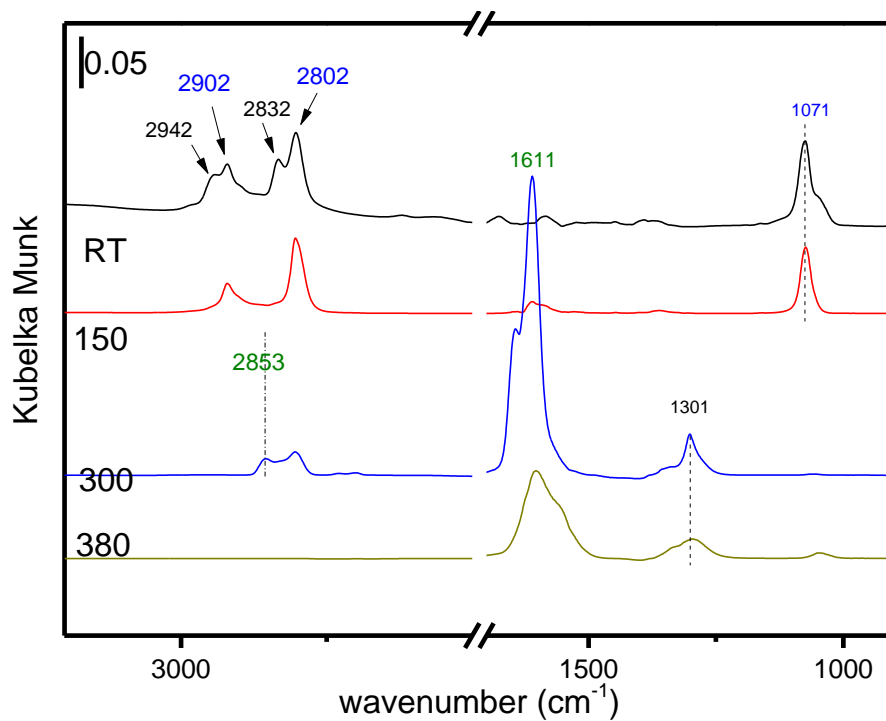
**Figure 3.6** Spectra of $Fe_2O_3$ with methanol desorption using kinetic collecting mode from RT to 380 °C black mark: physorbed methanol, blue mark :methoxy, red mark :formate,
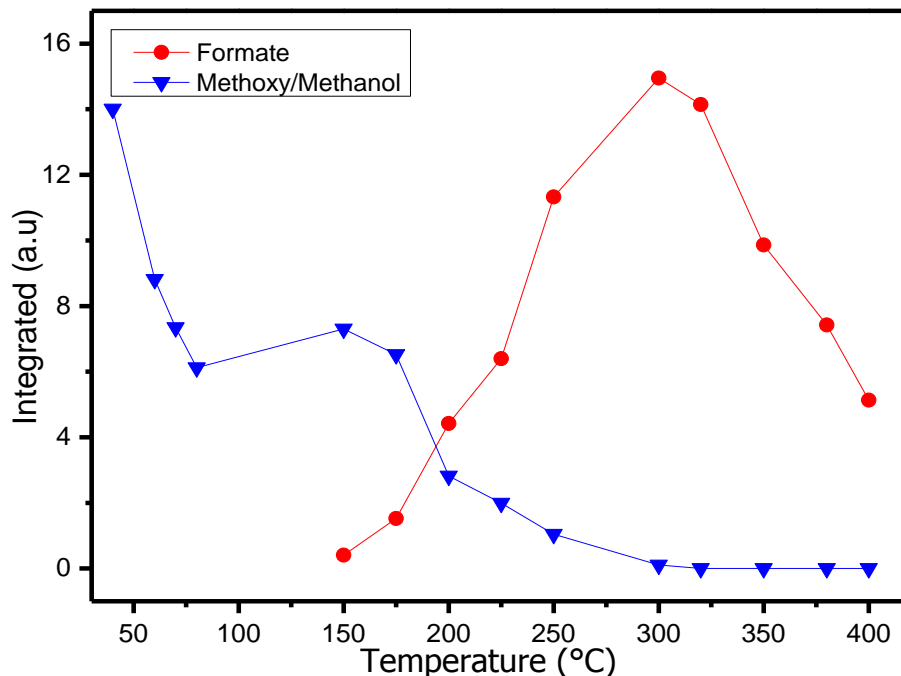
**Figure 3.7** Intergrated intensities of the $\nu(CO)$ bands from methanol and methoxy and the $\nu_{as}(COO)$ from formate species on the iron oxide surface as a function of temperature

### 3.2.1.4 Over Impregnated FeOx/MgO_1_10

The spectra recorded upon adsorption methanol on FeOx/MgO_1_10 sample at room temperature and outgassing at increasing temperatures are presented in **Figure 3.8**. Similarly to what was observed with the other two surfaces, at room temperature only physisorbed methanol and methoxy species are present on the surface (C-H vibrations between 2944 and 2807 cm$^{-1}$ and C-O stretching at 1073 and 1039 cm$^{-1}$). When increasing the temperature, physisorbed methanol rapidly dissociated to give methoxy species, which at 300 °C had been already completely converted into formate (peaks 1600 and between 1385 and 1330 cm$^{-1}$). Unexpectedly, a species that had not been observed over any other surface showed two peaks at 2787 cm$^{-1}$ (C-H vibration region) and 1121 cm$^{-1}$ (C-O stretching region). These vibration modes could indicate a methoxy species that formed on the interphase of FeOx and MgO, however, its high stability, even at 380 °C (when all other methoxy have disappeared), brings some doubt to this hypothesis.
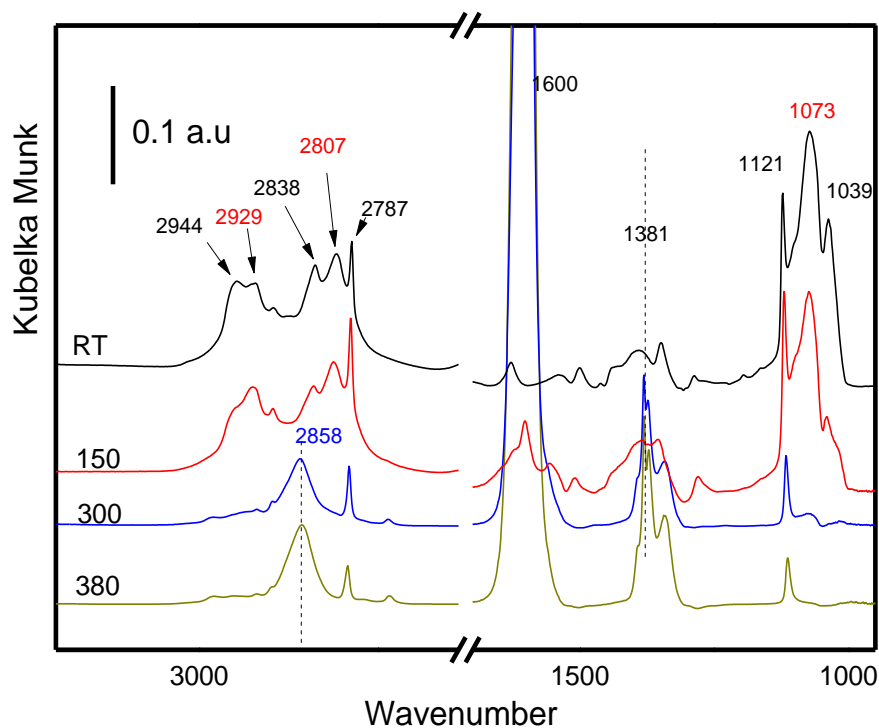
**Figure 3.8** Spectra of FeOx/MgO_1_10 with methanol desorption using kinetic collecting mode from RT to 380 °C black mark: physorbed methanol, blue mark :methoxy, red mark :formate,

### 3.2.1.5 Discussion of the DRIFTS results of methanol activation on different oxides

The experimental results on methanol adsorption and activation on the three oxides studies (MgO, $Fe_2O_3$, and FeOx/MgO_1_10.) presented above are summarized in **Table 3.2** where the assignments have been performed according to the literature precedents presented in **Table 3.1**.

**Table 3.2** Assignments for the bands observed in DRIFTS experiments

| Surface Species | Mode Assignment | Catalyst | | | Ref. |
|---|---|---|---|---|---|
| | | MgO | $Fe_2O_3$ | FeOx/MgO_1_10 | |
| Physisorbed Methanol | $v_S(CH)$ | 2942 | 2942 | 2944 | [111, 185- |
| | $2\delta(CH_3)$ | 2835 | 2832 | 2838 | |

| | | | | | |
|---|---|---|---|---|---|
| | $v_s(CO)$ | 1058 | _ | 1039 | 188] |
| Methoxy | $v_s(CH)$ | 2917[b] | 2902 | 2929 | [111, 182, 185] |
| | $2\delta(CH_3)$ | 2809, 2800 | 2802 | 2807 | |
| | $v_s(CO)$ | 1108 (Mono) 1092(Bridging) | 1071(Bridging) | 1073(Bridging) | |
| Formate | $v_s(CH)$ | 2846 | 2853 | 2846 | [113, 189, 190] |
| | $v_{as}(COO)$ | 1600-1610 | 1610-1620 | 1600-1665 | |
| | $v_s(COO)$ | 1330-1380 | 1300-1374 | 1330-1385 | |

As can be seen, the assignments agree within few wavenumbers with respect to the literature data and show that, as already discussed above: all oxide display a similar behavior : at moderate temperatures methanol physisorption and activation as methoxy species is observed; heating at higher temperature leads to the formation of formates. On magnesia such formate species appear stable until the highest temperatures explored (380°C). The spectra acquired on the mixed oxide are dominated by the magnesia feature. On the other hand, iron oxide promotes formate decomposition at higher temperature, most likely into light compounds.

### 3.2.2 DRIFTS Analysis under Steady-State Methanol Reaction

Steady-state methanol transformation was used to examine the change of species present on the metal oxide catalysts over time at the reaction temperature (380 °C) in the presence of excess methanol, an experimental condition present in our catalytic studies but not studied in the previous section, where only small quantities of methanol in batch condition where sent to the oxide surface.

Over MgO (**Figure 3.9**), a continuous flow of methanol generates methoxy (characteristic C-O bands around 1100 cm$^{-1}$) and formate species ($v_{as}(COO)$ at $\approx$ 1600 cm$^{-1}$) which coexist over

time, with no sign of catalyst degradation. Surprisingly, a very different behavior was observed when performing the same experiment over $Fe_2O_3$ (**Figure 3.10**). The baseline changed considerably during time, with the appearance of broad negative regions, implying that the catalyst (used as background) is suffering dramatic changes. This made impossible the identification of the species present on the surface. Finally, when the experiment was performed over FeOx/MgO_1_10 (**Figure 3.11**), a considerable amount of methoxy and formate species were observed, as in the MgO, but some negative bands, probably arising from the FeOx phase, could also be identified in the difference spectra reported here.[1] All samples containing the basic MgO showed an enhanced stability which was correspond to the results found in literature.[110]
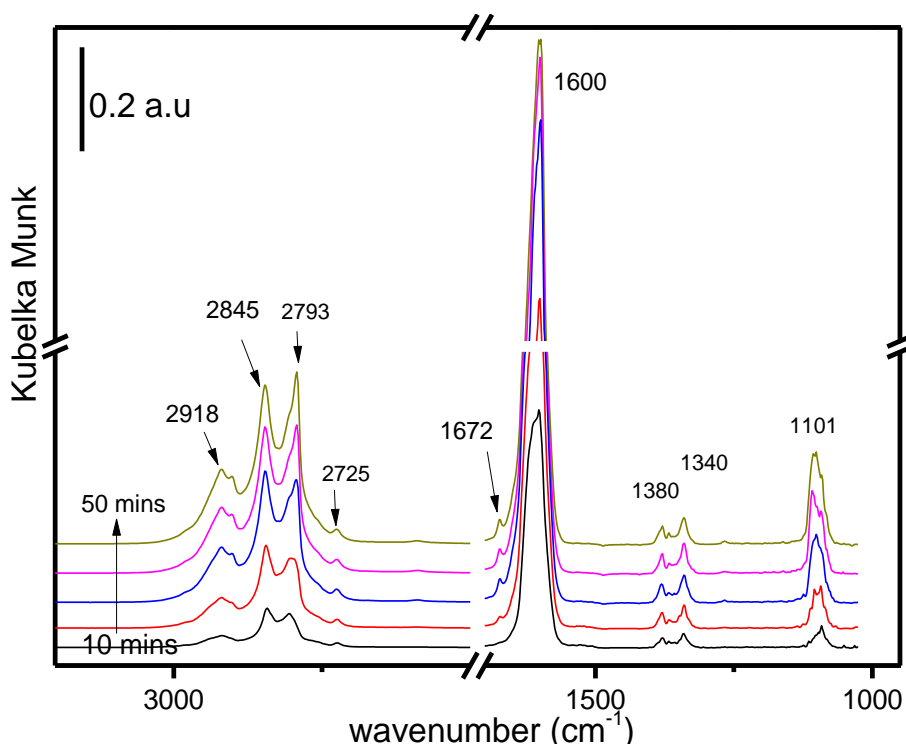


**Figure 3.9** MgO reaction at 380°C feeding with methanol under He flow

---

[1] As a reminder all the spectra presented here are difference spectra, where the background collected at the corresponding temperature has been subtracted from the sample spectrum.
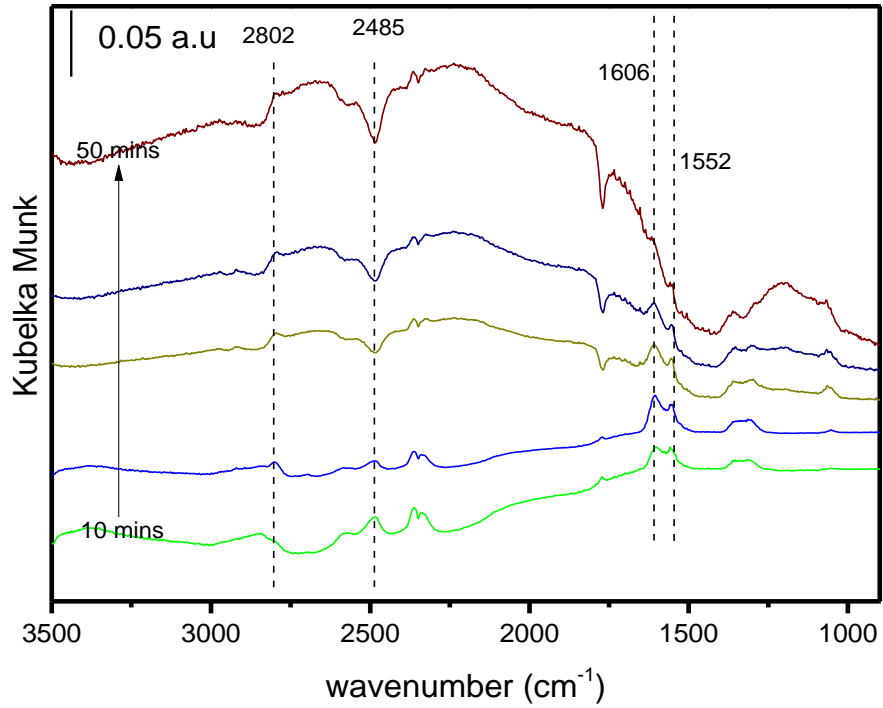
**Figure 3.10** $Fe_2O_3$ reaction at 380°C feeding with methanol under He flow
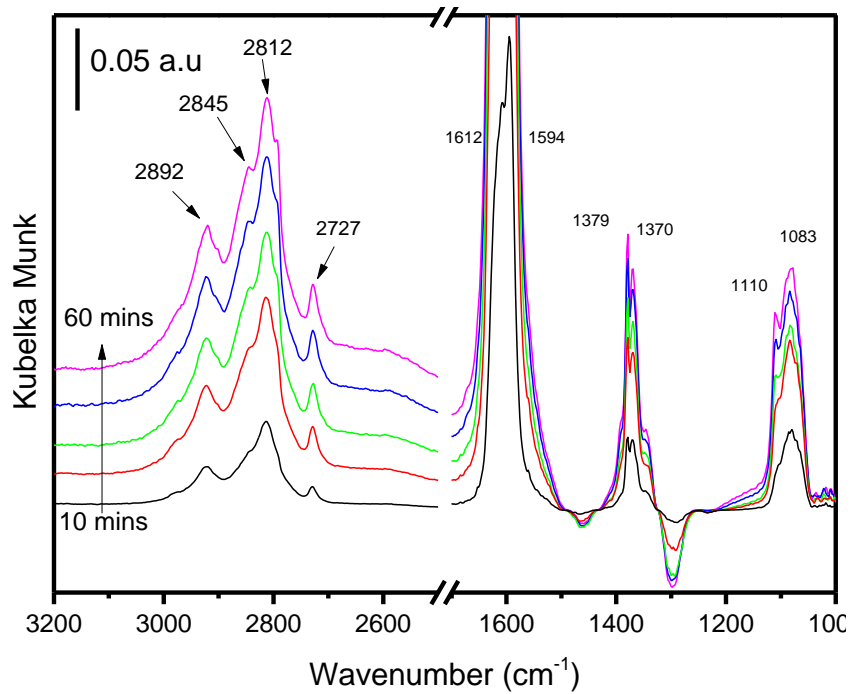


**Figure 3.11** FeOx/MgO_1_10 reaction at 380°C feeding with methanol under He flow

In summary, the DRIFTS experiment under methanol flow suggests that while magnesia displays the same surface reactivity over time (namely, creation of methoxy and formate species) even under excess methanol conditions, the iron oxide exposed to methanol undergoes profound structural changes during the thermal treatment. Noteworthy, such change in the iron oxide support is not observed in the absence of excess methanol, as discussed in the previous section (section **2.1.3** and section **2.1.5**).

### 3.2.3 Furfural and Furfuryl Alcohol Activation Analysis and Intermediates

The interest for this reaction system is methanol reduction of furfural (furfuryl alcohol) to methylfuran (see **Scheme 2.1 chapter II**). In order to identify the species involved during furfural (furfuryl alcohol) activation, we therefore investigated stepwise the furfural and then the furfuryl alcohol adsorption over different catalyst surfaces by FTIR. The goal is to acquire information about their geometric adsorption modes and their corresponded functional group activation.

The literature precedents which are relevant for this study mainly address furan [179] and aromatic aldehydes adsorption[191-193] on different types of oxides ($AuPd/TiO_2$ and $AuPd/MgO$). Meanwhile there are extensive investigations of the adsorption of aldehydes over different metals. [194, 195] It has been shown that over different type of metal surface aldehyde turn to either only the carbonyl O adsorbed $\eta^1$ (C=O) or both C and O interacting with the surface $\eta^2$ (C=O)

### 3.2.3.1 Furfural Adsorption-Desorption Investigations

The typical C=O stretching vibration modes of furfural appear at 1691 and 1674 $cm^{-1}$ [196]we independently confirmed this data by recording the IR spectrum of furfural over KBr pellet (see **Figure 3.12**). These vibration frequencies are lower than typical aldehydes (generally displaying at $v(CO) > 1700$ $cm^{-1}$, such as formaldehyde 1750 $cm^{-1}$.[197] The red shift in the spectra of furfural is due to the conjugation with the furan ring.
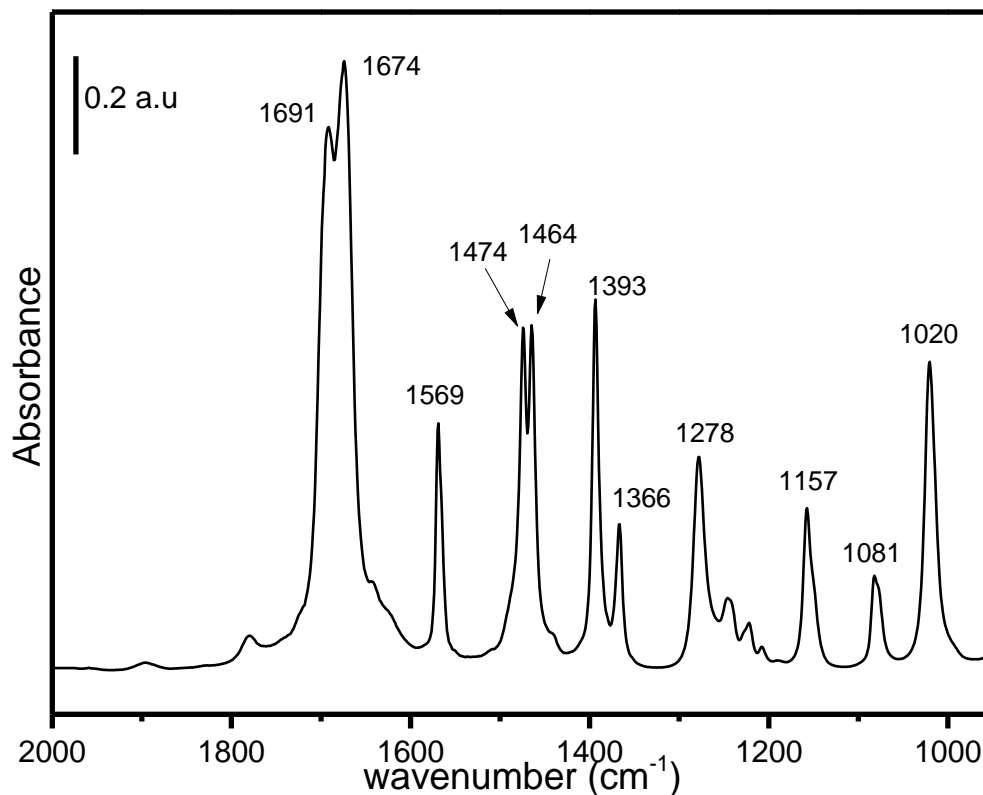
**Figure 3.12** Furfural IR spectra adsorption over pellet KBr surface**.**

Few studies reported the IR investigations of furfural after interaction with different surfaces, namely : Fe-Pt oxides/alumina[198], Fe-Ni/SiO$_2$ [22] and Cu/SiO$_2$ [18] interactions with the surface cause various types of shifts of $\nu$(C=O) frequency, these shifts can be at higher wavenumbers such as 1732 cm$^{-1}$ on FePt oxides/Al$_2$O$_3$ or at lower wavenumbers (1670 cm$^{-1}$ on Cu/SiO$_2$ and 1670 cm$^{-1}$.ove FeNi/SiO$_2$). The assignments proposed are respectively base on the asymmetric vibration model of C=O bond from furan side aldehyde, which can be influence by furan ring conjugation and surface interaction but overall a clear explanation of the reason for a blue or a red shift is not available.

Based on the previous literature review over furan, aldehyde, and furfural adsorption investigations we therefore propose the following interpretation scheme; furfural can interact with a surface either through its aldehyde group or through the furan ring (**Figure 3.13**).
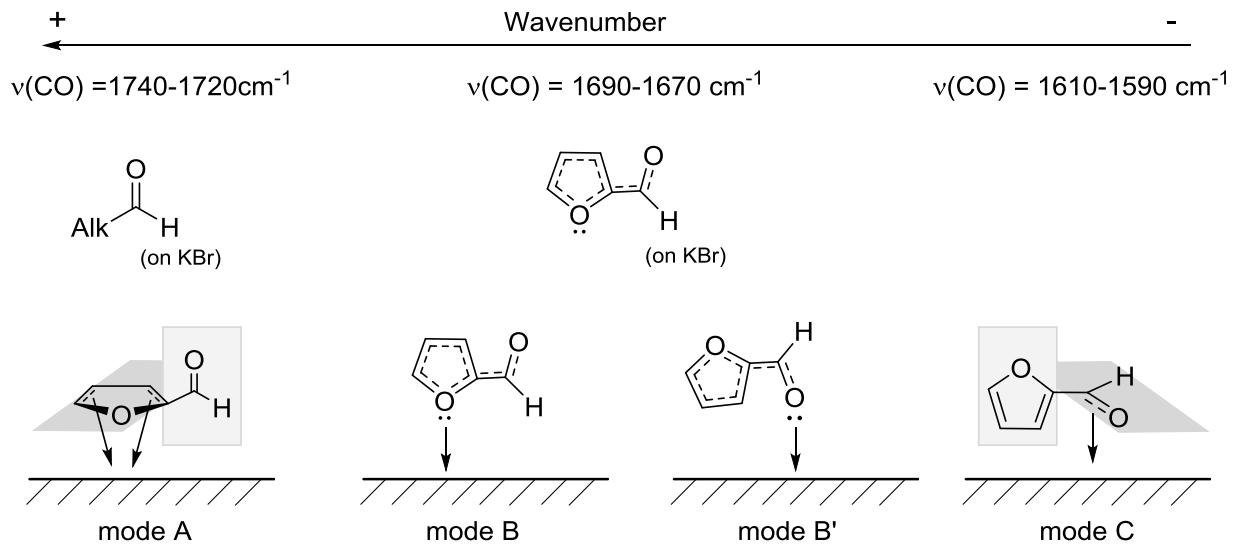
**Figure 3.13** Proposed rationalization of literature observed ν(CO) in free furfural and physisorbed furfural depending on the possible coordination modes (the planes represented in the picture help the reader visualize the planar moieties in the proposed structures)

Furfural surface coordination via the aldehyde can happen as a $\eta^1$(O) or $\eta^2$(C=O) mode (modes B' and C respectively, **Figure 3.13**), the latter inducing a greater red shifts due to a weakening of the C=O bond. Instead, coordination of the furfural through the furan ring should be possible through two different routes: namely through exclusively the oxygen lone pair (mode B) or through the ring double bonds (mode A).

While these modes of coordination are not expected to induce diagnostic changes in the furan-related bonding modes, we formulated the hypothesis that such modes can impact the aldehyde. The coordination modes involving only the oxygen lone pairs (mode B and B') do not disturb the furfural conjugation, thus similar C=O stretching frequencies to those of the free furfural are expected. However, when the furfural is coordinated through the furan ring (mode A), the aromaticity is partially disrupted and the ν(C=O) gets closer to that of an aliphatic aldehyde. On the other hand, when a $\eta^2$(C=O) coordination takes place (mode C), a remarkable red shift due to a weakening of the C=O bond should be observed.

Furthermore, as opposed to group IB metals, on which $\eta^1$-(O) aldehyde is the preferred surface species, group VIIIB metal surfaces tend to adsorb aldehydes in the so-called $\eta^2$(C,O) configuration.[195, 199]

**Over MgO**

When furfural was absorbed on MgO at room temperature (**Figure 3.14**), 3 peaks arising from the C=O stretching could be observed: at 1720, 1672 and 1600 cm$^{-1}$, corresponding to the modes A, B and C (**Figure 3.13**, respectively. The peak at 1569 cm$^{-1}$ arises from the C=C of the furan ring. As the temperature increases, the peaks at 1720 and 1672 cm$^{-1}$ decrease, and at 380 °C only the $\eta^2$(C=O) mode of activation is present (peak at 1600 cm$^{-1}$). This suggests that at this temperature we have an optimum activation of the C=O bond which might favor the formation of the furfuryl alcohol. [180, 200, 201] Furthermore, this experiment demonstrates that adsorbed furfural on MgO is stable even at high temperatures, as had already been confirmed by Albonetti *et al.*[149]
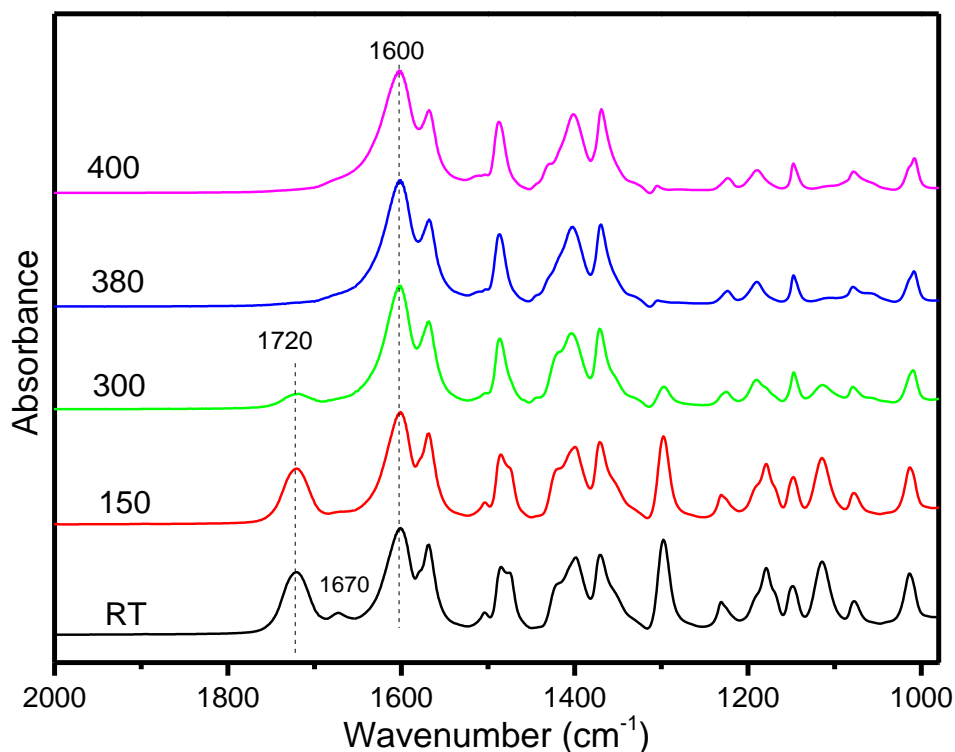


**Figure 3.14** Furfural adsorption and desorption over MgO sample from RT to 400°C

**Over FeOx/MgO_1_10**

The FTIR adsorption of furfural over $Fe_2O_3$ could not be performed due to the opacity of the obtained pellets, thus the experiment was directly carried out with FeOx/MgO_1_10 (see **Figure 3.15**). The obtained spectra were very similar to those of MgO, with the only exception that no peak at 1720 cm$^{-1}$ (corresponding to the furan ring adsorption on the surface) was observed. This may suggest that the presence of FeOx on the MgO causes a stronger interaction furfural-surface at lower temperatures.
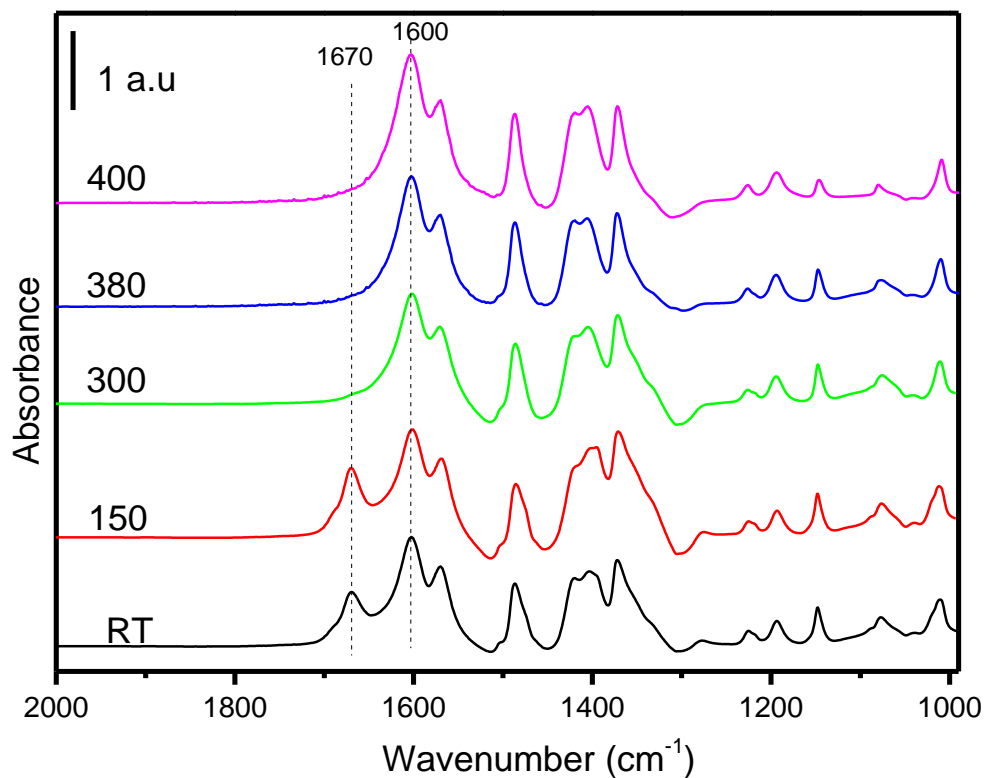


**Figure 3.15** Furfural adsorption / desorption over FeOx/MgO_1_10 sample from RT to 400°C

**3.2.3.2 Furfuryl Alcohol Adsorption Desorption Investigation**

Furfuryl alcohol adsorption-desorption FTIR was carried out at different temperatures. For comparison, the spectra of furfuryl alcohol adsorbed over KBr was recorded in **Figure 3.16**. The peak at 1505 cm$^{-1}$ corresponds to the furan ring C=C stretching, at 1146 cm$^{-1}$ to the C-O in the furan ring and at 1010 cm$^{-1}$ to the C-OH.
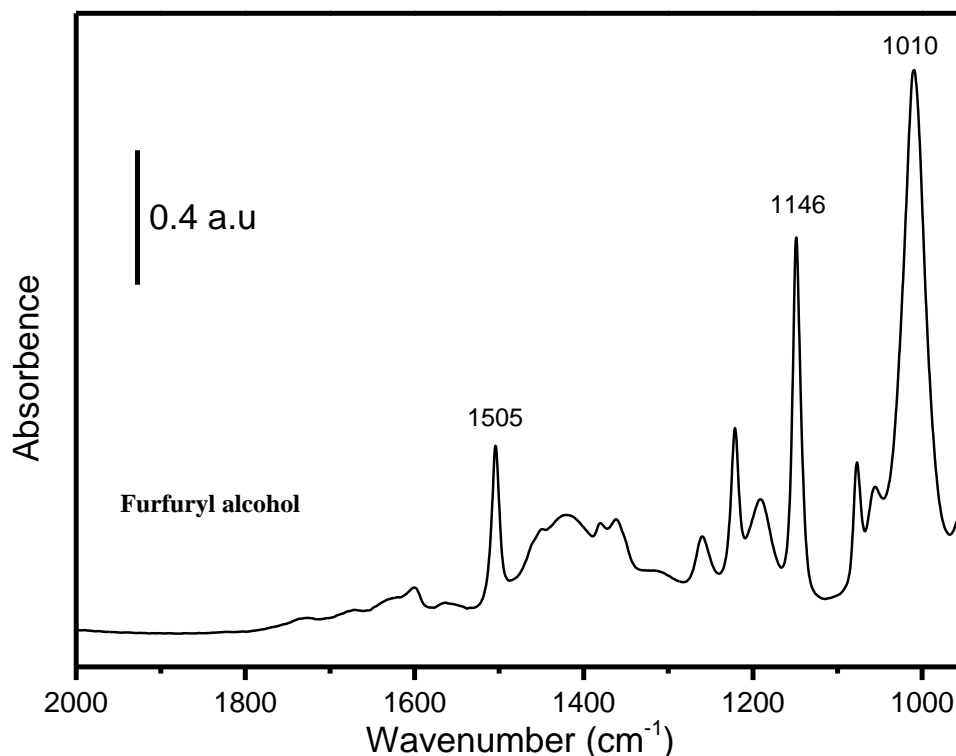
**Figure 3.16**. Furfuryl alcohol adsorption over KBr pellet surface**.**

**Over MgO**

When furfuryl alcohol was adsorbed over MgO at room temperature, almost no changes were observed with respect to the spectrum taken at over KBr, this meaning that very weak interactions are taking place. When the temperature increases, the furfuryl alcohol bands slowly decrease giving place to the appearance of a band at 1587 cm$^{-1}$, which at 400 °C is merged with a big band at 1602 cm$^{-1}$. This latter band is the same that had been observed for the adsorption of furfural on MgO (see **Figure 3.17**). Thus, this proves that, although high temperatures are required, furfuryl alcohol can be dehydrogenated on the MgO surface. Furthermore, it also shows the stability of these two compounds on MgO.
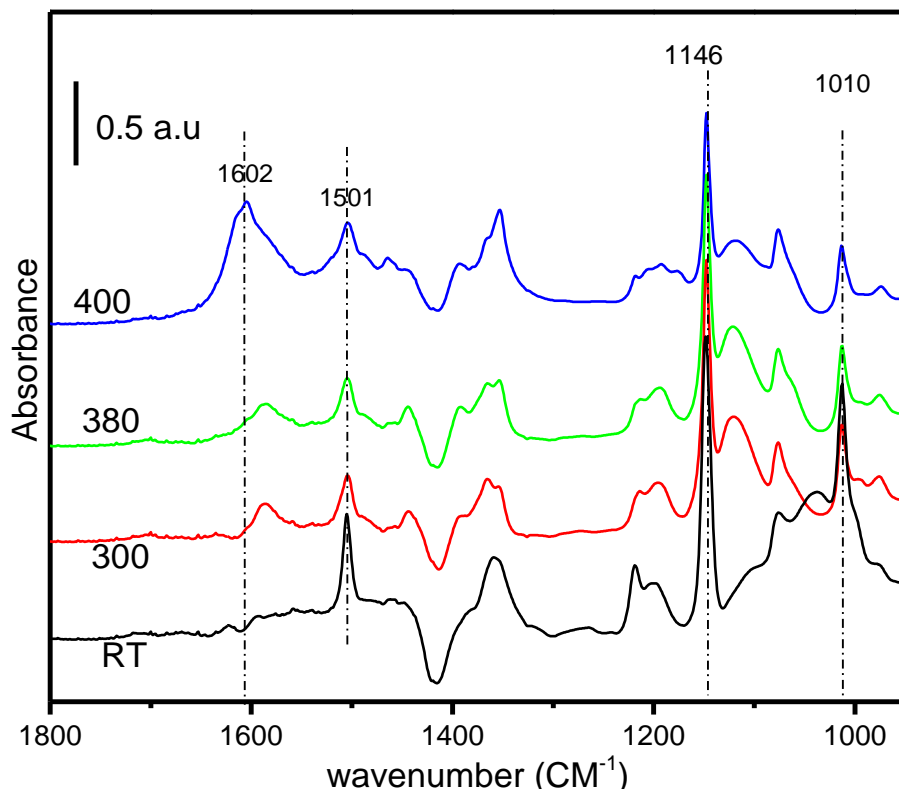
**Figure 3.17** FTIR Spectra of Furfuryl alcohol adosrption /desorption Over MgO at different temperature.

**Over FeOx/MgO_1_10**

A very similar spectrum was obtained when adsorbing furfuryl alcohol at room temperature on FeOx/MgO_1_10. (**Figure 3.18**) However, the dehydrogenation of the alcohol was initiated at lower temperatures (starting at 300 °C) than in the case of MgO. At 380 °C the furfuryl alcohol has almost disappeared and been converted quantitatively into furfural, as it can be followed by the band at 1505 cm$^{-1}$.
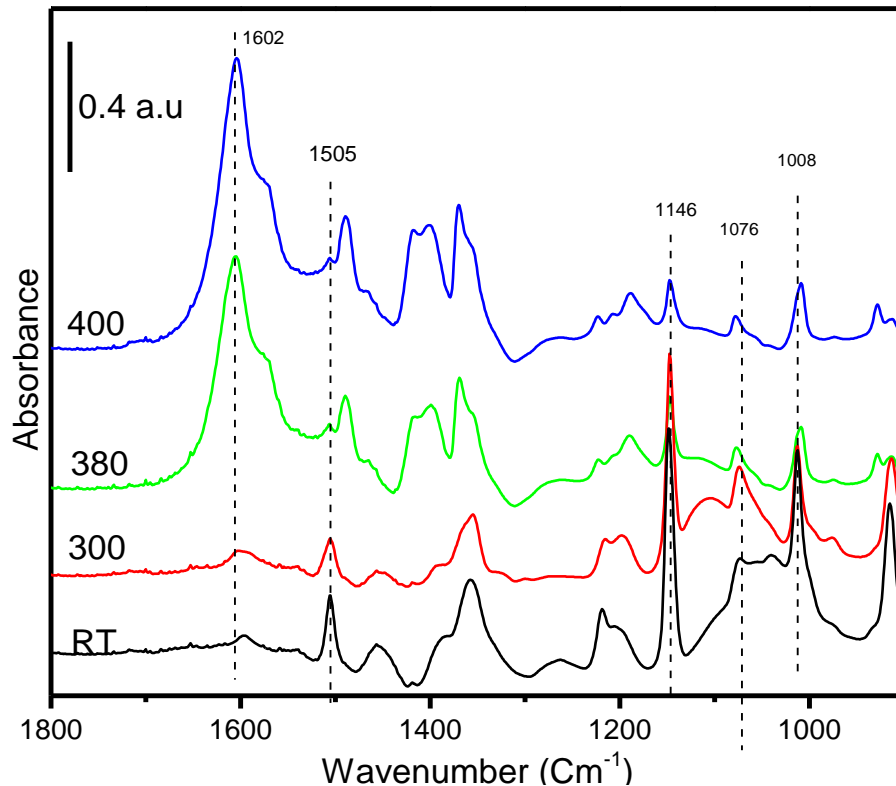
**Figure 3.18** Furfuryl alcohol adsorption /desorption over FeOx/MgO_1_10 within different temperature.

### 3.2.3 Isotopic Labeling Studies on the Catalytic Transfer Hydrogenation of Furfural to MF

**Hydrogenation of Furfural to FA**

As already described, the conversion of furfural to MFU entails, first, the hydrogenation of the carbonyl group of furfural to form FAL, and second, the hydrodeoxygenation of this latter to render MFU. To get a deeper mechanistic insight in the first step, an isotopic labeling experiment was performed. The reduction of FU to FAL was performed with FeOx/MgO_1_10 as catalyst at 200 °C and using $CD_3OD$ as solvent.

1H NMR analysis of the reaction mixture, after 3 h of reaction, showed that one deuterium atom had been incorporated in the methylene moiety of the FAL, as the integration of the peak at around 4.5 ppm integrates only for 1 H (**Figure 3.19**). The resulting alcohol must be also deuterated, due to the rapid H/D exchange of alcohols, although it cannot be observed by NMR.
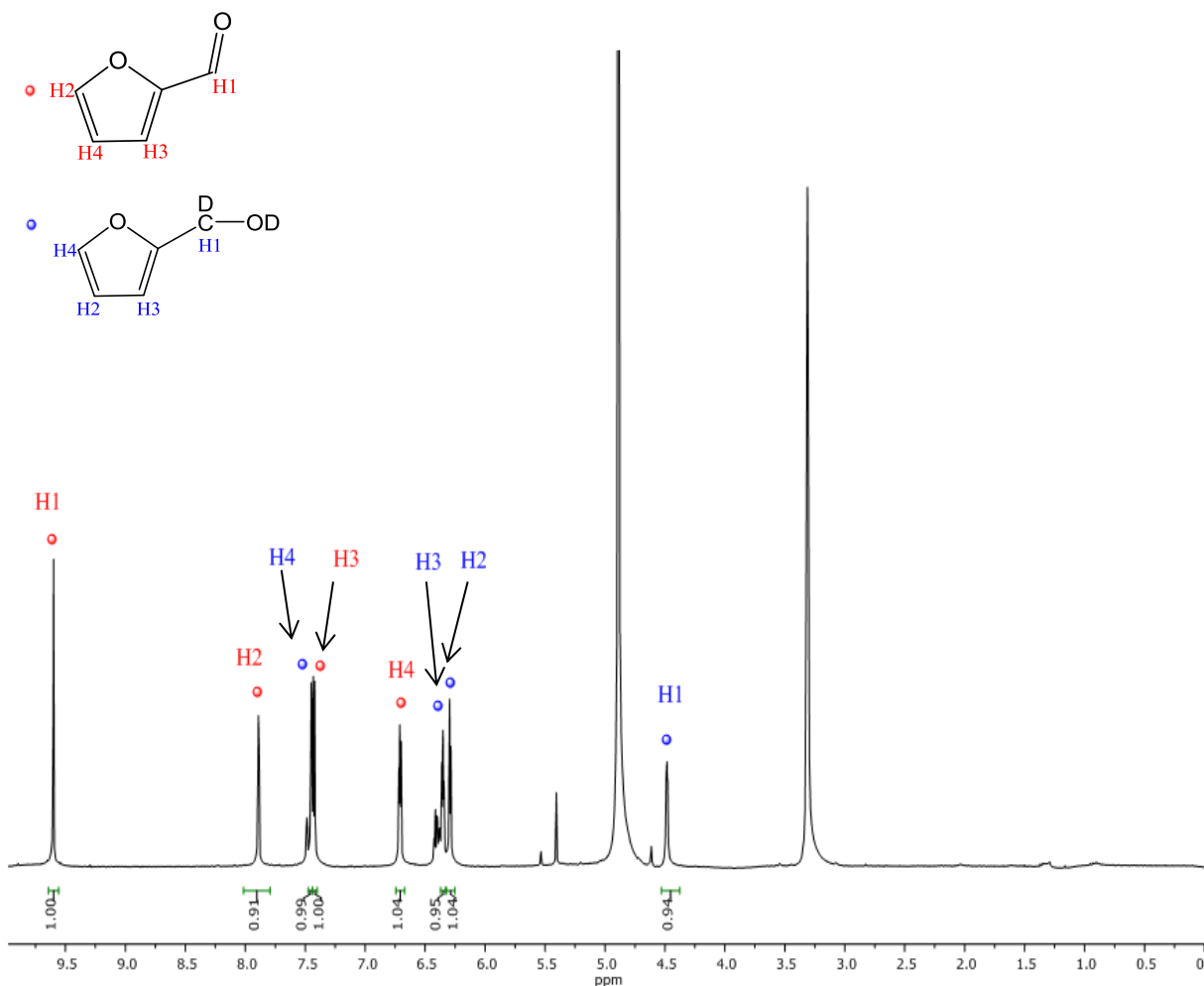
**Figure 3.19** Identification of product from furfural reaction at 380°C for 3 hours with $CD_3OD$ by ^{1}H NMR

Furthermore, GC-MS analysis was also performed. The parent ion of FAL (98 amu), in a reaction carried out with non-deuterated MeOH, is the most intense peak (red bars in Figure 3.18), and the small signal in 99 amu is attributed to the natural isotope abundance of [13]C. A clear mass shift by 1 amu was observed when $CD_3OD$ was used as the hydrogen donor (blue bars in **Figure 3.20**), indicating that the produced FAL molecule contains one D. The reason why only the addition of one deuterium atom, and not two, is observed can be rationalized by the fact that the deuterium in the OD group of FA can exchange with the OH groups in the capillary gas chromatograph (GC) column. Therefore, we conclude the 1 amu mass shift in the FAL formed

with $CD_3OD$ as the hydrogen donor originates from the D bonded to the hydroxymethyl carbon (**Figure 3.20**).
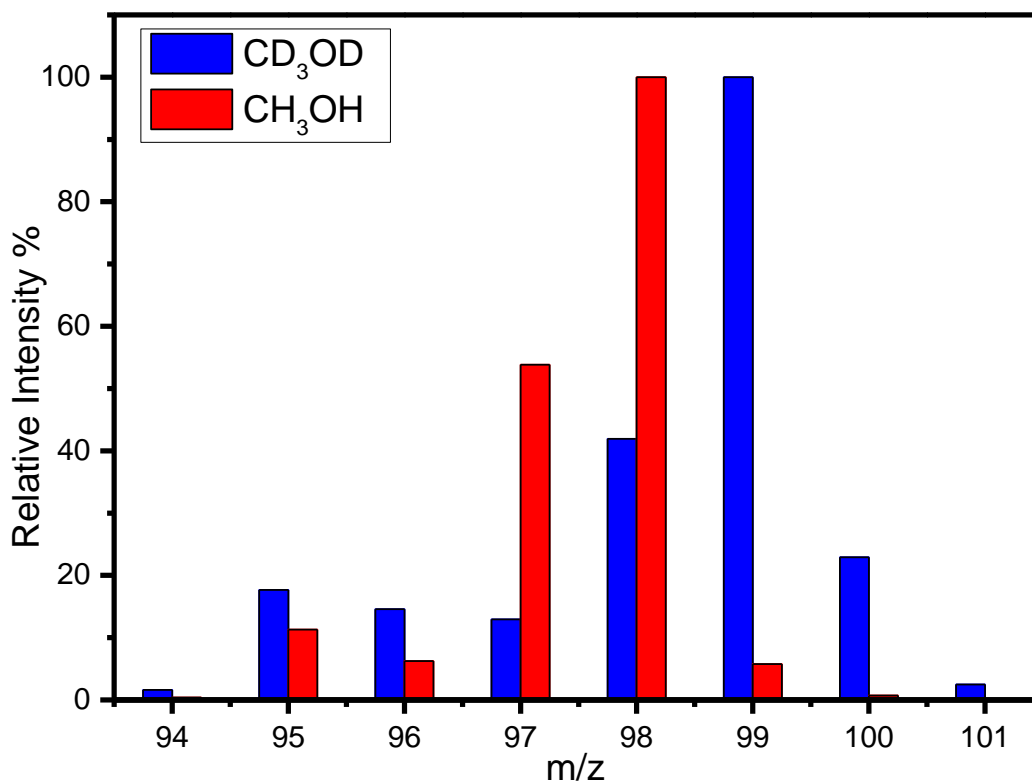


**Figure 3.20** Mass fragmentation analyses of the products of CTH of furfural. Mass spectra (all intensities scaled to 100%) of FA obtained from furfural hydrogenolysis in $CD_3OD$. Experimental conditions: 1 mmol furfural in 50 ml $CD_3OD$ solution; T = 200 °C, and reaction 3h

From these results, and comparing to literature precedent, two main pathways can be proposed for the hydrogenation of FU to FAL. A first option involves Lewis basic sites, as the ones that can be found in MgO. We have shown that MgO is able to catalyze the dehydrogenation of methanol (see section **2.1.2**), forming surface hydride species. The transfer of these hydrides to the aldehyde of furfural would reduce it to FAL (**Scheme.3.1 A**). A second option would involve a Meerwein–Ponndorf–Verley mechanism[75] at the Lewis acid sites of FeOx. This mechanism implies the formation of a six-membered ring where both the methanol and the aldehyde are coordinated to the Lewis acid and a hydride transfer from the methanol to the carbonyl group takes place (**Scheme. 3.1 B**).

However, in our system, the coexistence of basic sites (MgO) and acid sites (FeOx) makes possible that both pathways are taking place simultaneously. Although this experiment proved that all the hydrogenation come from the methanol, further deuterium experiments are needed to be able to distinguish if one of the two routes is predominant.
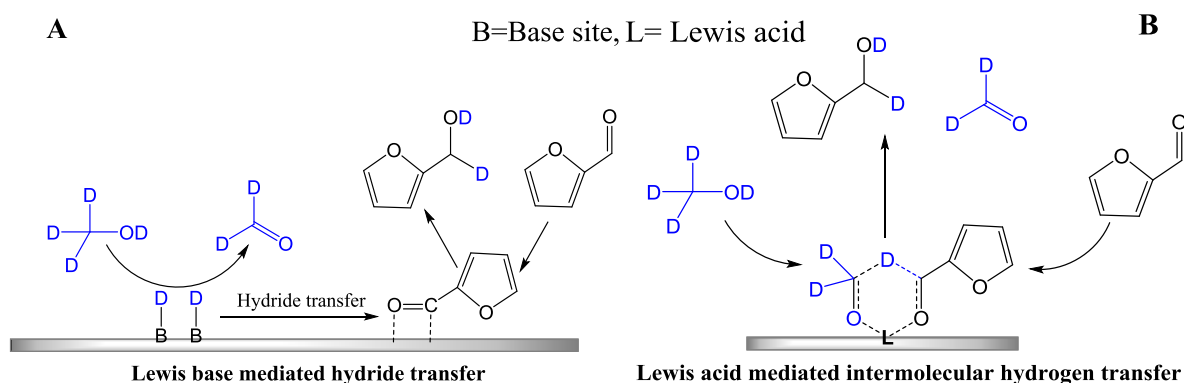


**Scheme.3.1** possible pathway for hydrogen transfer reduce of furfural into furfuryl alcohol over FeOx/MgO_1_10 using $CD_3OD$

## 3.3 Conclusion

### 3.3.1 Methanol Activation

To summarize the results described above, it can be concluded that adsorbed methanol dissociated at low temperatures to form methoxy species leading to the formation of surface formate species by at higher temperatures. The most accepted pathway for this transformation is via the formation of formaldehyde which rapidly disproportionates to give formate and methoxy species (**Figure 3.21**). The formation of formate and its stability is greatly improved when employing basic surfaces like MgO, compared to $Fe_2O_3$.
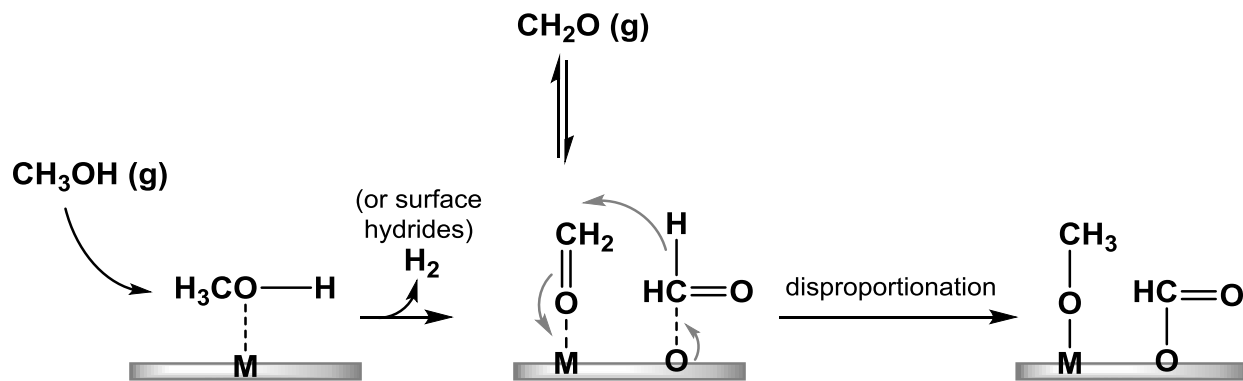
**Figure 3.21** The possible pathways responsible for the Methanol transformation

Furthermore, steady-state methanol reaction analysis at 380°C suggests that surface formate and methoxy species coexist over the surface; hence, both species and the surface hydrides should be considered as hydrogen donors.

### 3.3.2 Furfural & Furfuryl Alcohol Activation

Regarding furfural activation, no transformations were observed even at high temperatures, highlighting the high stability of it on MgO and FeOx in the absence of a reducing atmosphere. However, at the reaction temperature (380 °C), it seems that only the $\eta^2$(C=O) mode of furfural activation is present, and might be the necessary step for its further hydrogenation.

In contrast, furfuryl alcohol was dehydrogenated to furfural on both MgO and FeOx/MgO_1_10 at high temperatures, however, the latter is able to promote this transformation at lower temperatures (300 °C instead of 400 °C) and much more efficiently. This behavior was also confirmed by a previously reported catalytic experiment[149], where the loading furfuryl alcohol with methanol over MgO and Fe/Mg/O_1_2 catalyst, traces of furfural formation were identified.

The reduction of furfural to MF (**Scheme 3.2**), first involves the hydrogenation of the carbonyl group of furfural to produce furfuryl alcohol. The chemistry can proceed via hydride route, that is, the atomic hydrogen adsorbed on the surface formed by methanol dehydrogenation is the responsible of the reduction. An alternative pathway is the Lewis acid-mediated intermolecular hydride transfer of the β-H in the alcohol to the carbonyl group, following the Meerwein–Ponndorf–Verley mechanism. For the production of methyl furan, hydrogenolysis can proceed either via the direct route (i.e., the cleavage of the C–OH bond followed by H addition) or via the

activation of the furan ring, in which H is added to the ring to break the aromaticity and facilitate OH remove. Currently; more experiments are being performed to elucidate which are the predominant pathways in our gas phase system.
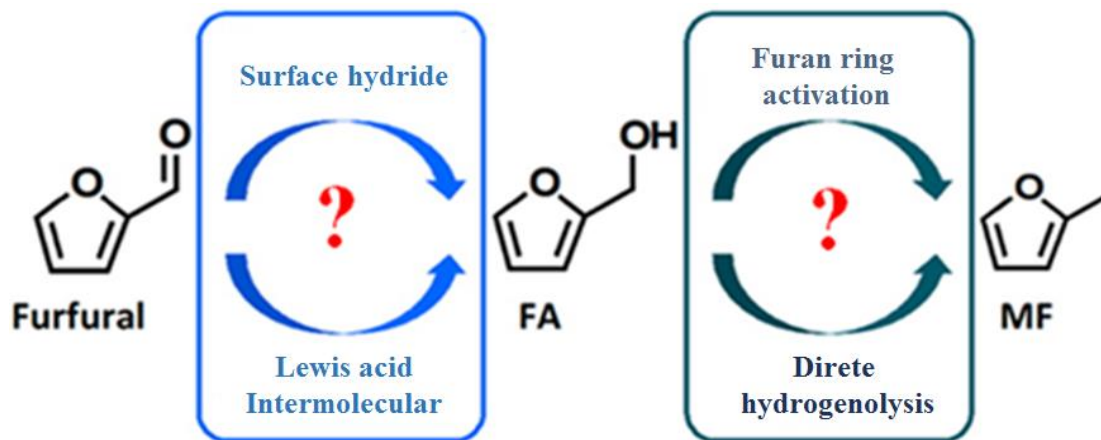


**Scheme 3.2** Possible Reaction Pathways in the HDO of Furfural to Methyl furan

## 3.4 Experimental Section

**Materials**

Methanol-$d_4$ (99.8%) and formic acid (96%) were purchased from Aldrich. all the chemical was used without purification.

**Fourier Transform infrared spectroscopy (FTIR) of supported catalysts**

The FTIR was used to record vibrational spectra of furfural adsorbed on the catalysts. The FTIR spectra of adsorbed furfural were recorded with 2 cm$^{-1}$ resolution using a Thermo Nicolet Nexus 470 spectrometer equipped with a MCT-A (mercury cadmium tellurid) detector.

**Operando DRIFTS Measurements**

New spectroscopic and kinetic methods for catalysis for the DRIFTS measurements, a commercial reaction cell (Harrick) fitted with $CaF_2$ windows was implemented into a Nicolet 6700 FTIR spectrometer (Thermo Fischer Scientific) equipped with a MCT detector.

**Steady state methanol DRIFT**

Sample was loaded in the DRIFT chamber and pretreated under He heating at 400°C for 60 min, after pretreatment, the background was collected at 380°C. The methanol was loaded by bubbling He through the methanol saturator. Kinetic spectra were collected per minutes using self-supported sample as background. The He flow was fixed at 15 ml/min and the methanol was loaded from a saturator which was kept in a liquid $N_2$/ethanol cooling bath (-80°C).

**In situ Furfural and Furfuryl alcohol FTIR study**

Measurements were carried out in Niocolet 6700, between 4000 and 400 cm$^{-1}$. Self-supported wafers of the samples containing around 30 mg (13 mm diameter) were evacuated at 10$^{-6}$ bar and 450 °C for 1 h, after cooling to room temperature, the spectrum was recorded as a background. The sample wafer was then exposed to furfuryl alcohol vapors at room temperature for 10 min until equilibrium was reached, and then a second spectrum was recorded. Subsequently, the wafer was subjected to evacuation for 10 min and then a room temperature spectrum was recorded. Subsequent evacuations were performed at 300, 320, 350 380 and 400 °C for 5 min followed by spectral acquisitions. The spectra presented were obtained by subtracting the spectra recorded after pretreatment and before furfuryl alcohol adsorption.

# General Discussion and Conclusion

This study has aimed at improving and understanding gas phase catalytic transfer hydrogenation of furfural (FU) to furfuryl alcohol (FAL) and sequential hydrogenolysis into methyl furan (MFU).

Initial results showed that MgO catalyst was a competent catalyst for the reduction of furfural to furfuryl alcohol (52% FU conversion and 75% FAL selectivity), see **Scheme 1**. However, when Fe doped MgO (Fe/Mg/O_1_2) was employed, methyl furan was preferentially formed (79% MFU selectivity with 93% FU conversion), see **Scheme 2.**
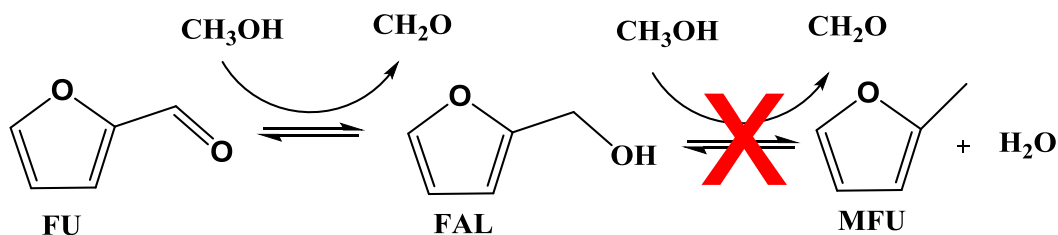


**Scheme 1** catalytic hydrogen transfer over MgO catalyst at 380 °C using methanol as hydrogen donor
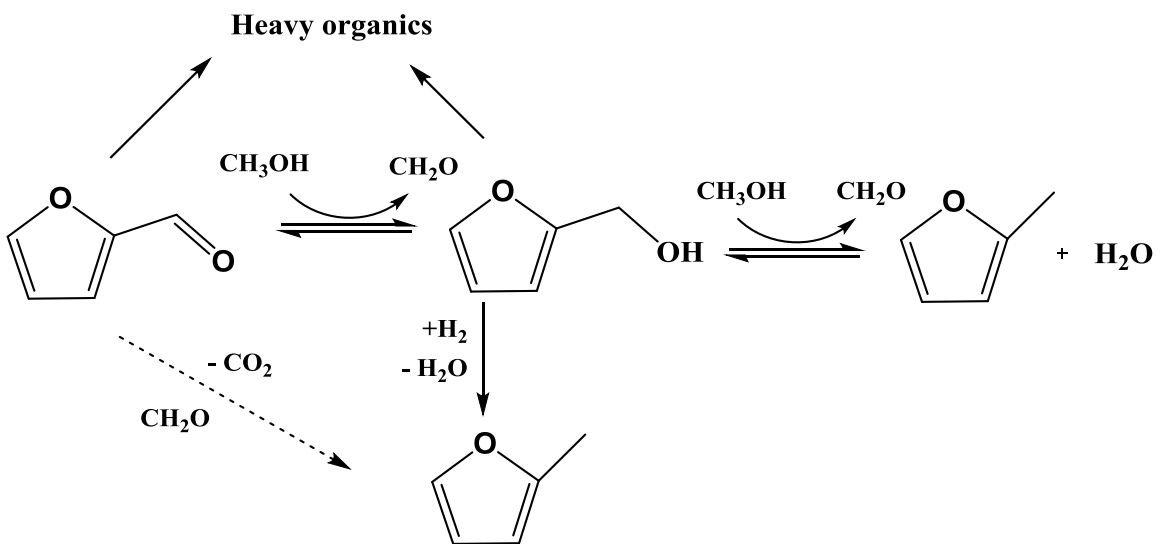


**Scheme 2** catalytic hydrogen transfer over Fe/Mg/O catalyst at 380 °C using methanol as hydrogen donor

These results led us to investigate how iron oxide influenced the product distribution, especially towards methyl furan formation. Series of catalysts with different iron and magnesium molar

ratios were prepared by co-precipitation or impregnation methods and were tested in the reduction of furfural (FU) using methanol as hydrogen source. As expected, furfuryl alcohol (FAL) and 2-methyl furan (MFU) were the main products obtained. The impregnated catalysts with a Fe/Mg ratio 1/10, namely FeOx/MgO_1_10, demonstrated to be the most active and selective towards MFU (FU conversion 89%, MFU selectivity 93%).

Reported data demonstrated that product distribution was strongly influenced by the iron content and from the resulting acid and redox properties of the material. As a matter of fact, the introduction of iron on the surface of the basic oxide led to the addition of Lewis acidity and redox capacity in the system, significantly enhancing FU conversion and MFU production. However, an optimal Fe/Mg ratio (observed both in co-precipitated and impregnated samples) is necessary for a high MFU selectivity.

The activation of different species on the catalyst surface has been studied by in situ methanol DRIFTS and furfural and furfuryl alcohol FTIR. Results indicated that, at the reaction temperature (380 °C), methanol is activated on the catalyst surface generating formate species. These latter species formate are quite stable over the FeOx/MgO_1_10 catalyst, but easily decompose over $Fe_2O_3$. As regard to furfural and furfuryl alcohol activation, FeOx was found more suitable for furfuryl alcohol activation, since it catalyzes the dehydrogenation to furfural more readily than MgO. These results do not clarify which is the final hydrogen donor, since many species coexist on the catalyst surface: methoxy, formate, hydrides… However, it seems reasonable to assume that MgO favors the initial transfer hydrogenation of furfural to furfuryl alcohol, and that the redox capacity from FeOx might be the responsible of furfuryl alcohol hydrogenolysis.

# Perspectives

Initially, biomass valorization was a new concept proposed to face the energy shortage and the requirement of sustainable chemistry. Thus, biomass utilization could tend to process real applications as the main goal, more like technology and development. Its investigation should not aim at creating new reaction. Instead, a smart integration of known reaction processes to optimally produce the required compounds should be the final goal. At the moment, routes towards fine chemicals are more competitive than transformation into fuels on the economic purpose.

Owing to the high diversity and complexity of products obtained from biomass transformation processes, efficient and fast analytical procedures are required to keep up to date with this fast development. Such as humin, there is still no conclusion about their structure and composition. As regard to fundamental investigations, analytical chemistry tools could help to understand the underlying mechanisms involved in the production control and determination of the reaction pathways. With the possibility to scale up the production pilot plants, concerns on the bio-fuels quality, the stability and up scaling rely strongly on analytical approaches. Analytical standards should be implemented to be able to compare these complex mixtures.

Synergies effects between acid–base sites and redox capacity should be emphasized and detailed investigations to real active site. With hypothesis, catalysts with tailored site compositions and well-defined structure, e.g., well defined metal nanoparticles supported on acidic basic supports, in model reactions, it will be helpful in illustrate the synergistic effects among different types of active sites. Most catalytic transfer reduction reactions are carried out in liquid phase, so the influence of solvent should also place more emphasis. Therefore, characterization capable of taking solvent effects on catalytic sites into account will be highly desirable.

As regard to hydrogen transfer reduction processes, starting from cellulose derived feedstocks, catalytic hydrogen transfer strategies show promise yield, but the application in lignin based precursors remain relatively unexplored. In this field, catalytic transfer hydrogenations have the potential to selectively activate C–O bonds in the depolymerization of lignin and HDO of phenolic monomers and dimers.

# Acknowledgement

# Reference

[1]     D.M. Alonso, J.Q. Bond, J.A. Dumesic, Green Chemistry 12 (2010) 1493-1513.

[2]     L.R. LYND, J.H. CUSHMAN, R.J. NICHOLS, C.E. WYMAN, Science 251 (1991) 1318-1323.

[3]     A.E. Atabani, A.S. Silitonga, I.A. Badruddin, T.M.I. Mahlia, H.H. Masjuki, S. Mekhilef, Renewable and Sustainable Energy Reviews 16 (2012) 2070-2093.

[4]     C.E. Wyman, B.E. Dale, R.T. Elander, M. Holtzapple, M.R. Ladisch, Y.Y. Lee, Bioresource Technology 96 (2005) 1959-1966.

[5]     H.-Y. Zheng, Y.-L. Zhu, B.-T. Teng, Z.-Q. Bai, C.-H. Zhang, H.-W. Xiang, Y.-W. Li, Journal of Molecular Catalysis A: Chemical 246 (2006) 18-23.

[6]     H.E. Hoydonckx, W.M. Van Rhijn, W. Van Rhijn, D.E. De Vos, P.A. Jacobs, Ullmann's Encyclopedia of Industrial Chemistry, Wiley-VCH Verlag GmbH & Co. KGaA, 2000.

[7]     J.Z. Karl, in: J.Z. Karl (Ed.), Sugar Series, Elsevier, 2000, pp. 98-103.

[8]     H.M.G. E.Ricard, US Pat., 1929.

[9]     W.Lazier, Process for hydrogenation furfural 1937, p. 2077422.

[10]    S.Swadesh, Catalytic production of furfuryl alcohol and catalyst therefor, USA, 1956.

[11]    J. Wu, Y. Shen, C. Liu, H. Wang, C. Geng, Z. Zhang, Catalysis Communications 6 (2005) 633-637.

[12]    J.O. M.Bankmann, T.Tacke US.pat., 1997.

[13]    L.R. Baker, G. Kennedy, M. Van Spronsen, A. Hervier, X. Cai, S. Chen, L.-W. Wang, G.A. Somorjai, Journal of the American Chemical Society 134 (2012) 14208-14216.

[14]    R. Rao, A. Dandekar, R.T.K. Baker, M.A. Vannice, Journal of Catalysis 171 (1997) 406-419.

[15]    D. Liu, D. Zemlyanov, T. Wu, R.J. Lobo-Lapidus, J.A. Dumesic, J.T. Miller, C.L. Marshall, Journal of Catalysis 299 (2013) 336-345.

[16]    H. Zhang, Y. Lei, A.J. Kropf, G. Zhang, J.W. Elam, J.T. Miller, F. Sollberger, F. Ribeiro, M.C. Akatay, E.A. Stach, J.A. Dumesic, C.L. Marshall, Journal of Catalysis 317 (2014) 284-292.

[17]    F. Dong, Y. Zhu, H. Zheng, Y. Zhu, X. Li, Y. Li, Journal of Molecular Catalysis A: Chemical 398 (2015) 140-148.

[18]    S. Sitthisa, T. Sooknoi, Y. Ma, P.B. Balbuena, D.E. Resasco, Journal of Catalysis 277 (2011) 1-13.

[19]    B.M. Nagaraja, V. Siva Kumar, V. Shasikala, A.H. Padmasri, B. Sreedhar, B. David Raju, K.S. Rama Rao, Catalysis Communications 4 (2003) 287-293.

[20]    D. Vargas-Hernández, J.M. Rubio-Caballero, J. Santamaría-González, R. Moreno-Tost, J.M. Mérida-Robles, M.A. Pérez-Cruz, A. Jiménez-López, R. Hernández-Huesca, P. Maireles-Torres, Journal of Molecular Catalysis A: Chemical 383–384 (2014) 106-113.

[21]    R.S. Rao, R.T.K. Baker, M.A. Vannice, Catalysis Letters 60 (1999) 51-57.

[22]    S. Sitthisa, W. An, D.E. Resasco, Journal of Catalysis 284 (2011) 90-101.

[23]    K. An, N. Musselwhite, G. Kennedy, V.V. Pushkarev, L. Robert Baker, G.A. Somorjai, Journal of Colloid and Interface Science 392 (2013) 122-128.

[24]    W. Huang, H. Li, B. Zhu, Y. Feng, S. Wang, S. Zhang, Ultrasonics Sonochemistry 14 (2007) 67-74.

[25]    B.M. Reddy, G.K. Reddy, K.N. Rao, A. Khan, I. Ganesh, Journal of Molecular Catalysis A: Chemical 265 (2007) 276-282.

[26]    C. Xu, L. Zheng, D. Deng, J. Liu, S. Liu, Catalysis Communications 12 (2011) 996-999.

[27]     F.N. Peters, US pat., 1933.
[28]     H.A.a.R. Connor, US pat., USA, 1937.
[29]     L.J.F.a.H.H. Fineberg, US pat., 1981
[30]     in: J.Z. Karl (Ed.), Sugar Series, Elsevier, 2000, pp. 150-155.
[31]     B.J. O'Neill, D.H.K. Jackson, A.J. Crisci, C.A. Farberow, F. Shi, A.C. Alba-Rubio, J. Lu, P.J. Dietrich, X. Gu, C.L. Marshall, P.C. Stair, J.W. Elam, J.T. Miller, F.H. Ribeiro, P.M. Voyles, J. Greeley, M. Mavrikakis, S.L. Scott, T.F. Kuech, J.A. Dumesic, Angewandte Chemie International Edition 52 (2013) 13808-13812.
[32]     P.D. Vaidya, V.V. Mahajani, Industrial & Engineering Chemistry Research 42 (2003) 3881-3885.
[33]     M. Pierre, US pat. , 1956.
[34]     M. Lesiak, M. Binczarski, S. Karski, W. Maniukiewicz, J. Rogowski, E. Szubiakiewicz, J. Berlowska, P. Dziugan, I. Witońska, Journal of Molecular Catalysis A: Chemical 395 (2014) 337-348.
[35]     M. Audemar, C. Ciotonea, K. De Oliveira Vigier, S. Royer, A. Ungureanu, B. Dragoi, E. Dumitriu, F. Jérôme, ChemSusChem 8 (2015) 1885-1891.
[36]     Q. Yuan, D. Zhang, L.v. Haandel, F. Ye, T. Xue, E.J.M. Hensen, Y. Guan, Journal of Molecular Catalysis A: Chemical 406 (2015) 58-64.
[37]     A.B. Merlo, V. Vetere, J.F. Ruggera, M.L. Casella, Catalysis Communications 10 (2009) 1665-1669.
[38]     V. Vetere, A.B. Merlo, J.F. Ruggera, M.L. Casella, Journal of the Brazilian Chemical Society 21 (2010) 914-920.
[39]     S. Liu, Y. Amada, M. Tamura, Y. Nakagawa, K. Tomishige, Green Chemistry 16 (2014) 617-626.
[40]     K. Fulajtárova, T. Soták, M. Hronec, I. Vávra, E. Dobročka, M. Omastová, Applied Catalysis A: General 502 (2015) 78-85.
[41]     S. Srivastava, P. Mohanty, J.K. Parikh, A.K. Dalai, S.S. Amritphale, A.K. Khare, Chinese Journal of Catalysis 36 (2015) 933-942.
[42]     H. Li, H. Luo, L. Zhuang, W. Dai, M. Qiao, Journal of Molecular Catalysis A: Chemical 203 (2003) 267-275.
[43]     B. Miya, US pat., USA, 1981.
[44]     K. Yan, A. Chen, Energy 58 (2013) 357-363.
[45]     K. Yan, A. Chen, Fuel 115 (2014) 101-108.
[46]     M.M. Villaverde, N.M. Bertero, T.F. Garetto, A.J. Marchi, Catalysis Today 213 (2013) 87-92.
[47]     R.V. Sharma, U. Das, R. Sammynaiken, A.K. Dalai, Applied Catalysis A: General 454 (2013) 127-136.
[48]     C. Xu, L. Zheng, J. Liu, Z. Huang, Chinese Journal of Chemistry 29 (2011) 691-697.
[49]     M.J. Climent, A. Corma, S. Iborra, Green Chemistry 16 (2014) 516-547.
[50]     W. Yu, Y. Tang, L. Mo, P. Chen, H. Lou, X. Zheng, Catalysis Communications 13 (2011) 35-39.
[51]     W. Yu, Y. Tang, L. Mo, P. Chen, H. Lou, X. Zheng, Bioresource Technology 102 (2011) 8241-8246.
[52]     J.G. Stevens, R.A. Bourne, M.V. Twigg, M. Poliakoff, Angewandte Chemie International Edition 49 (2010) 8856-8859.

[53]	Z. Li, S. Kelkar, C.H. Lam, K. Luczek, J.E. Jackson, D.J. Miller, C.M. Saffron, Electrochimica Acta 64 (2012) 87-93.
[54]	S.K. Green, J. Lee, H.J. Kim, G.A. Tompsett, W.B. Kim, G.W. Huber, Green Chemistry 15 (2013) 1869-1879.
[55]	B. zhao, M. Chen, Q. Guo, Y. Fu, Electrochimica Acta 135 (2014) 139-146.
[56]	R. Noyori, M. Yamakawa, S. Hashiguchi, The Journal of Organic Chemistry 66 (2001) 7931-7944.
[57]	M. Koehle, R.F. Lobo, Catalysis Science & Technology 6 (2016) 3018-3026.
[58]	J.J. Ramos, V.K. Díez, C.A. Ferretti, P.A. Torresi, C.R. Apesteguía, J.I. Di Cosimo, Catal Today 172 (2011) 41-47.
[59]	R. Cohen, C.R. Graves, S.T. Nguyen, J.M.L. Martin, M.A. Ratner, Journal of the American Chemical Society 126 (2004) 14796-14803.
[60]	M. Chia, J.A. Dumesic, Chemical Communications 47 (2011) 12233-12235.
[61]	X. Tang, L. Hu, Y. Sun, G. Zhao, W. Hao, L. Lin, RSC Advances 3 (2013) 10277-10284.
[62]	X. Tang, H. Chen, L. Hu, W. Hao, Y. Sun, X. Zeng, L. Lin, S. Liu, Applied Catalysis B: Environmental 147 (2014) 827-834.
[63]	J. Wang, S. Jaenicke, G.-K. Chuah, RSC Advances 4 (2014) 13481-13489.
[64]	L. Bui, H. Luo, W.R. Gunther, Y. Román-Leshkov, Angewandte Chemie International Edition 52 (2013) 8022-8025.
[65]	J. Song, L. Wu, B. Zhou, H. Zhou, H. Fan, Y. Yang, Q. Meng, B. Han, Green Chemistry 17 (2015) 1626-1632.
[66]	Z. Yang, Y.-B. Huang, Q.-X. Guo, Y. Fu, Chemical Communications 49 (2013) 5328-5330.
[67]	Y. Kuwahara, W. Kaburagi, T. Fujitani, RSC Advances 4 (2014) 45848-45855.
[68]	X.-L. Du, L. He, S. Zhao, Y.-M. Liu, Y. Cao, H.-Y. He, K.-N. Fan, Angewandte Chemie International Edition 50 (2011) 7815-7819.
[69]	X.-L. Du, Q.-Y. Bi, Y.-M. Liu, Y. Cao, K.-N. Fan, ChemSusChem 4 (2011) 1838-1843.
[70]	T. Thananatthanachon, T.B. Rauchfuss, Angewandte Chemie International Edition 49 (2010) 6616-6618.
[71]	J. Mitra, X. Zhou, T. Rauchfuss, Green Chemistry 17 (2015) 307-313.
[72]	S. De, S. Dutta, B. Saha, ChemSusChem 5 (2012) 1826-1833.
[73]	J. Tuteja, H. Choudhary, S. Nishimura, K. Ebitani, ChemSusChem 7 (2014) 96-100.
[74]	T.S. Hansen, K. Barta, P.T. Anastas, P.C. Ford, A. Riisager, Green Chemistry 14 (2012) 2457-2461.
[75]	T. Pasini, A. Lolli, S. Albonetti, F. Cavani, M. Mella, Journal of Catalysis 317 (2014) 206-219.
[76]	J. Jae, W. Zheng, R.F. Lobo, D.G. Vlachos, ChemSusChem 6 (2013) 1158-1162.
[77]	B. Saha, M.M. Abu-Omar, ChemSusChem 8 (2015) 1133-1142.
[78]	D. Scholz, C. Aellig, I. Hermans, ChemSusChem 7 (2014) 268-275.
[79]	A.S. Nagpure, A.K. Venugopal, N. Lucas, M. Manikandan, R. Thirumalaiswamy, S. Chilukuri, Catalysis Science & Technology 5 (2015) 1463-1472.
[80]	M.M. Villaverde, T.F. Garetto, A.J. Marchi, Catalysis Communications 58 (2015) 6-10.
[81]	P. Panagiotopoulou, N. Martin, D.G. Vlachos, Journal of Molecular Catalysis A: Chemical 392 (2014) 223-228.
[82]	M.J. Gilkey, P. Panagiotopoulou, A.V. Mironenko, G.R. Jenness, D.G. Vlachos, B. Xu, ACS Catalysis 5 (2015) 3988-3994.

[83]    L.-H. Gong, Y.-Y. Cai, X.-H. Li, Y.-N. Zhang, J. Su, J.-S. Chen, Green Chemistry 16 (2014) 3746-3751.
[84]    G. Warner, T.S. Hansen, A. Riisager, E.S. Beach, K. Barta, P.T. Anastas, Bioresource Technology 161 (2014) 78-83.
[85]    X. Wang, R. Rinaldi, Angewandte Chemie International Edition 52 (2013) 11499-11503.
[86]    X. Wang, R. Rinaldi, Energy & Environmental Science 5 (2012) 8244-8260.
[87]    L. Wang, B. Zhang, X. Meng, D.S. Su, F.-S. Xiao, ChemSusChem 7 (2014) 1537-1541.
[88]    D. Scholz, C. Aellig, C. Mondelli, J. Pérez-Ramírez, ChemCatChem 7 (2015) 1551-1558.
[89]    H. Kobayashi, H. Matsuhashi, T. Komanoya, K. Hara, A. Fukuoka, Chemical Communications 47 (2011) 2366-2368.
[90]    Y. Liu, H. Tuysuz, C.-J. Jia, M. Schwickardi, R. Rinaldi, A.-H. Lu, W. Schmidt, F. Schuth, Chemical Communications 46 (2010) 1238-1240.
[91]    A. Konaka, T. Tago, T. Yoshikawa, A. Nakamura, T. Masuda, Applied Catalysis B: Environmental 146 (2014) 267-273.
[92]    E. Arceo, P. Marsden, R.G. Bergman, J.A. Ellman, Chemical Communications  (2009) 3357-3359.
[93]    H.P. Reddy Kannapu, C.A. Mullen, Y. Elkasabi, A.A. Boateng, Fuel Processing Technology 137 (2015) 220-228.
[94]    M.a.A. Aramendía, V. Borau, C. Jiménez, J.M. Marinas, J.R. Ruiz, F.J. Urbano, Applied Catalysis A: General 244 (2003) 207-215.
[95]    A. Corma, M.E. Domine, S. Valencia, Journal of Catalysis 215 (2003) 294-304.
[96]    B.M. Nagaraja, A.H. Padmasri, P. Seetharamulu, K. Hari Prasad Reddy, B. David Raju, K.S. Rama Rao, Journal of Molecular Catalysis A: Chemical 278 (2007) 29-37.
[97]    B.M. Nagaraja, A.H. Padmasri, B.D. Raju, K.S. Rama Rao, International Journal of Hydrogen Energy 36 (2011) 3417-3425.
[98]    M.a.A. Aramendía, V. Borau, C. Jiménez, J.M. Marinas, J.R. Ruiz, F.J. Urbano, Journal of Molecular Catalysis A: Chemical 171 (2001) 153-158.
[99]    I. Gandarias, P.L. Arias, S.G. Fernández, J. Requies, M. El Doukkali, M.B. Güemez, Catalysis Today 195 (2012) 22-31.
[100]   F. Jin, J. Yun, G. Li, A. Kishita, K. Tohji, H. Enomoto, Green Chemistry 10 (2008) 612-615.
[101]   W. Leitner, Angewandte Chemie International Edition in English 34 (1995) 2207-2221.
[102]   T.C. Johnson, D.J. Morris, M. Wills, Chemical Society Reviews 39 (2010) 81-88.
[103]   S. Enthaler, J. von Langermann, T. Schmidt, Energy & Environmental Science 3 (2010) 1207-1217.
[104]   M. Grasemann, G. Laurenczy, Energy & Environmental Science 5 (2012) 8171-8181.
[105]   Q. Luo, G. Feng, M. Beller, H. Jiao, The Journal of Physical Chemistry C 116 (2012) 4149-4156.
[106]   J. Yu, J. B. Spencer, Chemical Communications  (1998) 1935-1936.
[107]   J. Yu, J.B. Spencer, Chemistry – A European Journal 5 (1999) 2237-2240.
[108]   S. Rajagopal, A.F. Spatola, Applied Catalysis A: General 152 (1997) 69-81.
[109]   J. Feng, C. Yang, D. Zhang, J. Wang, H. Fu, H. Chen, X. Li, Applied Catalysis A: General 354 (2009) 38-43.
[110]   M. Bowker, E.K. Gibson, I.P. Silverwood, C. Brookes, Faraday Discussions 188 (2016) 387-398.
[111]   M. Bensitel, O. Saur, J.C. Lavalley, Materials Chemistry and Physics 28 (1991) 309-320.

[112]   J.V. Evans, T.L. Whateley, Transactions of the Faraday Society 63 (1967) 2769-2777.

[113]   G. Busca, J. Lamotte, J.C. Lavalley, V. Lorenzelli, Journal of the American Chemical Society 109 (1987) 5197-5202.

[114]   M.D. Marcinkowski, C.J. Murphy, M.L. Liriano, N.A. Wasio, F.R. Lucci, E.C.H. Sykes, ACS Catalysis  (2015) 7371-7378.

[115]   R.H. Perry, K.R. Brownell, K. Chingin, T.J. Cahill, R.M. Waymouth, R.N. Zare, Proceedings of the National Academy of Sciences 109 (2012) 2246-2250.

[116]   N. Ballarini, F. Cavani, L. Maselli, S. Passeri, S. Rovinetti, Journal of Catalysis 256 (2008) 215-225.

[117]   M. Boronat, A. Corma, M. Renz, The Journal of Physical Chemistry B 110 (2006) 21168-21174.

[118]   C.P. Jiménez-Gómez, J.A. Cecilia, D.e. Durán-Martín, R.n. Moreno-Tost, J. Santamaría-González, J. Mérida-Robles, R. Mariscal, P. Maireles-Torres, Journal of Catalysis 336 107-115.

[119]   P. Panagiotopoulou, D.G. Vlachos, Applied Catalysis A: General 480 (2014) 17-24.

[120]   P. Panagiotopoulou, N. Martin, D.G. Vlachos, ChemSusChem 8 (2015) 2046-2054.

[121]   M. Manikandan, A.K. Venugopal, A.S. Nagpure, S. Chilukuri, T. Raja, RSC Advances 6 3888-3898.

[122]   B.M. Nagaraja, A.H. Padmasri, P. Seetharamulu, K. Hari Prasad Reddy, B. David Raju, K.S. Rama Rao, Journal of Molecular Catalysis A: Chemical 278 (2007) 29-37.

[123]   T.P. Sulmonetti, S.H. Pang, M.T. Claure, S. Lee, D.A. Cullen, P.K. Agrawal, C.W. Jones, Applied Catalysis A: General 517 187-195.

[124]   P. Biswas, J.-H. Lin, J. Kang, V.V. Guliants, Applied Catalysis A: General 475 379-385.

[125]   W.-S. Lee, Z. Wang, W. Zheng, D.G. Vlachos, A. Bhan, Catalysis Science & Technology 4 2340-2352.

[126]   Y. Liu, M.A. Mellmer, D.M. Alonso, J.A. Dumesic, ChemSusChem 8 (2015) 3983-3986.

[127]   W. Yu, K. Xiong, N. Ji, M.D. Porosoff, J.G. Chen, Journal of Catalysis 317 253-262.

[128]   R.M. Williams, S.H. Pang, J.W. Medlin, The Journal of Physical Chemistry C 118 27933-27943.

[129]   S. Sitthisa, T. Pham, T. Prasomsri, T. Sooknoi, R.G. Mallinson, D.E. Resasco, Journal of Catalysis 280 (2011) 17-27.

[130]   J.W. Medlin, ACS Catalysis 1 (2011) 1284-1297.

[131]   V. Vorotnikov, G. Mpourmpakis, D.G. Vlachos, ACS Catalysis 2 (2012) 2496-2504.

[132]   E. Montiel, J. Cruz, J.C. Gonzales, N. Jayanthi, T. Pandiyan, Journal of Cluster Science 22 459-471.

[133]   H. Sheng, R.F. Lobo, ChemCatChem  (2016) n/a-n/a.

[134]   G. Dimas-Rivera, J. de la Rosa, C. Lucio-Ortiz, J. De los Reyes Heredia, V. González, T.s. Hernández, Materials 7 527.

[135]   P. Mars, D.W. van Krevelen, Chemical Engineering Science 3 (1954) 41-59.

[136]   A.V. Mironenko, D.G. Vlachos, Journal of the American Chemical Society 138 (2016) 8104-8113.

[137]   C. Michel, P. Gallezot, ACS Catalysis 5 4130-4132.

[138]   M. Dusselier, B.F. Sels, in: K.M. Nicholas (Ed.), Selective Catalysis for Renewable Feedstocks and Chemicals, Springer International Publishing, Cham, 2014, pp. 85-125.

[139]   L.W. Burnett, I.B. Johns, R.F. Holdren, R.M. Hixon, Industrial & Engineering Chemistry 40 (1948) 502-505.

[140]  H. Xiao, P. Zeng, Z. Li, L. Zhao, X. Fu, Fuel 175 157-163.
[141]  X. Wang, R. Rinaldi, Energy & Environmental Science 5 (2012) 8244.
[142]  A. Lolli, Y. Zhang, F. Basile, F. Cavani, S. Albonetti, Chemicals and Fuels from Bio-Based Building Blocks, Wiley-VCH Verlag GmbH & Co. KGaA, 2016, pp. 349-378.
[143]  M.J. Gilkey, B. Xu, ACS Catalysis 6 (2016) 1420-1436.
[144]  T.P. Sulmonetti, S.H. Pang, M.T. Claure, S. Lee, D.A. Cullen, P.K. Agrawal, C.W. Jones, Applied Catalysis A: General 517 (2016) 187-195.
[145]  M. Manikandan, A.K. Venugopal, A.S. Nagpure, S. Chilukuri, T. Raja, RSC Advances 6 (2016) 3888-3898.
[146]  J. Lee, S.P. Burt, C.A. Carrero, A.C. Alba-Rubio, I. Ro, B.J. O'Neill, H.J. Kim, D.H.K. Jackson, T.F. Kuech, I. Hermans, J.A. Dumesic, G.W. Huber, Journal of Catalysis 330 (2015) 19-27.
[147]  C. Wang, H. Xu, R. Daniel, A. Ghafourian, J.M. Herreros, S. Shuai, X. Ma, Fuel 103 (2013) 200-211.
[148]  Y. Xu, S. Qiu, J. Long, C. Wang, J. Chang, J. Tan, Q. Liu, L. Ma, T. Wang, Q. Zhang, RSC Advances 5 (2015) 91190-91195.
[149]  L. Grazia, A. Lolli, F. Folco, Y. Zhang, S. Albonetti, F. Cavani, Catalysis Science & Technology 6 (2016) 4418-4427.
[150]  V. Crocella, G. Cerrato, G. Magnacca, C. Morterra, F. Cavani, L. Maselli, S. Passeri, Dalton Transactions 39 (2010) 8527-8537.
[151]  J.S. Valente, F. Figueras, M. Gravelle, P. Kumbhar, J. Lopez, J.P. Besse, Journal of Catalysis 189 (2000) 370-381.
[152]  T. Sato, T. Wakabayashi, M. Shimada, Industrial & Engineering Chemistry Product Research and Development 25 (1986) 89-92.
[153]  D. Tichit, M.H. Lhouty, A. Guida, B.H. Chiche, F. Figueras, A. Auroux, D. Bartalini, E. Garrone, Journal of Catalysis 151 (1995) 50-59.
[154]  Y. Zhang, J. Wang, J. Ren, X. Liu, X. Li, Y. Xia, G. Lu, Y. Wang, Catalysis Science & Technology 2 (2012) 2485-2491.
[155]  J.I. Di Cosimo, V.K. Diez, C. Ferretti, C.R. Apesteguia, Catalysis: Volume 26, The Royal Society of Chemistry, 2014, pp. 1-28.
[156]  V.K. Díez, C.R. Apesteguía, J.I. Di Cosimo, Catalysis Today 63 (2000) 53-62.
[157]  A.S. Rocha, A.M.S. Forrester, M.H.C. de la Cruz, C.T. da Silva, E.R. Lachter, Catalysis Communications 9 (2008) 1959-1965.
[158]  N. Ballarini, F. Cavani, L. Maselli, A. Montaletti, S. Passeri, D. Scagliarini, C. Flego, C. Perego, Journal of Catalysis 251 (2007) 423-436.
[159]  N. Hosseinpour, A.A. Khodadadi, A. Bahramian, Y. Mortazavi, Langmuir 29 (2013) 14135-14146.
[160]  A. Hakim, T.S. Marliza, N.M. Abu Tahari, R.W.N. Wan Isahak, R.M. Yusop, W.M. Mohamed Hisham, A.M. Yarmo, Industrial & Engineering Chemistry Research 55 (2016) 7888-7897.
[161]  Y.-W. Chen, P.-J. Wang, W.-J. Wang, Catalysis Letters 6 (1990) 187-193.
[162]  G.M. Lari, C. Mondelli, J. Pérez-Ramírez, ACS Catalysis 5 (2015) 1453-1461.
[163]  F. Wang, N. Ta, W. Shen, Applied Catalysis A: General 475 (2014) 76-81.
[164]  Y. Shao, Q. Xia, X. Liu, G. Lu, Y. Wang, ChemSusChem 8 (2015) 1761-1767.
[165]  D.-Y. Hong, S.J. Miller, P.K. Agrawal, C.W. Jones, Chemical Communications 46 (2010) 1038-1040.

[166]   J.I. Di Cosimo, V.K. Díez, M. Xu, E. Iglesia, C.R. Apesteguía, Journal of Catalysis 178 (1998) 499-510.

[167]   K. Tanabe, W.F. Hölderich, Applied Catalysis A: General 181 (1999) 399-434.

[168]   M. Choura, N.M. Belgacem, A. Gandini, Macromolecules 29 (1996) 3839-3850.

[169]   T.P. Martin, R. Merlin, D.R. Huffman, M. Cardona, Solid State Communications 22 (1977) 565-567.

[170]   J.-f. Lu, C.-J. Tsai, Nanoscale Research Letters 9 (2014) 1-8.

[171]   L. Slavov, M.V. Abrashev, T. Merodiiska, C. Gelev, R.E. Vandenberghe, I. Markova-Deneva, I. Nedkov, Journal of Magnetism and Magnetic Materials 322 (2010) 1904-1911.

[172]   D.L.A. de Faria, S. Venâncio Silva, M.T. de Oliveira, J Raman Spectrosc 28 (1997) 873-878.

[173]   I.S. Lyubutin, S.S. Starchikov, T.V. Bukreeva, I.A. Lysenko, S.N. Sulyanov, N.Y. Korotkov, S.S. Rumyantseva, I.V. Marchenko, K.O. Funtov, A.L. Vasiliev, Materials Science and Engineering: C 45 (2014) 225-233.

[174]   G.K. Reddy, P. Boolchand, P.G. Smirniotis, The Journal of Physical Chemistry C 116 (2012) 11019-11031.

[175]   P. Chandramohan, M.P. Srinivasan, S. Velmurugan, S.V. Narasimhan, Journal of Solid State Chemistry 184 (2011) 89-96.

[176]   O. Vozniuk, S. Agnoli, L. Artiglia, A. Vassoi, N. Tanchoux, F. Di Renzo, G. Granozzi, F. Cavani, Green Chemistry 18 (2016) 1038-1050.

[177]   F.G.E. Nogueira, J.H. Lopes, A.C. Silva, R.M. Lago, J.D. Fabris, L.C.A. Oliveira, Applied Clay Science 51 (2011) 385-389.

[178]   W. Yu, J.G. Chen, Surface Science 640 (2015) 159-164.

[179]   E. Montiel, J. Cruz, J.-C. Gonzales, N. Jayanthi, T. Pandiyan, Journal of Cluster Science 22 (2011) 459.

[180]   S. Sitthisa, D.E. Resasco, Catalysis Letters 141 (2011) 784-791.

[181]   A. Navajas, G. Arzamendi, F. Romero-Sarria, M.A. Centeno, J.A. Odriozola, L.M. Gandía, Catalysis Communications 17 (2012) 189-193.

[182]   K. Routray, W. Zhou, C.J. Kiely, I.E. Wachs, ACS Catalysis 1 (2011) 54-66.

[183]   L.J. Burcham, L.E. Briand, I.E. Wachs, Langmuir 17 (2001) 6175-6184.

[184]   O. Gamba, H. Noei, J. Pavelec, R. Bliem, M. Schmid, U. Diebold, A. Stierle, G.S. Parkinson, The Journal of Physical Chemistry C 119 (2015) 20459-20465.

[185]   A. Badri, C. Binet, J.-C. Lavalley, Journal of the Chemical Society, Faraday Transactions 93 (1997) 1159-1168.

[186]   W. Zhang, H. Wang, Q. Li, Q. Dong, N. Zhao, W. Wei, Y. Sun, Applied Catalysis A: General 294 (2005) 188-196.

[187]   F. Solymosi, A. Erdohelyi, T. Bansagi, Journal of the Chemical Society, Faraday Transactions 1: Physical Chemistry in Condensed Phases 77 (1981) 2645-2657.

[188]   C. Di Valentin, A. Del Vitto, G. Pacchioni, S. Abbet, A.S. Wörz, K. Judai, U. Heiz, The Journal of Physical Chemistry B 106 (2002) 11961-11969.

[189]   G.T. Whiting, S.A. Kondrat, C. Hammond, N. Dimitratos, Q. He, D.J. Morgan, N.F. Dummer, J.K. Bartley, C.J. Kiely, S.H. Taylor, G.J. Hutchings, ACS Catalysis 5 (2015) 637-644.

[190]   L. Chen, S. Wang, J. Zhou, Y. Shen, Y. Zhao, X. Ma, RSC Advances 4 (2014) 30968-30975.

[191]  E. Nowicka, J.P. Hofmann, S.F. Parker, M. Sankar, G.M. Lari, S.A. Kondrat, D.W. Knight, D. Bethell, B.M. Weckhuysen, G.J. Hutchings, Physical Chemistry Chemical Physics 15 (2013) 12147-12155.

[192]  C. Lucarelli, S. Galli, A. Maspero, A. Cimino, C. Bandinelli, A. Lolli, J. Velasquez Ochoa, A. Vaccari, F. Cavani, S. Albonetti, The Journal of Physical Chemistry C 120 (2016) 15310-15321.

[193]  A. Villa, D. Ferri, S. Campisi, C.E. Chan-Thaw, Y. Lu, O. Kröcher, L. Prati, ChemCatChem 7 (2015) 2534-2541.

[194]  R. Shekhar, M.A. Barteau, R.V. Plank, J.M. Vohs, The Journal of Physical Chemistry B 101 (1997) 7939-7951.

[195]  J.L. Davis, M.A. Barteau, Surface Science 235 (1990) 235-248.

[196]  J.C.I.L. Center, Spectral Database for

Organic Compounds SDBS  http://sdbs.db.aist.go.jp/sdbs/cgi-bin/direct_frame_top.cgi.

[197]  G. Socrates, Infrared and Raman Characteristic Group Frequencies: Tables and Charts, 3rd Edition, 3rd Edition ed., Weily, 2004.

[198]  G. Dimas-Rivera, J. de la Rosa, C. Lucio-Ortiz, J. De los Reyes Heredia, V. González, T. Hernández, Materials 7 (2014) 527.

[199]  S. Sitthisa, T. Sooknoi, Y. Ma, P.B. Balbuena, D.E. Resasco, Journal of Catalysis 277 1-13.

[200]  M. Rogojerov, G. Keresztury, B. Jordanov, Spectrochimica Acta Part A: Molecular and Biomolecular Spectroscopy 61 (2005) 1661-1670.

[201]  J. Shen, M. Wang, Y.-n. Wu, F. Li, RSC Advances 4 (2014) 21089-21092.